Department of Physics
Faculty of Science
University of Zagreb

Vesna Janicki

Design and optical characterisation of hybrid thin film systems

Doctoral Thesis
submitted to the Department of Physics
Faculty of Science, University of Zagreb
for the academic degree of
Doctor of Natural Sciences (Physics)

Zagreb, 2007.

This dissertation has been made in Zagreb, supervised by Ph. D. Hrvoje Zorc, as a part of university postgraduate study at Department of Physics, Faculty of Science, University of Zagreb.

Acknowledgements

I would like to thank to Ph. D. Hrvoje Zorc, Ph. D. Olaf Stenzel and Ph. D. Jordi Sancho Parramon for the support, guidance, valuable discussions and advices. Special thanks go to Heidi Haase for deposition of the samples. Thanks to Ph. D. Sergey Yulin and Ph. D. Marcel Flemming from IOF in Jena for XRD and AFM measurements, Fraunhofer IOF in Jena for hospitality, Fraunhofer IST in Braunschweig, Laser Zentrum in Hannover and Microschicht Optik in Jena for the designs used for comparison and additional samples, Ph. D. Uwe Richter from Fraunhofer IST in Braunschweig for ellipsometry measurements and S. Grözinger and A. Chuvilin from Universität Ulm for TEM measurements.

I would like to thank to Fraunhofer Society in Germany for a Fraunhofer Fellowship at IOF in Jena.

Contents

Doctoral thesis

University of Zagreb
Faculty of Science
Department of Physics

Design and optical characterisation of hybrid thin film systems

Vesna Janicki

Institut Ruđer Bošković, Bijenička 54, Zagreb, Croatia and
Fraunhofer Institut für Angewandte Optik und Feinmechanik, Albert-Einstein-Strasse 7, Jena, Germany

The subject of this work is design and optical characterisation of hybrid thin film systems. The hybrid antireflective and notch designs are synthesised and compared with classical HL designs prepared with the same requirements and restrictions. Hybrid antireflective design is refined and adapted for deposition by different co-deposition methods. These coatings are deposited and their optical performance compared. Optical characterisation is performed. Origin of discrepancies between the designs and the models obtained by characterisation is related with errors in deposition processes. The model obtained using only reflectance and transmittance measurements and including ellipsometric measurements, same as the one obtained from secondary ion mass spectrometry based initial design are compared. The appropriateness of Lorentz-Lorenz model for calculation of refractive index of mixtures in optical characterisation and therefore the necessity to introduce it into designing is tested. Appropriateness of this model is related to the structure of the mixtures by additional measurements.

Keywords: hybrid coating, material mixture, antireflective coating, gradient index, optical characterisation, thin film design, optical properties
Supervisor: Ph. D. Hrvoje Zorc
Reviewers: Ph. D. Hrvoje Zorc, Ph. D. Olaf Stenzel, Ph. D. Dinko Babić.
Thesis accepted: 18.9.2007.

Doktorska dizertacija

Sveučilište u Zagrebu
Prirodoslovno-matematički fakultet
Fizički odsjek

Oblikovanje i optička karakterizacija hibridnih tankoslojnih sustava

Vesna Janicki

Institut Ruđer Bošković, Bijenička 54, Zagreb, Hrvatska i
Fraunhofer Institut für Angewandte Optik und Feinmechanik, Albert-Einstein-Strasse 7, Jena, Njemačka

Tema rada je dizajn i optička karkterizacija hibridnih tankoslojnih sustava. Hibridni antirefleksni dizajn i dizajn uskopojasnog reflektora su sintetizirani i uspoređeni s klasičnim HL dizajnima napravljenim prema istim zahtjevima i ograničenjima. Hibridni antirefleksni dizajn je dooptimiziran i prilagođen za kodepoziciju različitim tehnikama. Ovi slojevi su napravljeni i uspoređene su njihove optičke karakteristike. Provedena je optička karakterizacija. Uzroci odstupanja između dizajna i modela dobivenih optičkom karakterizacijom su dovedeni u vezu s greškama u procesu depozicije. Uspoređeni su modeli dobiveni upotrebom samo spektroskopijskih i uključujući i elipsometrijska mjerenja, kao i onaj dobiven iz početnog dizajna zasnovanog na masenoj spektroskopiji sekundarnih iona. Testirana je opravdanost Lorentz-Lorenzovog modela za izračun indeksa loma mješavina u optičkoj karakterizaciji te stoga potreba da ga se ugradi u dizajniranje. Dodatnim mjerenjima je povezana opravdanost ovog modela sa strukturom mješavina.

Ključne riječi: hibridni slojevi, smjese materijala, antirefleksni slojevi, gradijent indeksa, optička karakterizacija dizajn tankih filmova, optička svojstva
Mentor: Dr. sc. Hrvoje Zorc
Ocjenjivači: Dr. sc. Hrvoje Zorc, Dr. sc. Olaf Stenzel, Dr. sc. Dinko Babić.
Rad prihvaćen: 18.9.2007.

Extended abstract in Croatian language

1. Uvod

1.1. Općenito

Optički tanki slojevi kojima se indeks loma kontinuirano mijenja kroz debljinu sloja poznati su kao slojevi s gradijentom indeksa loma ili nehomogeni slojevi. Ako je promjena indeksa loma k tome još i periodična, tada se sloj naziva naboranim (engl. rugate). Sustavi s gradijentom indeksa loma mogu imati bolje optičke i mehaničke karakteristike od konvencionalnih HL dizajna gdje se izmjenjuju slojevi visokog i niskog indeksa loma. Slojevi s gradijentom indeksa loma (nehomogeni slojevi) su obećavajući u slučaju sustava s antirefleksnim svojstvima u širokom rasponu kutova upada svjetlosti, a također su vrlo interesantni u dizajnu uskopojasnih reflektora. Dodatne odlike koje se mogu očekivati od nehomogenih slojeva su dobra mehanička svojstva, kao što je nizak stres i velika tribološka otpornost, te viši prag na oštećenja uzrokovana laserom nego kod klasičnih višeslojnih sustava.

Hibridni slojevi predstavljaju alternativni pristup dizajniranju jer kombiniraju homogene slojeve i one s linearnim gradijentom indeksa loma. Ovaj pristup ujedinjuje prednosti slojeva s gradijentom indeksa loma i mogućnosti izrade nehomogenih slojeva u industrijskim uređajima za depoziciju.

U ovoj radnji predstavljen je dizajn hibridnih antirefleksnih (AR) i uskopojasnih reflektorskih filtera, a njihove teorijske optičke karakteristike su uspoređene s onima odgovarajućih klasičnih dizajna. Hibridni AR sustav je napravljen različitim tehnikama depozicije. Optička karakterizacija izrađenih uzoraka daje naputke koja poboljšanja bi trebalo napraviti u procesu depozicije. Model za izračunavanje indeksa loma materijala u smjesi koji je primijenjen u karakterizaciji je eksperimentalno provjeren i doveden u vezu sa strukturom materijala.

1.1.1. Dizajn tankoslojnih optičkih sustava

Dva su pristupa dizajniranju tankoslojnih filtera. Prvi pristup kreće od početnog dizajna koji se zasniva na prethodnom teorijskom znanju o strukturi različitih interferentnih filtera. Početne debljine slojeva se zatim optimiziraju dok se ne dobije najmanje odstupanje od zadanih vrijednosti optičkih karakteristika (željena refleksija, transmisija). Drugi pristup kreće od samo jednog sloja

materijala u koji se onda postepeno dodaju slojevi drugog materijala te nakon toga slijedi optimizacija[10].

Nasuprot klasičnom dizajnu, komercijalni program za dizajn naboranih slojeva još nije dostupan. U ovoj vrsti dizajna dopušteni su i indeksi loma vrijednosti između onih čistih materijala i to su dodatni parametri u optimizaciji koje treba dobro kontrolirati.

Optičke konstante slojeva koji su mješavina materijala računaju se pomoću različitih modela koji povezuju optičke konstante mješavine s onima čistih materijala, kao što Bruggemanov, Lorentz-Lorenzov (LL), Maxwell-Garnettov ili linearna kombinacija indeksa loma. Za slučaj TiO_2-SiO_2 mješavina pokazano je da je Lorentz-Lorenzov model prikladniji od Bruggemanovog, iako se sve objavljene studije ne slažu.

Različite vrijednosti indeksa loma u dizajnu se postižu odgovarajućom smjesom materijala. Zbog poteškoća u pripremi materijala željenog indeksa loma nehomogeni slojevi su izazov za izradu. Jedna od standardnih tehnika izrade nehomogenih slojeva je kodepozicija (istovremeno naparavanje) dva materijala s promjenom omjera njihovih čestica koje se kondenziraju na podlogu.

1.1.2. Optička karakterizacija tankoslojnih sustava

Izrađeni uzorci se analiziraju kako bi se provjerilo da li zadovoljavaju zahtjevima. Pri tome se koriste metode optičke karakterizacije kojima se iz optičkih mjerenja određuje indeks loma, debljina sloja, te varijacija indeksa loma (nehomogenost). Većina tih metoda polazi od početne aproksimacije uzorka koja je dana preko skupa parametara. Minimalizacijom odstupanja simuliranih podataka od izmjerenih podataka pronalaze se optimalne vrijednosti parametara.

Numeričke tehnike koje se koriste u optimizaciji bazirane su obično na spektrofotometrijskim ili elipsometrijskim mjerenjima spektra, a rijetko se koristi i njihova kombinacija. Česti problem optičke karakterizacije je višestrukost rješenja, te je stoga preporučljivo imati više mjerenja istog uzorka (npr. mjerenja pod različitim kutovima upada svjetlosti, kombinacija spektrofotometrijskih i elipsometrijskih mjerenja) ili kombinirati optičke metode s drugim metodama.

Korisno je usporediti profil indeksa loma pronađen optičkom karakterizacijom s ciljanim profilom koji je trebalo izraditi jer se time mogu detektirati pogreške u procesu izrade uzorka te poboljšati proces. Važno je razmotriti i uspješnost ne-optičkih metoda dubinske analize materijala u određivanju profila indeksa loma sloja.

1.1.3. Rad predstavljen u ovoj dizertaciji

Predmet istraživanja ove dizeratacije je dizajn i optička karakterizacija hibridnih tankoslojnih sustava. Predstavljeni hibridni antirefleksni slojevi i uskopojasni reflektor. Oni su uspoređeni s klasičnim HL dizajnima napravljenim prema istim kriterijima i ograničenjima. Antirefleksni slojevi su posebno uspoređeni s obzirom na suzbijanje refleksije na većim kutovima upada i na osjetljivost na greške u procesu izrade, a uskopojasni reflektori su posebno uspoređeni s obzirom na ukupnu debljinu i optičku gustoću. Hibridni antirefleksni sloj je usavršen i prilagođen za izradu pomoću različitih metoda kodepozicije: naparavanju uz pomoć elektronskog topa, magnetronskom radio frekvencijskom raspršivanju i raspršivanju pomoću ionskog snopa. Svi usavršeni dizajni imaju iste karakteristike i kvalitetu, a uspoređene su i analizirane i optičke karakteristike izrađenih uzoraka. Također, provedena je optička karakterizacija ovih uzoraka te su predložene mogućnosti za poboljšanje procesa izrade. Model dobiven optičkom karakterizacijom koristeći samo spektroskopska mjerenja uspoređen je s modelom dobivenim kad su bila uključena i elipsometrijska mjerenja, kao i onim dobivenim iz početnog dizajna zasnivanom na masenoj spektrometriji sekundarnih iona. Izradom različitih slojeva koji su mješavina materijala, te usporedbom njihovog indeksa loma s teorijskim vrijednostima koje daju različiti modeli miješanja, eksperimentalno je pokazana prikladnost primjene LL modela i potreba da se taj model implementira u program za dizajn naboranih slojeva. Prikladnost LL modela je povezana sa strukturom mješavina dodatnim mjerenjima.

1.2. Materijali

U Leybold Syrus Pro 1100 depozicijskoj komori za izradu slojeva je korištena kombinacija oksida koji se uobičajeno koriste u naparivanju, a to su Nb_2O_5 i SiO_2. Niti jedan od ova dva materijala nema značajniju apsorpciju u području spektra od interesa (400-900 nm), osim ako ne dolazi do manjka kisika tokom izrade sloja. Silicij dioksid u sloju ima amorfnu strukturu koja je stabilna na zagrijavanje do 1100°C. Karakteristične veze u SiO_2 koje se mogu detektirati infracrvenom spektroskopijom su na 121 cm^{-1}, 1080 cm^{-1}, 804 cm^{-1}, i 461 cm^{-1}. Niobij pentoksid je također amorfan u sloju dobivenom naparavanjem pomoću elektronskog topa. Ako se radi o sloju čistog Nb_2O_5, do kristalizacije dolazi zagrijavanjem već između 400^oC i 500°C. Strukture karakteristične za infracrveni dio spektra čistog Nb_2O_5 su oko 600 cm^{-1}. Miješanjem sa SiO_2 temperatura

kristalizacije diže i na preko 1000°C budući da SiO_2 stabilizira amorfni Nb_2O_5. Kada se preko Si-O-Nb veza uspostavi jako međudjelovanje između dva materijala smanjuje se mobilnost Nb_2O_5 te se zato povećava temperatura na kojoj dolazi do kristalizacije. Ovaj je zaključak zasnovan na proučavanju infracrvene vrpce između 930 cm^{-1} i 920 cm^{-1} koja nestaje nakon tretiranja uzoraka na visokoj temperaturi.

2. Teorija, tehnike za optičku karakterizaciju i numerički programi

2.1. Teorija

Predstavljeni su teorijski aspekti širenja svjetlosti kroz materiju. Definirane su optičke konstante koje su parametri za karakterizaciju međudjelovanja svjetla i sredstva u kojem se svjetlo širi. Objašnjen je i njihov odnos s mikroskopskim svojstvima, kao i ovisnost o frekvenciji elektromagnetskog zračenja. Disperzijski modeli su uvedeni kao jednadžbe koje povezuju ovisnost optičkih konstanti s frekvencijom. Opisani su Cauchyjev i Tauc-Lorentzov model disperzije. Opisano je i širenje svjetla kroz višeslojne strukture pri čemu dolazi do interferencije reflektiranih i transmitiranih dijelova snopa svjetlosti. Matrična metoda je predstavljena kao način da se izračunaju optička svojstva tankoslojne strukture. Opisane su i teorije efektivnog sredstva kao način da se optičke konstante mješavina materijala definiraju pomoću optičkih konstanti komponenata.

2.2. Spektrofotometrija i elipsometrija

Spektrofotometrija i elipsometrija su najraširenije i najbolje razvijene eksperimentalne tehnike za karakterizaciju optičkih svojstava materijala. Budući da su korištene za optičku karakterizaciju uzoraka u ovoj radnji, dan je njihov opis.

2.3. Program za naborane slojeve i program za optičku karakterizaciju

2.3.1. Program za dizajn naboranih slojeva

Najčešći pristup sintezi naboranih filtera je zasnovan na inverziji relacije Fourierovog transformata između spektralne funkcije $Q(\lambda)$ i profila indeksa loma. Jedan od problema ove metode je da Q-funkcija nije točno poznata, nego se koriste njene približne vrijednosti. Alternativna metoda za sintezu naboranih slojeva je upotrebom programa koji se služi tehnikom numeričke optimizacije i koji je posebno prilagođen naboranim sustavima.

Polazi se od početnog dizajna, tj. profila indeksa loma koji je definiran preko točaka u kojima se mijenja gradijent indeksa loma. Te su točke zadane preko dvije varijable, a to su debljina sloja u kojem se mijenja gradijent i vrijednost indeksa loma od kojeg započinje promjena. Na taj način svaki kontinuirani profil indeksa loma može biti dobro aproksimiran, ovisno o broju zadanih točaka. Za računanje spektra ovako definiranog sloja, svaki je segment između dviju točaka podijeljen na podslojeve jednakih debljina i konstantnog indeksa loma čija je vrijednost jednaka srednjoj vrijednosti indeksa loma svakog podsloja. Broj podslojeva treba biti dovoljan za razumno dobru aproksimaciju gradijenta u sloju.

2.3.2. Program za optičku karakterizaciju

Za optičku karakterizaciju je korišten program koji prilagodbom na eksperimentalne podatke omogućava određivanje optimalne vrijednosti skupa parametara koji definiraju uzorak. Nehomogenost svakog segmenta je prikazana podjelom na odgovarajući broj podslojeva jednakih debljina. Svaki podsloj i svaki sloj konstantnog indeksa loma modelirani su kao mješavina dva materijala visokog i niskog indeksa loma sa odgovarajućim volumnim udjelima, gdje je zbroj tih udjela jednak jedan. Za modeliranje indeksa loma smjese primijenjen je Lorentz-Lorenzov model, ali testirani su i Bruggemanov i linearni model. Indeksi loma čistih materijala su uzimani iz podataka koji su određeni optičkom karakterizacijom iz uzoraka s jednim slojem čistog materijala, ili su predstavljeni preko disperzijskih modela.

Ovakvim načinom modeliranja moguće je predstaviti uzorak preko ograničenog broja parametara: volumnog udjela i debljine svakog sloja, te parametara koji definiraju disperzijski model za svaki materijal. Program dozvoljava fiksiranje ovih parametara na zadanu vrijednost ili njihovu optimizaciju unutar zadanih granica. Također, moguće je povezati parametre različitih slojeva i tako, na primjer, osigurati kontinuitet volumnih udjela na granicama između slojeva.

3. Dizajni

U Leybold Syrus Pro 1100 depozicijskoj komori prethodno su već napravljene uspješne probe kodepozicije niobij pentoksida i silicij dioksida. Minimalni i maksimalni indeks loma slojeva s linearnim gradijentima su ograničeni tehnikom depozicije i poteškoćama u preciznoj kontroli niskih brzina depozicije. Stoga su izvedive vrijednosti indeksa loma ograničene između vrijednosti 2.1 i 1.6 na valnoj duljini 570 nm. Osim toga, nije moguće dobiti proizvoljno strmi gradijent,

također zbog tehničkih razloga. Tako je maksimalno dozvoljena promjena indeksa loma ograničena na 0.5 na svakih 25 nm debljine.

3.1. Dizajn antirefleksnog sloja

Antirefleksni slojevi se koriste u većini optičkih sustava kako bi se povećao intenzitet transmitiranog svjetla, te spriječila višestruka refleksija na površinama unutar sustava. Klasični HL sustavi, napravljeni od dva materijala, su najefikasniji u slučaju okomitog upada svjetlosti. No, kada se radi o svjetlosti koja ulazi u sustav pod nekim drugim kutom i ako su još neophodna i dobra antirefleksna svojstva u velikom rasponu kutova upada, potrebno je uvesti barem još jedan dodatni materijal i zapravo je najpogodnije primijeniti sloj s gradijentom indeksa loma.

Idealni antirefleksni sloj za dani raspon valnih duljina i kutova bio bi struktura s gradijentom indeksa loma koji se mijenja od vrijednosti indeksa loma podloge, na strani podloge, do indeksa loma okoline, na površini sloja. Neki od načina kako dobiti dovoljno niske indekse loma na površini su izrada struktura moljčevog oka ili povećana poroznost prema ulaznom sredstvu. Glavni nedostatak ovih rješenja je slaba mehanička otpornost i čišćenje takvih površina.

U ovom je radu predstavljen alternativni hibridni antirefleksni dizajn sintetiziran pomoću programa koji je nedavno razvio Tikhonravov sa suradnicima. Ovaj je sloj optimiziran za vidljivi dio spektra za BK7 staklo, a korišteni su materijali uobičajeni za depoziciju Nb_2O_5 i SiO_2, imajući na umu ograničenja depozicijske tehnologije koja je na raspolaganju u Leybold Syrus Pro 1100 depozicijskoj komori gdje su slojevi kasnije izrađeni. Napravljena su dva hibridna dizajna, različitih debljina i uspoređeni su s klasičnim dizajnom. Za tanji dizajn je provedena analiza pogrešaka u debljini i indeksu loma, a određeni su i najosjetljiviji slojevi.

Usavršeni i prilagođeni hibridni antirefleksni sloj je izrađen s tri različite depozicijske tehnike: evaporacije pomoću elektronskog topa, radiofrekvencijskog magnetronskog raspršivanja i raspršivanja pomoću ionskog topa. Spektri uzoraka jednostrano i obostrano prekrivenih ovim slojem su uspoređeni s teorijskim spektrima dizajna, a provjerena je i reproducibilnost rezultata za svaki proces.

3.1.1. Specifikacije i ograničenja na dizajn

Traženi antirefleksni sloj mora minimalizirati refleksiju R u području 480-680 nm za kutove upada 0-50°. R je srednja vrijednost refleksije od s i p polarizacije (R_s i R_p). Dodatni je zahtjev da razlika

refleksije od obje polarizacije bude što manja za kut od 50° u zadanom području. Podloga je BK7 staklo.

3.1.2. Hibridni dizajni

Kao rezultat sinteze dobivena su dva hibridna dizajna definirana u 9 i u 13 točaka. Zadnje četiri točke predstavljaju slojeve čistih materijala i konstantnog indeksa loma. Ukupna debljina ovih dizajna je 526 nm (dizajn definiran u 9 točaka) i 839 nm (dizajn definiran u 13 točaka). Odstupanje od zadanih zahtjeva je 40% manje u slučaju debljeg dizajna. Ipak, oba dizajna dobro zadovoljavaju zahtjeve. Osim dobrih optičkih karakteristika i male debljine, kvaliteta hibridnih antirefleksnih dizajna je u njihovoj jednostavnosti tj. malom broju točaka u kojima su definirani. Početne i završne točke svakog segmenta su uvijek minimalni i maksimalni dozvoljeni indeks loma mješavine, tako da samo dva indeksa loma mješavina trebaju biti dobro kontrolirani i reproducibilni.

3.1.3. Usporedba s klasičnim HL dizajnom

Klasični HL višeslojni dizajn antirefleksnog sloja je dobiven korištenjem programa Optilayer, uz zadavanje istih zahtjeva, podloge i materijala. Ovaj je dizajn debljine 553 nm i ima 7 slojeva, te daje 19% bolju prilagodbu na zahtjeve od tanjeg hibridnog dizajna. Nedostatak je da je prvi sloj visokog indeksa loma debljine samo 4.6 nm, a ako bi ga se izostavilo, prilagodba na zahtjeve bi bila 10% lošija od one hibridnog dizajna.

3.1.4 Osjetljivost i analiza grešaka

Poznavanje osjetljivosti na greške u izradi, te kritičnih točaka u dizajnu je vrlo važno za proces naparavanja. Da bi se utvrdile najosjetljivije točke za tanji dizajn, debljina i indeks loma svake točke u kojoj je dizajn definiran varirani su ±1% i provjeravana je kvaliteta prilagodbe na zahtjeve. Utvrđeno je da je prilagodba najslabija u slučaju povećanog indeksa loma četvrte točke u dizajnu, smanjene debljine zadnjeg sloja prema površini ili smanjenog indeksa loma pete točke. Simulacijom pogrešaka od 1% u debljini i indeksu loma u programu Optilayer (jedino u slojevima čistih materijala nije dozvoljena greška u indeksu loma), generiranjem 100 spektara sa slučajnom pogreškom u dizajnu, najširi pojas vjerojatnosti je dobiven za deblji hibridni dizajn, što je posljedica većeg broja parametara. Pojas vjerojatnosti tanjeg hibridnog i klasičnog dizajna je podjednao širok za kut od 0°, a u slučaju klasičnog za kut od 50° je uži.

3.1.5. Usavršeni dizajni

Usavršeni dizajni koji su sintetizirani kako bi se usporedila efikasnost različitih tehnika depozicije su uspoređeni i utvrđeno je da svi imaju podjednake debljine (531-537 nm za tanji dizajn), najniži dopušteni indeks loma mješavine je 1.6 na 570 nm, a usporedive su i kvalitete prilagodbe na zahtjeve. Apsorpcija materijala (Ta_2O_5 i TiO_2) je zanemarena jer je niska u zadanom području valnih duljina i jer je ukupna debljina materijala visokog indeksa loma u dizajnu mala.

3.2. Dizajn uskopojasnih reflektora

Idealni uskopojasni reflektor bi imao sto postotnu refleksiju u zadanom području, a izvan njega refleksija bi bila nula. Kvaliteta filtera se ocjenjuje prema širini područja refleksije, brzine prelaska između područja refleksije i transmisije, debljini sloja i optičkoj gustoći. Optička gustoća je mjera snage refeleksijskog maksimuma, a definira se kao negativni logaritam vrijednosti transmisije u ovom maksimumu.

Poznato je da četvrtvalni HL sustav daje fundamentalno blokirajuće područje, tj. područje visoke refleksije, kao i blokirajuća područja neparnih harmonika. Što je manja razlika indeksa loma korištenih materijala to će biti uže područje refleksije, ali isto tako i manja optička gustoća za danu ukupnu debljinu sloja.

Zbog nepoklapanja ekvivalentnih indeksa loma sloja i okolnog medija, uz maksimum se javljaju i oscilacije u refleksiji. Profil indeksa loma četvrtvalnog sustava se može shvatiti kao stepenasta valna funkcija i kao takva biti predstavljena Fourierovim redom. Da bi se uklonile oscilacije koje se javljaju uz maksimum refleksije, primjenjuje se funkcija amplitudne apodizacije na prvi član Fourierovog reda. Gaussova apodizacija i apodizacija polinomom petog reda, dodane na sinusnu funkciju, su se pokazale jako dobrima u tu svrhu. Potiskivanje dodatnih oscilacija često ide na uštrb refleksije u blokirajućem području. Zato se obično koristi samo djelomična apodizacija na jedan broj početnih i završnih perioda strukture ili se jednostavno poveća broj perioda budući da optička gustoća raste gotovo linearno s njihovim brojem.

U ovome radu je predstavljen hibridni dizajn uskopojasnog reflektora centriranog na valnoj duljini 532 nm, te je uspoređen s druga dva dizajna. Jedan od tih dizajna je klasični HL sustav, a drugi je apodizirana sinusoidalna struktura koja je aproksimirana homogenim slojevima, tj. slojevima konstantnog indeksa loma. Hibridni dizajn je kombinacija ova dva pristupa. Također je

zasnovan na apodiziranoj sinusnoj strukturi, ali je aproksimiran kombinacijom dijelova s linearnom promjenom indeksa loma između slojeva s najnižim i najvišim u dizajnu dopuštenim indeksima loma.

3.2.1. Specifikacije

Pod okomitim upadom svjetla, uskopojasni reflektor treba zadovoljavati slijedeće zahtjeve: refleksija treba biti manja od 10% u području 400-515 nm i 550-700 nm (bez refleksije sa zadnje strane), transmisija u području 530-534 nm treba biti manja od 0.01%, a ukupna debljina ne smije prelaziti 10 μm za više od 10%. Podloga je BK7 staklo. Radi jednostavnije usporedbe rezultata pretpostavljeno je da korišteni materijali i podloga ne apsorbiraju.

3.2.2. Usporedba uskopojasnih reflektora

U originalnom klasičnom HL dizajnu uskopojasnog reflektora originalni materijali su zamijenjeni s SiO_2 i Nb_2O_5 istog indeksa loma kao i materijali korišteni u dizajnu hibridnih AR sustava. Tako izmijenjeni dizajn je onda dodatno optimiziran na tražene specifikacija. Isto je napravljeno s originalnim naboranim sustavom.

Hibridni dizajn je dobiven od početnih 45 cik-cak perioda s rasponom indeksa loma 1.6-1.75 i ukupne debljine oko 7 μm. Optimizacija je dovela do apodiziranog profila oblika sinusoide s pola perioda. U sredini profila sve su gornje vrijednosti indeksa loma fiksirane na 1.80. Dodavanjem novih perioda, optimizacijom debljina, te uvođenjem SiO_2 sloja na kraj dizajna, kako bi se poboljšala transmisija izvan refleksijskog maksimuma, dobiven je konačni dizajn.

Sva tri dizajna imaju slične refleksijske spektre. Klasični dizajn ima najbolju optičku gustoću u području refleksijskog maksimuma i time najvišu refleksiju. Ovaj dizajn također ima i najmanju debljinu i broj perioda, zahvaljujući najvećem kontrastu između najvećeg i najmanjeg indeksa loma u dizajnu, u odnosu na druga dva dizajna. Općenito je za dizajne s gradijentom indeksa loma karakteristično da im je potrebna veća debljina nego klasičnima za istu kvalitetu refleksije. Strmina prijelaza između propuštajućeg i blokirajućeg pojasa za sva tri dizajna je 1 nm za promjenu od 20% do 80%, dok je širina na pola refleksijskog maksimuma 32 nm. Uspoređujući hibridni i naborani dizajn može se primijetiti nešto širi propuštajući pojas za hibridni i nešto bolja optička gustoća, te manja debljina za naborani. Hibridni dizajn je lakši za izradu od naboranog zahvaljujući linearnim gradijentima i konstantnoj amplitudi perioda.

4. Eksperiment

4.1. Depozicija

4.1.1. Tehnike depozicije

4.1.1. Evaporacija pomoću elektronskog topa (EBE)

Leybold Syrus Pro 1100 komora za depoziciju opskrbljena je s dva elektronska topa i Advanced Plasma Source (APS). Katoda od LaB_6 i anoda APS-a se nalaze u cilindričnoj magnetskoj zavojnici koja proizvodi magnetsko polje što daje spiralnu putanju elektronima koji izlaze iz anode tokom njihova ubrzanja. U cilindar se dovode atomi argona koji se ioniziraju sudarima s elektronima, te nastaju dodatni elektroni. Elektroni čine izbojnu struju I_D između katode i anode. Elektroni se ubrzavaju izvan APS-a, duž magnetskih silnica, te za sobom ostavljaju pozitivni naboj koji daje napon između APS-a i nosača podloge koji onda ubrzava ione argona prema podlogama. Sudari iona argona doprinose također i energiji čestica koje se kondenziraju na podlozi povećavajući tako gustoću i indeks loma sloja, smanjujući poroznost i mogućnost apsorpcije vode, te povećavaju tenzilni stres u sloju.

Naparavanje materijala (Nb_2O_5 i SiO_2) se odvija u atmosferi argona (radni plin) i kisika (reaktivni plin) kako bi se zadržala stehiometrija materijala koji se naparavaju. Prije početka depozicije podloge se zagrijavaju na temperaturu 150^oC, koja se održava i tokom procesa. Da bi se osigurala uniformnost debljine sloja, podloge su stavljene na nosače koji rotiraju brzinom od oko 20 okreta u minuti. Lončići s materijalima također rotiraju kako bi se izbjegla deformacija oblaka pare zbog snižavanja nivoa u lončiću potrošnjom materijala za vrijeme dugotrajnih procesa. Proces naparavanja se kontrolira računalnim programom koji automatski vrši mjerenja i očitavanja parametara (brzina naparavanja, tlaka, temperature, itd.).

Indeks loma se mijenja zbog promjene omjera koncentracije materijala u sloju. Ovo se postiže kontinuiranom promjenom brzine naparavanja materijala promjenom emisijske struje elektronskog topa. Nehomogeni profil indeksa loma u sloju je, prema tome, zaista kontinuirana promjena u svojstvima sloja, a ne niz tankih slojeva konstantnog indeksa loma, tj. kvazi nehomogeni sloj.

Brzina naparavanja svakog materijala je kontrolirana računalom i mjerena monitorima s kvarcnim kristalićem, zasebnim za svaki materijal. Zbroj brzina naparavanja oba materijala je

održavan konstantnim za vrijeme depozicije. Kvarcni monitori su zaštićeni kako bi se smanjila eventualna depozicija jednog materijala na monitor za praćenje debljine sloja drugog materijala. Efikasnost ove zaštite je testirana eksperimentalno. Test je napravljen s različitim brzinama depozicije kako bi se uzela u obzir eventualna promjena oblika oblaka pare materijala koji bi se onda više ili manje kondenzirao na dani kvarcni monitor. Pokazano je da kvarcni monitor za mjerenje debljine silicij dioksida broji u prosjeku 7.9% debljine niobij pentoksida, a kvarcni monitor debljine niobij pentoksida oko 1.5% debljine silicij dioksida. Kada se ovo uzme u obzir, brzine naparavanja su postavljene da se mijenjaju od 0.3 nm/s do 1.2 nm/s, što znači realnu brzinu od 0.205-1.178 nm/s za SiO_2 i 0.282-1.183 nm/s za Nb_2O_5 i minimalni i maksimalni indeks loma mješavine od 1.589 do 2.15 za valnu duljinu 570 nm.

4.1.1.2. Radiofrekvencijsko magnetronsko raspršivanje (RFS)

Uzorci izrađeni ovom tehnikom načinjeni su u FhG-IST, Braunschweig, Njemačka, u komori koja je dizajnirana i konstruirana u samom laboratoriju. Korištene su keramičke SiO_2 i Ta_2O_5 mete. Željeni sastav sloja se postiže mijenjanjem omjera snage na ove dvije mete, te time brzine depozicije pojedinog materijala. Za vrijeme procesa održavana je konstantna ukupna snaga od 800 W i konstantni tok plina u komoru (Ar=59 sccm, O_2=4 sccm, čistoće: Ar=99.998 i O_2=99.995).

4.1.1.3. Raspršivanje pomoću ionskog topa (IBS)

Uzorci izrađeni ovom tehnikom načinjeni su u prilagođenoj Varian 3125 depozicijskoj komori U Lazer Zentrum Hannover, Njemačka, koja je opremljena radiofrekvencijskim ionskim izvorom. Ioni argona se ubrzavaju do energije oko 1.2 keV za reaktivno raspršivanje s metalne mete. Materijali mete, SiO_2 i TiO_2, se nalaze na istoj ploči, jedan uz drugoga, a ploča je montirana na nosač koji se može linearno pomicati. Na taj način oba materijala mogu biti raspršivana istovremeno. Pozicija ove zonske mete s obzirom na ionski snop definira koncentraciju mješavine dva materijala. U komoru je ugrađen širokopojasni CCD monitoring sustav koji snima transmisijske spektre direktno s rotirajuće podloge. Spektri se mjere od 475 do 950 nm te se iz njih kontinuirano izračunava trenutna debljina sloja i točka u kojoj treba završiti naparavanje.

4.1.2. Napravljeni uzorci

Za svaki proces depozicije obično su stavljene tri vrste podloge u komoru: BK7 staklo, Suprasil i komadić silicijskog wafera radi kasnije analize.

4.1.2.1. Nb_2O_5 i SiO_2

Slojevi ovih materijala su naneseni uz konstantne brzine depozicije i upotrijebljeni za određivanje indeksa loma čistih materijala koji će se kasnije koristiti u optičkoj karakterizaciji naboranog i hibridnih AR uzoraka. Također su upotrijebljeni za određivanje faktora pretvorbe za treći kvarcni monitor, smješten u centru rotirajuće kalote, koji služi za kontroliranje debljine tokom depozicije čistih materijala.

4.1.2.2. Uzorak s deset perioda

Uzorak s deset perioda rastućeg i padajućeg indeksa loma je napravljen da bi se provjerile optičke karakteristike naboranog sustava.

4.1.2.3. Hibridni AR slojevi

Hibridni antirefkleksni slojevi su nanešeni na BK7 podloge na jednu i na obje strane. Nakon vađenja uzoraka iz komore izmjerena im je transmisija i refleksija na Perkin Elmer Lambda 900 spektrofotometru za kut upada 0^o, te s i p polarizacija za kut 45^o. Korišten je dodatak za apsolutno mjerenje refleksije koji omogućava izvođenje oba mjerenja (transmisije i refleksije) bez pomicanja uzorka.

4.1.2.4. Usporedba uzoraka napravljenih različitim tehnikama

Iz spektralnih krivulja se vidi da je postignuto dobro slaganje optičkih karakteristika uzoraka sa očekivanim teorijskim vrijednostima. Mjerenja napravljena pod 45° ukazuju na to da je dobro zadovoljen i uvjet postavljen za 50°. Najbolje slaganje sa teorijskim spektrima ima uzorak izrađen tehnikom raspršivanja pomoću ionskog snopa. Ova tehnika pokazuje i najbolju reproducibilnost.

4.1.2.5. Slojevi mješavine materijala

Pet uzoraka sa slojem mješavine materijala, konstantnog indeksa loma, razlikujući se međusobno u koncentraciji SiO_2 u odnosu na Nb_2O_5 su napravljeni kako bi se potvrdilo koja teorija efektivnog sredstva najbolje opisuje optičke konstante smjese SiO_2 i Nb_2O_5.

4.2. Spektroskopska optička karakterizacija

4.2.1. Transmisija, refleksija i elipsometrijska mjerenja

Refleksija (R) i transmisija (T) su mjerene svaka 2 nm: srednja R i T su mjerene pod kutem 6°, a Rs, Rp, Ts i Tp pod kutem 45°. Greška mjerenja za R i T i normalni upad su 0.2%, a za mjerenja pod 45° 0.5%. Mjerenja spektra elipsometrijskih Δ i Ψ funkcija su napravljena na standardnom SENTECH SE800 elipsometru s mikrotočkom (200μm). Korištenjem mikrotočke, te relativno debele podloge (2 mm) izbjegava se doprinos refleksije stražnje strane uzorka u mjerenjima. Elipsometrijska mjerenja su napravljena u istom području valnih duljina kao i spektrofotometrijska mjerenja, pod kutevima 50, 55 i 60 stupnjeva, u 575 točaka po kutu. Ovi kutevi su izabrani jer daju najveću amplitudu u spektru izmjerenih funkcija. U optičkoj karakterizaciji su korišteni $\cos\Delta$ i $\cos 2\Psi$. Greške u ovim elipsometrijskim funkcijama, zajedno s težinskim faktorom koji je bio uzet u obzir u odnosu na spektrofotometrijska mjerenja, su procijenjene na 0.0018 za $\cos\Delta$ i 0.0072 za $\cos 2\Psi$.

4.2.2. Podloge: BK7 i Suprasil

Prije optičke karakterizacije uzoraka napravljena je karakterizacija golih podloga BK7 i suprasila pomoću spektrofotometrijskih mjerenja.

4.2.3. Karakterizacija napravljenih uzoraka

4.2.3.1. Nb_2O_5 and SiO_2

Mjereni su refleksija i transmisija uzoraka na Suprasilu pod kutom od 0^o u pojasu valnih duljina 350-950 nm, svaka 2 nm, te su ta mjerenja korištena za optičku karakterizaciju. Rezultati sugeriraju da su prave brzine depozicije bile 0.675 nm/s za SiO_2 i 0.775 nm/s za Nb_2O_5.

4.2.3.2. Uzorak s deset perioda

Za karakterizaciju ovog uzorka mjereni su refleksija i transmisija uzoraka na Suprasilu pod kutom od 0^o u pojasu valnih duljina 350-950 nm, svaka 2 nm, ali također i *s* i *p* polarizacije pod kutom 45^o. U optičkoj karakterizaciji su korišteni indeksi loma čistih materijala dobiveni iz prethodno opisana dva uzorka. Uspoređeni su očekivani profil (dizajn), profil dobiven optičkom karakterizacijom i profil dobiven iz brzina naparavanja.

4.2.3.3. Hibridni AR uzorci

U svrhu optičke karakterizacije za početni dizajn su uzeti teorijski dizajni koje je trebalo napraviti, te su tako definirane početne vrijednosti parametara koji su zatim optimizirani. Svaki linearni gradijent u EBE i RFS uzorku bio je podijeljen u 8 podslojeva. Na taj je način potrebno optimizirati samo početni i završni volumni udio jednog materijala u segmentu, te debljinu segmenta. Na početku su granice debljine za RFS i IBS uzorak bile postavljene na 3% debljine dizajna. U slučaju EBE uzorka očekivana je veća greška zbog toga što su brzine naparavanja kontrolirane samo kvarcnim monitorom te zato što su te brzine bitno veće od onih za druge dvije tehnike depozicije. Zato su bile postavljene na 6%. Za čiste materijale su korišteni indeksi loma dobiveni iz mjerenja uzorka samo sa slojem danog materijala. U slijedećem koraku, kako bi se poboljšala prilagodba na izmjerene vrijednosti spektara, dozvoljena je optimizacija indeksa loma preko disperzijske relacije. U slučaju RFS uzorka spektrofotometrijska su mjerenja ukazala na prisustvo gubitaka ($R+T<1$). Budući da je apsorpcija kod materijala s visokim indeksom loma korištenim u ovoj tehnici bila zanemarena, uvedena je u optimizaciju preko disperzijske formule za koeficijent apsorpcije.

Kod EBE uzorka samo je debljina četvrtog segmenta više od 6% deblja od one u originalnom dizajnu. Srednja pogreška indeksa loma je 2.62%. Greške indeksa loma niobij pentoksida nema jer nije bilo dozvoljeno da se ovaj indeks optimizira. Kod RFS uzorka debljina drugog segmenta je 8% veća od one u originalnom dizajnu, a debljina sloja tantal pentoksida je 27% veća (11 nm). Debljine ostalih slojeva su unutar pogreške od 3%. Srednja greška indeksa loma je 2.17%. Greške indeksa loma tantal pentoksida također nema jer nije bilo dozvoljeno da se ovaj indeks optimizira. Kod IBS uzorka sve su greške debljina unutar 3%. Srednja greška indeksa loma je 1.09%.

4.2.3.4. Optička karakterizacija EBE hibridnog AR uzorka zasnovana na početnom profilu dobivenom iz SIMS-a

Volumni udio molekula Nb_2O_5 kroz debljinu hibridnog AR EBE uzorka je izračunat iz mjerenja dobivenih iz masene spektroskopije sekundarnih iona. Iz toga je onda pomoću prethodno dobivenih indeksa loma čistih materijala i LL modela napravljen profil indeksa loma zasnovan na SIMS-u, koji je uspoređen s profilom dobivenim iz optičke karakterizacije i originalnim dizajnom. Taj je profil također kasnije iskorišten kao početni dizajn za optičku karakterizaciju hibridnog AR EBE uzorka.

4.2.3.5. Usporedba rezultata optičke karakterizacije dobivenih sa i bez elipsometrije

Model hibridnog AR EBE uzorka dobiven optičkom karakterizacijom iz spektrometrijskih i elipsometrijskih mjerenja je uspoređen s novim, dobivenim korištenjem samo spektrofotometrijskih mjerenja. Da bi se bolje utvrdila kvaliteta jednog i drugog modela provedena je analiza statističke nesigurnosti optimizacijskih parametara.

4.2.3.6. Optička karakterizacija slojeva mješavine materijala

Uzorci su mjereni nakon depozicije (AD), nakon pet sati zagrijavanja na 500^{o}C, te nakon pet sati na 750^{o}C. Mjereni su refleksija i transmisija u području 350-950 nm, svakih 1 nm pod kutom 0^o, te su ti podatci iskorišteni za optičku karakterizaciju. Također je izmjereno i raspršenje svjetla na uzorcima koji su prošli termički tretman na 750^{o}C. Ovisnost indeksa loma o volumnom udjelu SiO_2 je uspoređena s LL modelom.

4.3. Struktura slojeva mješavine materijala

Strukturu slojeva mješavine materijala treba povezati s teorijom efektivnog sredstva koja najbolje opisuje njihove indekse loma kao funkciju omjera komponenata. Tako bi infracrvena spektroskopija trebala pokazati postoje li Si-O-Nb apsorpcijske u spektrima danih uzoraka vrpce koje ukazuju na stupanj miješanja faza. Ova tehnika bi pokazala i ovisnost intenziteta tih vrpci u ovisnosti o koncentraciji Nb_2O_5 i temperature zagrijavanja. Sa zagrijavanjem bi intenzitet Si-O-Si veza trebao slabiti i time ukazati na separaciju u faze.

Difrakcija X-zrakama također pokazuje nivo miješanja materijala. Ako nema difrakcijskih maksimuma znači da je materijal amorfan ili su kristalna zrna vrlo mala. U tom slučaju nije moguće

razlikovati faze. Mikroskopija atomskom silom može pokazati kristalna zrna eventualno formirana na površini uzoraka nakon zagrijavanja. Difraktogrami transmisijske elektronske mikroskopije također mogu potvrditi postojanje kristalizacije. Slike dobivene ovom metodom mogu pokazati strukturu sloja u smislu distribucije materijala i zrna opet ukazujući na separaciju faza, odnosno stupanj pomiješanosti materijala.

4.3.1. Dodatne mjerne tehnike

Mjerne tehnike korištene za određivanje strukture uzoraka slojeva mješavine materijala su infracrvena spektroskopija (FTIR), difrakcija X-zraka (XRD), mikroskopija atomskom silom (AFM) i transmisijska elektronska mikroskopija (TEM).

4.3.2. Rezultati dodatnih mjerenja

Uspoređeni su FTIR spektri uzoraka različitih koncentracija SiO_2 prije i nakon zagrijavanja na 500^{o}C i 750^{o}C u području 400-7000 cm^{-1}. Izračunate su i uspoređene površine ispod apsorpcijskog spektra molekula vode. Tretirani i netretirani uzorci su podvrgnuti XRD-i. Osim difraktograma, ovom tehnikom su dobivene i vrijednosti površinske hrapavosti te gustoća slojeva. Vrijednosti površinske hrapavosti su uspoređene s onima dobivenim iz AFM. Napravljene su TEM slike Nb_2O_5 uzorka, te smjesa s najvećom i najmanjom koncentracijom Nb_2O_5 prije i nakon zagrijavanja.

5. Diskusija

5.1. Antirefleksni dizajn

Osim dobrih optičkih svojstava i male debljine, kvaliteta hibridnih antirefleksnih dizajna je i u njihovoj jednostavnosti zbog malog broja točaka u kojima se mijenja gradijent indeksa loma. Početni i završni indeks loma svakog segmenta odgovara minimalnom i maksimalnom dopuštenom indeksu loma. Tako je potrebno dobro kontrolirati i osigurati ponovljivost samo tih krajnjih vrijednosti. Time se smanjuje vjerojatnost greške indeksa loma u točkama u kojima se mijenja gradijent.

Hibridni slojevi imaju jednako dobre ili čak nešto bolje spektralne i kutne karakteristike kao i klasični HL dizajn. Najlošije karakteristike za tanji dizajn se dobiju u slučaju pogreške kod povećanja indeksa u četvrtoj točki, povećane debljine zadnjeg sloja ili smanjenog indeksa loma pete točke.

5.2. Dizajn uskopojasnog reflektora

Klasični HL dizajn je postigao najnižu optičku gustoću u području refleksijskog maksimuma i stoga najbolju (najnižu) transmisiju na traženoj valnoj duljini od 532 nm. Istovremeno, ovaj dizajn ima i najmanji broj perioda te najmanju debljinu, što je posljedica veće razlike u indeksu loma korištenih materijala u odnosu na ostala dva dizajna. Hibridni dizajn je jednostavnijeg profila indeksa loma jer se sastoji od segmenata s linearnim gradijentima te segmenata konstantnog indeksa loma i stoga je manje zahtjevan za izradu od druga dva.

5.3. Napravljeni AR uzorci

Najmanje odstupanje od teorijskog spektra pokazuje IBS uzorak, a raspršivanje pomoću ionskog topa je tehnika koja ima najbolju ponovljivost u izradi uzoraka s gradijentom indeksa loma. Ove kvalitete potječu od stabilnosti procesa i sofisticirane *in-situ* širokopojasne optičke kontrole. Veliko odstupanje od teorijskih vrijednosti RFS uzorka i slaba ponovljivost može se pripisati spektralnom pomaku koji je uzrokovan sistematskom greškom u debljini sloja.

5.4. Optička karakterizacija napravljenih uzoraka

5.4.1. Nb_2O_5 i SiO_2

Optička karakterizacija čistih materijala je standardna procedura koja se koristi za kalibraciju kontrole debljine i određivanje optičkih konstanti. Pronađene optičke konstante su se kasnije koristile u optičkoj karakterizaciji uzorka s deset perioda i hibridnih uzoraka.

5.4.2. Uzorak s deset perioda

Model ovog uzorka dobiven optičkom karakterizacijom pokazuje samo malu grešku u debljini, ali je cijeli profil podignut prema većim vrijednostima indeksa loma što ukazuje na pomaknut omjer SiO_2 i Nb_2O_5 u korist ovog drugog.

5.4.3. Hibridni AR uzorci

Općenito, optička karakterizacija je dala jako dobro slaganje između simuliranih i eksperimentalnih podataka, te modele koji su blizu početnih dizajna. Razlike između modela i

početnih dizajna mogu se vrlo dobro objasniti odstupanjima u procesu depozicije. Ako se za optičku karakterizaciju koriste samo spektrofotometrijska mjerenja, dobiju se simulirani spektri koji su vrlo dobro prilagođeni na eksperimentalne R i T podatke, no profil indeksa loma ne daje elipsometrijske spektre u skladu s izmjerenima. Tek istovremeno korištenje spektrofotometrijskih i elipsometrijskih podataka daje smislene fizičke modele.

Optimizacija indeksa loma silicij dioksida EBE i RFS uzoraka, modeliranih Cauchyjevom disperzijskom formulom, omogućava značajno poboljšanje prilagodbe simuliranih podataka na eksperimentalne. Nasuprot tome, optimizacija materijala visokog indeksa loma (osim uvođenja apsorpcije za tantal pentoksid), ili silicij dioksida korištenog u IBS-u, nije dala poboljšanja, bez obzira na to koji je disperzijski model korišten. Razlika prema podatcima za indekse loma EBE i RFS uzoraka određenih iz sloja čistog silicij dioksida je 1% i 2% (veći postotak odgovara RFS uzorku). Ova razlika se može objasniti promjenom uvjeta naparavanja tokom procesa (različit tlak ili temperatura podloge), ili razlikom u rastu sloja kada se naparava na već postojeći sloj ili na golu podlogu. Ipak, za RFS uzorak najvjerojatnije objašnjenje bi bila kontaminacija s materijalom visokog indeksa loma. Pronađena razlika u indeksu loma silicij dioksida odgovara onečišćenju s 5% volumnih udjela tantal pentoksida. Porijeklo ovog onečišćenja bi mogla biti kontaminacija SiO_2 mete za vrijeme raspršivanja s Ta_2O_5 mete. Drugo moguće objašnjenje bi bilo kako slijedi: za vrijeme depozicije moraju biti uključena oba izvora, pa tako za vrijeme depozicije jednog materijala, izvor za raspršivanje drugog materijala je također uključen, iako je na vrlo niskoj snazi. Ovaj mod niske snage može biti nestabilan, ovisno o prethodnom procesu. Ako onečišćenje dolazi zbog ovog razloga, trebalo bi ga se moći izbjeći potpunim isključivanjem izvora za materijal koji se u danom trenutku ne raspršuje i stavljanjem zaštite preko mete koja se ne koristi.

Indeks loma sloja za koji je bilo pretpostavljeno da je čisti silicij dioksid kod IBS uzorka je također viši nego što bi se očekivalo za ovaj materijal. Slično kao u slučaju RFS SiO_2, razlog za ovo bi mogla biti kontaminacija s TiO_2. Tako dobiveni indeks loma odgovara sloju silicij dioksida s 4% volumnih udjela TiO_2. Za depoziciju tehnikom IBS bila je korištena posebno napravljena zonska meta. Neslaganje, tj. pogreška u ovisnosti indeksa loma o položaju ionskog snopa na meti može rezultirati u istovremenom raspršivanju oba materijala umjesto samo jednog. Ova pogreška može biti uzrokovana proširenjem ionskog snopa.

Debljine slojeva ostaju u očekivanim granicama 6% za EBE i 3% za RFS i IBS. Samo četvrti segment kod EBE modela i drugi i tantal pentoksid sloj kod RFS modela izlaze van ovih granica, ali

značajno poboljšavaju prilagodbu na eksperimentalne podatke. Linearni gradijenti kod modela EBE uzorka završavaju s indeksom loma višim nego što je u dizajnu. To upućuje da je brzina naparavanja niobij pentoksida bila veća od očekivane, tj. da nije bila dobro kalibrirana. Nasuprot tome, debljina sloja čistog Nb_2O_5 je kao u dizajnu jer je bila kontrolirana kvarcnim monitorom, a ne vremenom depozicije kao što je slučaj tokom naparavanja mješavine.

Osim Lorentz-Lorenz modela, za izračunavanje indeksa loma mješavine testirane su i druge teorije efektivnog sredstva. Tako se, na primjer, korištenjem Bruggemanove formule prilagodba simulacije na eksperimentalne vrijednosti pogoršala 50% u odnosu na prilagodbu gdje se koristila Lorentz-Lorenz formula, što ukazuje na to da je upravo ova zadnja dobar izbor za materijale koji su bili naparavani.

5.4.3. Uzorci mješavine materijala

Debljine dobivene optičkom karakterizacijom su veće od onih izračunatih iz brzine depozicije vjerojatno zbog poroznosti ili promjene uvjeta depozicije od jednog do drugog procesa. Indeksi loma rastu s temperaturom zagrijavanja. Ovakav trend debljine i indeksa loma ukazuje na povećanje gustoće sloja zagrijavanjem. Disperzijske krivulje AD uzoraka vrlo dobro slijede teorijske disperzijske krivulje LL modela. To potvrđuje opravdanost primjene ovog modela u optičkoj karakterizaciji. Pokazano je da LL model vrijedi i za AD i za termički tretirane uzorke, što je u suprotnosti s očekivanjem da se nakon zagrijavanja smjesa razdvaja u faze i njen indeks loma bi bolje trebao biti opisan Bruggemanovim ili linearnim modelom.

Postojanje Si-O-Nb vrpce u FTIR spektru ukazuje da su materijali pomiješani na atomskom nivou i da nema značajne separacije u faze. Smanjenje intenziteta ove vrpce i jačanje Si-O-Si vrpce sa zagrijavanjem ukazuje na separaciju u faze. Si-O-Nb veze ipak ostaju u spektru nekih uzoraka i nakon tretmana na 750^oC što znači da proces separacije nije dovršen.

XRD pokazuje da se kristalizacija pojavljuje zagrijavanjem uzoraka između 500^oC i 750^oC i to samo za uzorke s najvećom koncentracijom Nb_2O_5. TEM difraktogram potvrđuje strukturu utvrđenu XRD-om. Na visokorezolucijskoj TEM slici kristaliničnog uzorka se vidi da zrna različitih faza nisu dobro definirana, tj. da proces separacije nije završen, što je u skladu s rezultatima FTIR-a i može se dovesti u vezu s razlogom što smjese i nakon zagrijavanja slijede LL model. Da bi Bruggemanova i Maxwell-Garnettova teorija vrijedile u vidljivom dijelu spektra te do srednje infracrvenog, faze trebaju biti veličine 3-30 nm, a to prema analizi, u ovim uzorcima nije postignuto.

6. Zaključci

Antirefleksni hibridni slojevi predstavljeni u ovom radu su sinteza dielektričnih slojeva s konstantnim indeksom loma i s gradijentom indeksa loma. Utvrđeno je da takvi slojevi pokazuju odlične optičke karakteristike u širokom rasponu kutova upada svjetlosti. U usporedbi s klasičnim dizajnom, ovi sustavi daju jednako dobra ili čak bolja optička svojstva. Hibridni dizajni mogu biti praktički izrađeni koevaporacijom materijala visokog i niskog indeksa loma. Mala debljina, mali broj točaka u kojima se mijenja gradijent, segmenti koji počinju i završavaju uvijek u istim vrijednostima indeksa loma i odsustvo indeksa loma koji bi trebao biti blizu indeksa loma okoline (zraka) čine ove dizajne izvedivima i prikladnima za antirefleksne slojeve koji moraju imati dobre karakteristike u širokom pojasu kutova upada.

Usporedbom klasičnog HL, naboranog i hibridnog dizajna uskopojasnog reflektora, optimiziranih da zadovoljavaju iste zahtjeve, pokazano je da dizajni s gradijentom indeksa loma trebaju veću debljinu da bi imali jednako dobra svojstva. Ipak, njihova je prednost u tome što bolje potiskuju oscilacije koje se javljaju uz refleksijski maksimum, što se osobito odnosi na naborani dizajn. Hibridni dizajn ima jednostavniji profil indeksa loma u odnosu na naborani i jednostavnije ga je prilagoditi sustavu za depoziciju. Pokazano je da je za postavljene zahtjeve klasični dizajn bolji od druga dva. U stvari, iz principa maksimuma se zaključuje da je u slučaju okomitog kuta upada za optimalni dizajn dovoljno koristiti samo dva materijala sa što većom razlikom indeksa loma. Prema tome, bez obzira na to što su u dizajnima korišteni različiti materijali, nije iznenađujuće da HL dizajn daje najbolje rezultate. U slučaju upada pod nekim drugim kutom ovaj zaključak više ne vrijedi i tada dizajni s gradijentom indeksa loma mogu pokazati jednaka ili bolja svojstva, kao što je pokazano u slučaju antirefleksnih slojeva.

Pokazana je uspješna izrada hibridnih antirefleksnih slojeva. Uzorci su izrađeni različitim tehnikama i uspoređena je njihova reproducibilnost. Najbolje uzorke i reproducibilnost je dala IBS tehnika, pokazujući najveću stabilnost i najbolju kontrolu procesa. Jako dobri rezultati su dobiveni i RFS tehnikom. Tehnike rasprašivanja, budući da imaju male brzine depozicije, omogućavaju stabilnu i preciznu depoziciju mješavina. Antirefleksni slojevi dobiveni EBE tehnikom, koja dozvoljava znatno veće brzine depozicije, također pokazuju dobra optička svojstva. Iako su EBE slojevi, očekivano, bili slabiji zbog poteškoća u kontroli procesa zbog velike brzine depozicije,

vrijedi uložiti napora i vremena u poboljšanje ove tehnike jer upravo zbog brzine naparavanja treba najmanje vremena za izradu sloja, a osim toga, ovo je i najčešće korištena tehnika.

Optička karakterizacija je uspješno primijenjena za analizu hibridnih antirefleksnih slojeva. Pokazano je da je kombinacija spektrofotometrijskih i elipsometrijskih mjerenja pod različitim kutovima pravi izbor za karakterizaciju sustava kao što su antirefleksni slojevi, gdje u optičkom spektru nema detalja koji bi pomogli u karakterizaciji. Hibridni dizajni su reprezentirani odgovarajućim modelima čiji su broj i vrijednosti parametara maksimalno kontrolirani u procesu optimizacije kako bi se dobilo što jednostavnije i realnije moguće rješenje. U proračunima indeksa loma mješavina potvrđena je prikladnost Lorentz-Lorenz modela za dane materijale.

Dobiveni modeli su bili od koristi za određivanje pogrešaka u procesu depozicije svake od tehnika, a to je i bio glavni cilj optičke karakterizacije. Tako je utvrđeno da su debljine kontrolirane uglavnom s očekivanom točnošću. Glavni problem u depoziciji proučavanih uzoraka je kontrola indeksa loma boljom kalibracijom brzina depozicije i izbjegavanjem neželjene kodepozicije oba materijala kada se treba naparavati samo jedan od njih.

Pokazano je da SIMS nije dovoljno dobra metoda za određivanje profila indeksa loma danih uzoraka. Ipak, početni profil zasnovan na SIMS-u daje nakon optičke karakterizacije model vrlo blizu onome dobivenom iz dizajna kao početnog modela. Usporedbom modela dobivenih karakterizacijom koja uključuje samo spektrometrijska ili također i elipsometrijska mjerenja, nakon analize statističkih nesigurnosti, utvrđeno je da je model dobiven uz pomoć oba tipa mjerenja znatno pouzdaniji. To potvrđuje opravdanost uvođenja elipsometrijskih mjerenja u optičku karakterizaciju.

Rezultati optičke karakterizacije slojeva mješavina materijala pokazuju da indeksi loma smjesa Nb_2O_5 i SiO_2 slijede LL model i prije i nakon zagrijavanja. Iako je utvrđena separacija komponenata u faze nakon zagrijavana, taj proces nije dovršen i granica veličine faza potrebne da počne vrijediti neka druga teorija efektivnog sredstva nije zadovoljena. Zbog toga je potrebno ugraditi LL model u program za dizajn naboranih slojeva kako bi se olakšao prijelaz s dizajna na parametre u procesu depozicije koje treba kontrolirati kako bi se dobio željeni profil indeksa loma.

1. Introduction

1.1. General

Optical thin film coatings having refractive index that is continuously changing through the depth of the layer are known as gradient index films or inhomogeneous films. If the change of the refractive index is also periodic with coating thickness the coating is called rugate. Rugate structures, as well as gradient refractive index films in general, attract a lot of interest in the field of optical thin films. Gradient index systems may provide advantages in both, optical performance and mechanical properties in comparison to conventional HL-stack designs with alternating layers of materials of high and low refractive index. A lot of excellent theoretical work on optical behaviour of rugates and gradient index films has been done during the last decades[1,2,3]. Gradient index coatings are promising due to their superior optical properties, e.g. broadband antireflection. Rugates have been shown to be especially interesting for design of notch filters. Additional profits that can be expected from inhomogeneous coatings are low stress, tribological resistance[4,5,6] and higher laser induced damage threshold[7] than classical multilayer stacks.

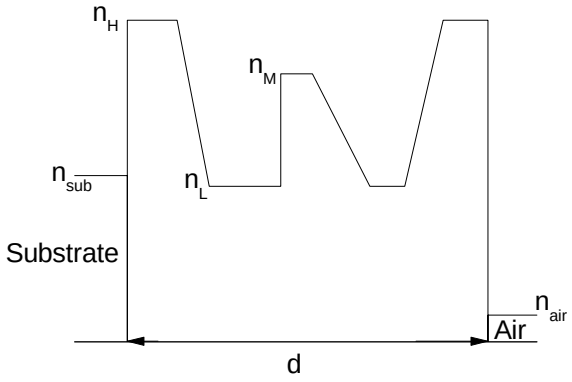

Figure 1. General refractive index profile of a hybrid coating of thickness d. Here, n_H and n_L are the refractive indices given by pure materials (pure in sense that they were not mixtures) and n_M stands for any achievable intermediate refractive index in the profile. Substrate's refractive index is denoted by n_{sub}, while n_{air} is the ambient one.

Hybrid coatings present an alternative approach to designs, combining homogeneous and linearly graded index layers. Figure 1 presents a general refractive index profile of a hybrid coating. This approach merges the advantages of gradient index layers, e.g. reduced scatter losses and thermal

stress due to the absence of abrupt changes of refractive indices at interfaces, and the capability of fabrication inhomogeneous coatings using industrial deposition plants.

Hybrid antireflective (AR) and notch filters have been designed in this work and their theoretical optical performance compared with the one of classical designs. The hybrid antireflective coating has been deposited by different deposition techniques in a round robin experiment where the composition of two materials mixture has been controlled. The resulting optical performances of thus obtained samples were compared. Optical characterisation of the deposited samples suggested improvements that should be done in the deposition processes. The mixture model used in characterisation has been experimentally verified and related to the structure of the mixture.

In the next sections of this Chapter it is given an overview of design and optical characterisation strategies of classical and gradient index structures, with highlighted common features, differences and problems in approach to the one and the other kind of coatings. Then, the main subject of the work is presented. In addition, the properties of materials used for design and preparation of the samples are described.

1.1.1. Thin film optical design

There are two general approaches to obtain classical thin film design, i.e. the combination of layers of appropriate thickness, refractive index and their sequence that will have the required optical properties. The first approach is to start with an initial design that is based on previous theoretical knowledge about the structure of different interferential filters[8,9]. The thicknesses of layers in the initial designs are then refined according to the required specifications to minimise the discrepancies between targeted optical properties and optical properties of the design. The other approach is so called “push button” when the initial design is just a single layer of one material and into which layers of the other material are added gradually, followed by optimisation[10]. The best known method of introducing new layers is needle method[11].

Contrary to the classical designs, there is no commercially available software for the design of rugates at the moment. In the design of gradient index and hybrid structures the same materials as in generation of HL stacks are used, but also intermediate values of indices are allowed. In this way smooth transition from one value to another is enabled. Therefore, the additional parameters in optimisation process are refractive indices in extreme points and the gradients. This last parameter must be well controlled because high gradients might not be practically feasible. The other reason is avoiding maximum principle[12], i.e. that for oblique incidence of light designs consisting of only two

materials of highest index contrast (HL stacks) are preferable. The mathematical apparatus for calculation of optical properties of classical multilayers and rugates is basically the same since parts with gradients are approximated with sequence of sublayers of constant refractive index[13].

Adjacent layers of high and low refractive index in classical design correspond roughly to the appropriate single gradient in rugates. In this way it is possible to use a classical design where abrupt changes of refractive index are replaced by gradients as a rugate initial design. It is also possible to use the other approach described for HL stacks, with a layer of constant refractive index with the points defined along the thickness as possible beginnings and ends of gradients. The third way of creating the initial design, that is specific to rugates, is based on Fourier transform relation between a spectral function $Q(\lambda)$ and the refractive index profile. The spectral function is, in fact, a function of the desired optical performance of the final system. One of the problems of this method is that Q-function is not known exactly, but only its approximate values[3,14,15].

Apart from the previously mentioned advantages that are expected from gradient index coatings, regarding lower scattering and mechanical wear resistance than in HL stacks, the optical properties of corresponding classical and gradient index designs should be compared to enable better evaluation of different coatings and make the choice for the required application easier. Also, relating design and the optical performance of the sample that will be deposited, care should be taken how to calculate the optical constants of the material mixture that is used in the design and later deposited. The optical constants for each mixture layer can be calculated using different mixing models that relate the optical constants of the mixture of given composition with the optical constants of the pure materials. Several models, known as effective medium theories, have been proposed: Bruggeman[16], Lorentz-Lorenz[17], Maxwell Garnett[18] or a linear combination of refractive indices[19]. For example, in the case of TiO_2-SiO_2 mixture layers it has been shown[20,21], that Lorentz-Lorenz model is more appropriate then the Bruggeman, although not all the studies are in accordance[22].

Gradient index coatings and optical filters are a challenge for fabrication. Only few of the designs could be deposited, which is often caused by practical problems, e.g. preparing materials with the desired refractive index values. Each refractive index value in the design can be achieved by an appropriate mixture of materials. Besides sol-gel methods[23,24], there are two more standard techniques for obtaining gradient layers with varying composition and refractive index in growth direction. The first approach is based on changing the composition of ternary compounds during growth of the layer by controlling the composition of the reactive gas[25]. The second technique involves co-evaporation of

two materials where the ratio of particles of the two co-deposited materials condensing at a substrate is varied[26].

1.1.2. Optical characterisation of thin film coatings

The deposited samples are analysed in order to check how well their performance meets the requirements. Optical characterisation methods are very helpful in analysis of thin films. From optical measurements it is possible to determine refractive index, thickness of the coating and variation of refractive index through the depth of the coating (i.e. inhomogeneity). Optical characterisation can be applied to both, layer of only one material and multilayer stacks. Same as in design, if the layer is inhomogeneous it can be represented as a multilayer stack by dividing the layer into homogeneous sublayers of different refractive indices.

Numerous methods for optical characterisation of thin films have been developed. Similar to the design, most of these methods start from the modelling of optical behaviour of the sample through a set of parameters which represent some kind of initial approximation. The optimal values of these parameters are found by minimisation of a merit function that quantifies the agreement between experimental measurements and the data simulated from the model. The optimisation procedure is normally carried out using numerical techniques. Some of these methods are based on analysis of spectrophotometric measurements[27], i. e. reflectance ($R(\lambda)$) and transmittance ($T(\lambda)$) as function of the wavelength (λ) in a certain spectral range, and some on analysis of ellipsometric Δ and Ψ angles[28,29]. The combination of the two sets of measurements has been also applied[30,31,32]. A typical problem of these methods is the multiplicity of solutions, i.e. the existence of different combination of parameters values that minimise the merit function. This is especially important in inhomogeneous coatings, where mathematical description of the refractive index profile may involve a large set of parameters. To avoid this problem it is useful to have more measurements of the same sample, like measurements with different angles of incidence, to combine spectrophotometry and spectroscopic ellipsometry, or to combine these optical with other, non-optical, methods[33]. This leads to a significant reduction of the solution multiplicity, thus facilitating the selection of the physically meaningful one. Effective medium theories appropriate to the material mixture deposited by the given technique should be applied.

An important benefit from optical characterisation, i.e. finding the model of refractive index profile of deposited sample, would be if from the comparison with the targeted profile that was aimed to be deposited it would be possible to detect the errors and critical points in the process of deposition and propose improvements to the manufacturing procedures. To perform a good optical

characterisation and obtain a realistic model it is crucial to know how many measurements should be taken into account and what benefits of the additional measurements are. It is also important to consider the possibility that non-optical methods for depth profiling of the samples, like secondary ion mass spectrometry or electron energy loss spectroscopy, could be sufficient for definition of refractive index profile of the sample or at least give an initial design close enough to the real profile able to be refined into the reliable and realistic solution.

1.1.3. The research done in this thesis

The main subject of this work is design and optical characterisation of hybrid thin film systems. The hybrid antireflective[34] and notch[35] designs are synthesised utilising the numerical optimisation software recently developed by Tikhonravov et al[19,36]. They are compared with classical HL designs prepared with the same requirements and restrictions. Antireflective designs are compared specially in respect to the quality of suppression of reflectance at higher angles of incidence and sensitivity to errors in deposition[37]. Besides with the classical, the hybrid notch design is compared also with the rugate, regarding total thickness of the layers and optical density.

Antireflective design has been chosen for deposition since its refractive index profile is simpler and therefore easier for both, manufacturing and analysis. Also, it is expected that it will be applied in real optomechanical systems. Hybrid antireflective design is refined and adapted for deposition by different co-deposition methods, taking into account characteristics and limitations of the each method. It is shown that all the refined designs are of the same quality and physical and optical characteristics. Hybrid antireflective coatings have been deposited and their optical performance compared[38]. Thus, comparison of deposition techniques was enabled. Optical characterisation of the samples has been performed and origin of discrepancies between the designs and the models obtained by characterisation has been related with errors in deposition processes[39]. The model obtained using only reflectance and transmittance measurements and including ellipsometric measurements, same as the one obtained from secondary ion mass spectrometry based initial design have been compared.

Finally, the appropriateness of Lorentz-Lorenz model for calculation of refractive index of mixtures in optical characterisation, and therefore the necessity to introduce it into designing, has been tested. The result has been checked experimentally by deposition of mixture layers of constant composition throughout the layer and comparing their refractive indices to the theoretical values of different effective medium theories. Appropriateness of Lorentz-Lorenz model has been related to the structure of the mixtures by additional measurements.

In Chapter 2 theoretical concepts regarding multilayer optics are given, together with an overview of optical characterisation techniques and the numerical software for design and characterisation of the coatings. Chapter 3 deals with antireflective and notch hybrid designs and comparison of their theoretical optical performance with the performance of corresponding classical designs. Chapter 4 is devoted to the experimental part of the work including description of properties of deposition techniques and deposited samples, spectroscopic optical characterisation and results of additional measurements done at mixture samples in order to asses their structure. Chapter 5 follows with discussion and Chapter 6 with conclusions.

1.2. Materials

Different materials are used for deposition of thin film coatings depending on the optical range important for the application, mechanical and aging properties and environmental stability. In this work visible range (400-700 nm) is of interest, so silica (SiO_2) was used as low index material and niobia (Nb_2O_5) as high index material. In examples for comparison of designed and deposited AR hybrid coatings, also titania (TiO_2) and tantala (Ta_2O_5) were used. All of the mentioned materials have to be deposited in reactive oxygen atmosphere to prevent reduction and formation of sub-oxides that contribute to undesirable absorption in the optical range.

SiO_2 is a favourable low index material with refractive index 1.45-1.50 at 500 nm. Although it is not the material with the lowest refractive index, that is MgF_2 with refractive index approximately 1.38 at 500 nm, it can be deposited with less porosity and scattering than MgF_2, having good adhesion to the substrate and good mechanical durability. It is appropriate for applications in UV and visible range, i.e. for range 250-1100 nm. Films are amorphous, having compressive stress. Crystallisation occurs upon thermal treatment at temperatures above 1100^{o}C. When evaporated with electron beam gun the amount of material deposited on a monitor chip or control quartz crystal doesn't have the expected reproducible ratio to that received at other positions in the chamber. This is explained by erratic melting/sublimation of silica in both, granular and solid disc forms[9]. It is also the reason why it is difficult to obtain stable rate of deposition for SiO_2. The characteristic bonds of fused silica detectable by infrared spectroscopy are at[40] 1218 cm^{-1}, 1080 cm^{-1}, 804 cm^{-1} and 461 cm^{-1}.

Niobia has high refractive index approximately 2.25 at 500 nm, close to TiO_2. Among sputtered materials Nb_2O_5 films have the lowest stress[9]. It is suitable for coatings for near UV (400 nm) to IR (8500 nm), with very little absorption if the film is stoichiometric. Films do not crystallise easily and are mainly amorphous as deposited. Coatings are wear resistant and fairly hard. For pure Nb_2O_5 onset

of crystallisation is between 400°C and 500°C[21,41,42,43] resulting in hexagonal structure (Powder Diffraction File[44]: card No. 28-0317) while at temperature between 600°C and 700°C orhtorhombic structure (Powder Diffraction File[44]: card No. 30-0873 or 27-1003) appears[43]. Characteristic features of infrared spectra of pure Nb_2O_5 are absorption band around 600 cm^{-1} corresponding to Nb-O bonds of slightly distorted NbO_6 octahedra[43]. This band increases with increase of temperature, splits and shifts to lower frequency, suggesting the existence of different Nb-O species or in equivalent Nb-O groups. Band at 850 cm^{-1} corresponds to Nb-O-Nb stretching[21].

There are studies in literature reporting that SiO_2 stabilises amorphous Nb_2O_5[45]. It is known that how Nb_2O_5 crystallisation takes place can be different according to the interactions between the compounds. Considering this fact, the structure of pure Nb_2O_5 is very different than when it is a system with other species. The interaction between Nb_2O_5 and other materials affect its stability and, consequently, the final structure. When a strong interaction is established via Si-O-Nb linkages, the superficial Nb_2O_5 presents only the amorphous phase after thermal treatment at 500°C for 2 hours. Even after 48 hours of treatment at 1000°C only weak peaks of diffraction were attributed to the hexagonal phase. The interactions between Nb_2O_5 and SiO_2 are responsible for Nb_2O_5 stabilisation, as they reduce Nb_2O_5 mobility thus preventing crystallisation. It has been shown that a strong interaction between SiO_2-Nb_2O_5 is established during the sol-gel process, i.e. it involves the formation of Si-O-Nb bonds. This conclusion was made based on the observation of infrared band between 930 cm^{-1} and 920 cm^{-1} that disappears with agglomeration process after treatment at high temperature.

Due to its high refractive index of 1.9-2.6 at 500 nm and good mechanical properties TiO_2 is the most widely used material in optical coatings for the visible range. Sub-oxide free films start to absorb below 400 nm and therefore the material is not appropriate for UV coatings. In combination with SiO_2, due to mutual compensation of stress, it is possible to obtain multilayers of high number of layers having excellent durability and stability. The films are crystalline with rutile or anatase phase or their mixture. Refractive index varies a lot depending on deposition technique and conditions, especially on pressure and rate of deposition[9].

Stoichiometric Ta_2O_5 films have high refractive indices of 1.9-2.0 at 500 nm and low absorption. Therefore, they are appropriate for coatings in near UV to IR, i.e. 350-8000 nm. A particular advantage over TiO_2 layers for near IR laser and band pass coatings is the absence of absorption above 900 nm. The films generally grow with crystalline structure. Post-deposition

annealing in air can raise the refractive index and decrease absorption and stress in electron beam evaporated and resistance-heated deposition coatings[9].

To enable extensive analysis of the samples, each sample was deposited onto different kinds of substrates: BK7 glass, Suprasil and intrinsic (non-doped) crystalline silicon wafer chunks.

BK7 is widely used borosilicate glass of optical quality, meaning that it has homogeneous and well controlled optical properties. Samples deposited on this substrate were used for optical characterisation by means of spectrophotometry and spectroscopic ellipsometry, in the range of 380 to 1100 nm. BK7 glass has significant absorption at wavelengths below 380 nm.

To study and analyse absorption of materials and samples of interest, non absorbing substrates in the required range are necessary. Therefore, samples prepared at Suprasil substrates were used. Suprasil is a commercial name for a high purity synthetic quartz glass made by flame hydrolysis of silicon tetrachloride. Since Suprasil has metallic impurity content less than 8 ppm, the UV transmission is superior to that of BK7. It starts absorbing at wavelengths below 200 nm. Suprasil exhibits high strength and low thermal expansion. Its softening point is rather high 1120°C, compared to that of BK7 which is 550°C. Therefore, the samples deposited at Suprasil were used also in annealing experiments.

Finally, both BK7 and Suprasil are opaque in IR region above 2700 nm. Silicon is a material that is transparent in the range of 50 μm to more than 100 μm, so for analysis in IR region were used samples deposited on silicon.

2. Theory, techniques for optical characterisation and numerical software

2.1. Theory

In this Section briefly will be introduced theoretical aspects of propagation of light through matter in order to understand the optical behaviour of the materials and samples that have been used in this work. Optical constants (complex dielectric function and refractive index), that are parameters characterizing the interaction between light and medium, will be defined. Their relationship with microscopic properties (atomic polarisability) and their dependence on frequency of electromagnetic radiation will be explained. Then, dispersion models will be introduced as the equations that mathematically relate the dependence of the optical constants with the frequency. The two dispersion models used to characterise materials used in this work will be derived: Cauchy model for dispersion of refractive index for low absorption combined with zero or exponential absorption that has been used for SiO_2, TiO_2 and Ta_2O_5, and Tauc-Lorentz that takes into account the dispersion of optical constants near the band gap and is applied to Nb_2O_5.

The propagation of light through multilayer structures will also be described. In these structures the beam reflected and transmitted at each interface between two media recombine and contributions from all the interfaces should be taken into account. This results in the typical interferential characteristics of multilayers that can be designed with targeted performances. The method of characteristic matrices will be introduced as a way to calculate optical properties of the multilayer structure.

As mentioned in Introduction, most of the layers in this work are material mixtures. However, in the classical multilayer theory it is assumed that every layer consists of only one material. Effective medium theories are presented as a way to define optical constants of the mixture of materials in terms of optical constants of the components of the mixture. Four of these theories, differing in the assumed model of the structure will be presented in this Section.

2.1.1. Optical constants and dispersion models

2.1.1.1. Optical constants

Propagation of the electromagnetic radiation through non-magnetic and electrically neutral medium is described by wave equation that follows from Maxwell equations:

Equation 1 $$\nabla^2\vec{\mathcal{E}} = \varepsilon\mu_o \frac{\partial^2\vec{\mathcal{E}}}{\partial t^2} + \sigma\mu_o \frac{\partial\vec{\mathcal{E}}}{\partial t},$$

where $\vec{\mathcal{E}}$ is vector of electric field, ε dielectric constant (permittivity) of the medium ($\varepsilon=\varepsilon_r\varepsilon_o$, ε_r- relative permittivity, ε_o – permittivity of vacuum), μ_o permeability of vacuum and σ specific conductivity of the medium. The solutions of this equation are oscillatory functions of electric field of frequency ω that for plane waves propagating in direction of z axes, have the following form:

Equation 2 $$\vec{\mathcal{E}} = \vec{\mathcal{E}}_o e^{-i\omega\left(t - z\sqrt{\varepsilon\mu_o\left(1+\frac{i\sigma}{\varepsilon\omega}\right)}\right)}.$$

If dielectric complex function ε^* is introduced

Equation 3 $$\varepsilon^* = \varepsilon_r + \frac{i\sigma}{\omega\varepsilon_o} = \varepsilon_1 + i\varepsilon_2$$

and $1/\sqrt{\mu_o\varepsilon_o}$ is replaced by c (velocity of light in vacuum), the solution of wave equation can be written in a more compact way as

Equation 4 $$\vec{\mathcal{E}} = \vec{\mathcal{E}}_o e^{i\frac{\omega}{c}\sqrt{\varepsilon^*}z - i\omega t} = \vec{\mathcal{E}}_o e^{i\frac{\omega}{c}Nz - i\omega t},$$

where N is complex refractive index defined as $N = \sqrt{\varepsilon^*} = n + ik$. Real and imaginary parts of ε^* and N are called optical constants and are related by

Equation 5 $$\varepsilon_1 = n^2 - k^2$$
$$\varepsilon_2 = 2nk$$

Real part of the complex refractive index n, known simply as refractive index, determines phase velocity of the wave in medium, while imaginary part is known as extinction coefficient and quantifies attenuation of the field propagating through the medium. In a transparent medium $k = 0$. In absorbing media intensity of light I, defined as time averaged Pointing vector over long period of time, attenuates exponentially as Beer-Lambert law:

Equation 6 $$I = \left\langle\left|\vec{S}\right|\right\rangle = \frac{1}{\mu_o}\left\langle\left|\vec{\mathcal{E}}\times\vec{\mathcal{H}}\right|\right\rangle = I_o e^{-\alpha z}.$$

$\vec{\mathcal{H}}$ is magnetic field, I_o intensity in the origin $z = 0$ and $\alpha = 2\omega k/c$ is absorption coefficient.

In the case of harmonic fields Kramers-Kronig relation[46] holds, that relates real and imaginary part of the complex refractive index:

Equation 7

$$n(\omega) = 1 + \frac{2}{\pi} P \int_0^{\infty} \frac{\omega' k(\omega')}{\omega'^2 - \omega^2} d\omega'$$

$$k(\omega) = -\frac{2\omega}{\pi} P \int_0^{\infty} \frac{n(\omega') - 1}{\omega'^2 - \omega^2} d\omega',$$

where *P* denotes principal (Cauchy) integral. Kramers-Kroning analysis consists of the calculation of the real (imaginary) part of refractive index when the imaginary (real) part is known over the entire frequency spectrum. Kramers-Kroning relations show that optical constants depend on the frequency of the interacting electric field.

2.1.1.2. Relation of optical constants with microscopic world

The interaction of light with matter can be described in terms of macroscopic and microscopic interactions. Macroscopically, the electric polarisation of a medium can be quantified with the electric polarisation vector $\vec{\mathcal{P}}$ that is linearly related to the external field $\vec{E}$ and the electric susceptibility χ:

Equation 8

$$\vec{\mathcal{P}} = \varepsilon_o \chi \vec{E},$$

$$\chi = \varepsilon_r - 1.$$

In microscopic description, the polarisation can be defined as the sum of $\mathcal{N}$ dipole moments $\vec{p}$ per volume unit, where each of the moments is linearly related to the local electric field $\vec{E}$', that is effective electric field affecting molecules, with α' representing the local microscopic polarisability:

Equation 9

$$\vec{\mathcal{P}} = \mathcal{N}\vec{p} = \mathcal{N}\alpha' \vec{E}'.$$

The local electric field $\vec{E}$' differs from the externally applied $\vec{E}$ (the observed electric field) because of the atomic and molecular dipole contributions to the field:

Equation 10

$$\vec{E}' = \vec{E} + \frac{\vec{\mathcal{P}}}{3\varepsilon_o}.$$

From the two expressions for $\vec{\mathcal{P}}$, Equation 8 and Equation 9, and taking into account Equation 10 relation between atomic (α') and macroscopic (ε) scale can be written:

Equation 11

$$\varepsilon_r - 1 = \frac{3\mathcal{N}\alpha'}{3\varepsilon_o - \mathcal{N}\alpha'}.$$

2.1.1.3. Dispersion models

The phenomenon of dispersion is the change of dielectric constant or complex refractive index with frequency. A simple way to approach to dispersion is to consider classical description of motion of an electron of mass m_o bounded to an atom by an elastic restoring force $\vec{F} = -q\vec{r}, q = m_o\omega_o^2$ in presence of an electric field of amplitude $\mathcal{E}_o'$ oscillating with frequency ω, where $\vec{r}$ is the displacement of electron from its equilibrium position:

Equation 12 $$m_o\ddot{\vec{r}} + m_o\gamma\dot{\vec{r}} + q\vec{r} = -e\vec{\mathcal{E}}'.$$

The solution is:

Equation 13 $$r = -\frac{e\mathcal{E}_o'}{m_o}\frac{1}{\omega_o^2 - \omega^2 - i\gamma\omega},$$

where $\omega_o = \sqrt{q/m_o}$ is the resonance frequency and γ is the damping coefficient. If polarisation is considered in terms of sum of dipolar moment $\vec{p} = e\vec{r}$, $\vec{\mathcal{P}} = \mathcal{N}e\vec{r}$, combining Equation 13 with Equation 11 and taking into account Equation 9, Clausius-Mosotti relation for Lorentz oscillator model of atomic dipoles[46] can be expressed as:

Equation 14 $$\frac{\varepsilon_r - 1}{\varepsilon_r + 2} = \frac{\mathcal{N}e^2}{3m_o\varepsilon_o}\frac{1}{\omega_o^2 - \omega^2 - i\gamma\omega}$$

that for several resonance frequencies can be written as summation of contributions of different oscillators with strength f_k:

Equation 15 $$\frac{\varepsilon_r - 1}{\varepsilon_r + 2} = \frac{\mathcal{N}e^2}{3m_o\varepsilon_o}\sum_k \frac{f_k}{\omega_k^2 - \omega^2 - i\gamma\omega}.$$

In the case of dielectric material $\varepsilon_r \cong n^2$ and with $\gamma\omega \to 0$ the terms in Equation 15 can be rearranged to obtain Sellmeier's formula for refractive index dispersion:

Equation 16 $$n^2 = \varepsilon_\infty + \sum_k \frac{A_k}{\omega_k^2 - \omega^2} = \varepsilon_\infty + \sum_k \frac{B_k\lambda^2}{\lambda^2 - \lambda_k^2}$$

with $\lambda_k = \frac{2\pi c}{\omega_k}$ and $B_k = \frac{\mathcal{N}e^2 f_k \lambda_k^2}{4\pi^2\varepsilon_o m_o c^2}$. ε_∞ is a contribution of polarisation from other mechanisms to the complex dielectric function, and λ is wavelength of light.

Cauchy model of dispersion is approximation of Sellmeier's but for only one resonance. It is obtained by expanding Sellmeier's formula into power series with $\lambda_1/\lambda << 1$:

Equation 17 $$n(\lambda) = A + \frac{B}{\lambda^2} + \frac{C}{\lambda^4},$$

where the correspondence among the parameters is given by:

Equation 18 $$A = \sqrt{\varepsilon_\infty + A_1}$$

$$B = \frac{A_1 \lambda_1^2}{2\sqrt{\varepsilon_\infty + A_1}}$$

$$C = \frac{A_1(4\varepsilon_\infty + 3A_1)\lambda_1^4}{8(\varepsilon_\infty + A_1)^{3/2}}.$$

The Sellmeier and Cauchy models are valid for frequencies well below electronic transitions. In this range the absorption coefficient is very low and usually can be neglected. However, absorption phenomena in solids that are related to defects, impurities or excitons, for example[47], can appear even for frequencies below electronic transitions, i.e. below the band gap. In this case the phenomenological model for dispersion of imaginary part of refractive index that is combined with Sellmeier and Cauchy models is the one proposed by Urbach. So, for most of the materials and frequencies lower than the gap, absorption coefficient follows the law:

Equation 19 $$\frac{d(\log\alpha)}{d\omega} = -\frac{1}{k_a T}.$$

Here T is temperature and k_a is phenomenological constant. Based on Equation 19, the following phenomenological expression for optical materials has been widely used:

Equation 20 $$k(\lambda) = k_A e^{k_B/\lambda},$$

where k_A and k_B are parameters of the model.

Combination of Cauchy (Sellmeier) and exponential model (Equation 20) is appropriate for absorbing materials in the range of energies $E = h\omega/2\pi$, h is Planck constant, that is far from the band gap and where absorption is small. If the range around band gap is studied, more realistic model is Tauc-Lorentz one. G. E. Jellison and F. A. Modine[48,49] have proposed parameterisation of optical constants of amorphous materials that is based on the work of Tauc[50] who proposed another relation for the imaginary part of the dielectric function for amorphous materials:

Equation 21

$$\varepsilon_2(E) = A_T \frac{(E-E_g)^2}{E^2} \quad E > E_g$$
$$= 0 \qquad\qquad E < E_g$$

Here A_T is a constant associated to the transition probability and E_g is energy of optical band gap. Tauc-Lorentz model is based on combination of Equation 21 with classical Lorentz oscillator, that although has been derived for a classical model of atom is valid for the dispersion of optical constants for frequencies around electronic transitions in atoms and solids. In this way both are taken into account: broadening associated to a single electron transition (Lorentz) and density of joint states (Tauc). Finally, complex dielectric function is given by:

Equation 22

$$\varepsilon_2(E) = \left[\frac{AE_0C\left(E-E_g\right)^2}{\left(E^2-E_0^2\right)^2 + C^2E^2} \frac{1}{E} \right] \quad E > E_g$$
$$= 0 \qquad\qquad E < E_g$$

The real part is obtained from Kramers-Kronig relations:

Equation 23

$$\varepsilon_1(E) = \varepsilon_\infty + \frac{AC}{\pi\zeta^4} \frac{a_{\ln}}{2\alpha E_0} \ln\left(\frac{E_0^2 + E_g^2 + \alpha E_g}{E_0^2 + E_g^2 - \alpha E_g} \right)$$
$$- \frac{A}{\pi\zeta^4} \frac{a_{a\tan}}{E_0} \left(\pi - \arctan\frac{2E_g + \alpha}{C} + \arctan\frac{-2E_g + \alpha}{C} \right)$$
$$+ 2\frac{AE_0}{\pi\zeta^4\alpha} \cdot E_g(E^2 - \gamma^2) \cdot \left[\pi + 2 \cdot \arctan\left(2\frac{\gamma^2 - E_g^2}{\alpha C} \right) \right]$$
$$- \frac{AE_0C}{\pi\zeta^4} \frac{E^2 + E_g^2}{E} \ln\frac{\left|E - E_g\right|}{E + E_g} + 2\frac{AE_0C}{\pi\zeta^4} E_g \ln\frac{\left|E - E_g\right|\left(E + E_g\right)}{\sqrt{\left(E_0^2 - E_g^2\right)^2 + E_g^2C^2}}$$

with

Equation 24

$$a_{\ln} = \left(E_g^2 - E_0^2\right)E^2 + E_g^2C^2 - E_0^2\left(E_0^2 + 3E_g^2\right)$$
$$a_{a\tan} = \left(E^2 - E_0^2\right)\left(E_0^2 + E_g^2\right) + E_g^2C^2$$
$$\zeta^{\$} = \left(E^2 - \gamma^2\right)^2 + \frac{\alpha^2C^2}{4}$$
$$\alpha = \sqrt{4E_0^2 - C^2}$$
$$\gamma = \sqrt{E_0^2 - C^2/2}\,.$$

2.1.2. Optics of multilayers, method of characteristic matrices

Multilayer structure is defined as a sequence of m plane-parallel layers of thickness d_j of different materials that are characterised by their complex refractive index $N_j = n_j + ik_j$ (Figure 2). The quantity $n_j d_j$ is known as optical thickness. The structure is situated among incident medium *0* and exit medium *m+1* that are in the most cases air and substrate, respectively. The light beam incides at multilayer structure at incidence angle Φ_o in respect to normal to the interface that separates incidence medium and the structure (z axes). It is partially reflected at this same angle and partially transmitted into medium *m+1* at angle Φ_{m+1}. The relation between these two angles is given by Snell's law:

Equation 25
$$N_o \sin\Phi_o = N_{m+1} \sin\Phi_{m+1}.$$

The incident, reflected and transmitted beam are contained in one common plane that is called plane of incidence.

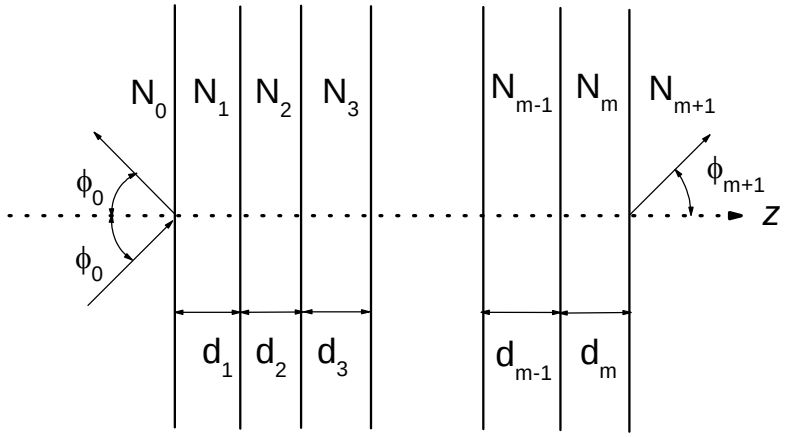

Figure 2. Schematic presentation of multilayer structure.

In the case of plane waves it is possible to define reflection r and transmission t coefficients as:

Equation 26
$$r = \frac{\mathcal{E}_r}{\mathcal{E}_i}$$

$$t = \frac{\mathcal{E}_t}{\mathcal{E}_i}.$$

$\mathcal{E}_i, \mathcal{E}_r$ and $\mathcal{E}_t$ are complex amplitudes of incident, reflected and transmitted electric field, respectively. The coefficients are complex quantities that relate amplitude and phase shift of electric field of

reflected and transmitted wave with the incidence one. Reflectance R and transmittance T are defined as ratio of reflected (I_r) and incident (I_i) and transmitted (I_t) and incident beam intensity, respectively:

Equation 27

$$R = \frac{I_r}{I_i} = |r|^2$$

$$T = \frac{I_t}{I_i} = |t|^2 \frac{n_{m+1}}{n_0}.$$

Absorptance A is defined as the intensity that is lost in interaction with the structure. Sum of R, T and A in the case when there are no other losses (for example scattering) must be unity: $R + T + A = 1$.

The defined coefficients depend on the state of polarisation of light. Thus, *s* state of polarisation is defined by electric field oscillating perpendicularly to the plane of incidence and *p* polarisation by electric field oscillating parallel with the plane of incidence (Figure 3). Then the quantities r_s, r_p, t_s, t_p, R_s, R_p, T_s, and T_p can be defined in a similar way. In the case of circular polarisation, when *s* and *p* components of electric field have the same value, it can be written:

Equation 28

$$R = \frac{R_s + R_p}{2}.$$

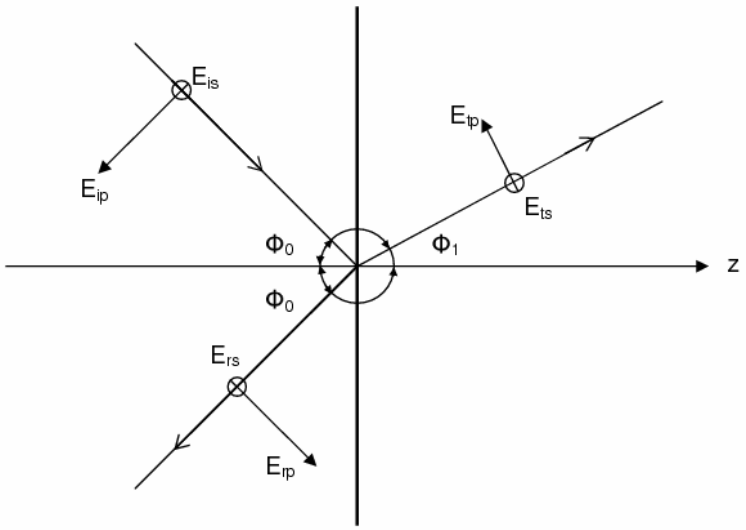

Figure 3. Schematic presentation of *s* and *p* components of electric field incidence, reflected and transmitted at the interface between two media, shown in the plane of incidence.

The waves reflected and transmitted at multilayer are result of interference of all the fractions of the incidence wave that are reflected and transmitted at each boundary between different layers of the structure. One of the most widely used approaches to relate the transmitted and reflected waves with the incidence one, method of characteristic matrices[51] will be presented here.

Characteristic matrix relates tangential components of electric field $\mathcal{E}$ and magnetic field $\mathcal{H}$ at interfaces between layers. It can be written as:

Equation 29
$$\begin{pmatrix} \mathcal{E}_{j-1} \\ \mathcal{H}_{j-1} \end{pmatrix} = \begin{pmatrix} \cos\beta_j & \frac{i}{\eta_j}\sin\beta_j \\ i\eta_j \sin\beta_j & \cos\beta_j \end{pmatrix} \begin{pmatrix} \mathcal{E}_j \\ \mathcal{H}_j \end{pmatrix},$$

where η_j is the generalised complex refractive index:

Equation 30
$$\eta_j = N_j \cos\Phi_j \qquad s \text{ polarisation}$$
$$= \frac{N_j}{\cos\Phi_j} \qquad p \text{ polarisation.}$$

Here β is phase factor defined as

Equation 31
$$\beta_j = \frac{2\pi d_j N_j}{\lambda}\cos\Phi_j,$$

and Φ_j is the angle between the wave transmitted into the layer j and z axis (see Figure 2).

The recursive form of relation of incidence and transmitted tangential component of fields as product of characteristic matrices of layer interfaces (Figure 4) is written as:

Equation 32
$$\begin{pmatrix} \mathcal{E}_o \\ \mathcal{H}_o \end{pmatrix} = \left[\prod_{j=1}^{m} \begin{pmatrix} \cos\beta_j & \frac{i}{\eta_j}\sin\beta_j \\ i\eta_j \sin\beta_j & \cos\beta_j \end{pmatrix} \right] \begin{pmatrix} \mathcal{E}_{m+1} \\ \mathcal{H}_{m+1} \end{pmatrix} = \begin{pmatrix} a_{11} & a_{12} \\ a_{21} & a_{22} \end{pmatrix} \begin{pmatrix} \mathcal{E}_{m+1} \\ \mathcal{H}_{m+1} \end{pmatrix}$$

Reflection and transmission coefficients are calculated as[52]:

Equation 33
$$r = \frac{2\eta_o}{\eta_o a_{11} + \eta_{m+1} a_{22} + \eta_o \eta_{m+1} a_{12} + a_{21}}$$
$$t = \frac{\eta_o a_{11} - \eta_{m+1} a_{22} + \eta_o \eta_{m+1} a_{12} - a_{21}}{\eta_o a_{11} + \eta_{m+1} a_{22} + \eta_o \eta_{m+1} a_{12} + a_{21}}.$$

Matrix formalism enables direct analysis of the effect of each layer to the optical properties of multilayers structure. For the case of periodic structure, this formalism enables reduction of computational demands by using the matrices to appropriate powers.

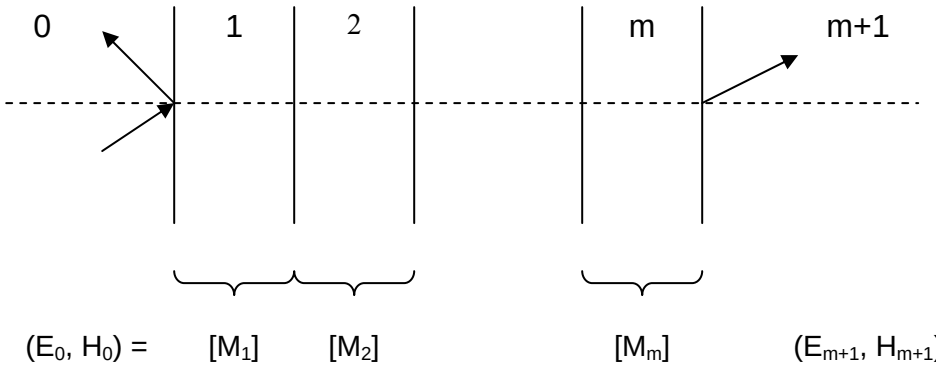

Figure 4. Schematic presentation of matrix method relating incidence and transmitted field as a product of different matrices.

Since the real substrates are not semi-infinite the reflection from the back side of the substrate (in respect to the direction of propagation of light) must be taken into account when calculating the reflectance and transmittance of a sample. Due to the substrate thickness, that is usually much bigger than the coherence length of the light, there will be no contribution in interference i.e. adding of amplitudes, but intensities. Only in the case of the absorbing substrate this contribution can be neglected.

In-depth inhomogeneous films can be represented for calculations as multilayer structure consisting of a number of very thin layers of homogeneous refractive index, which is changing gradually from layer to layer through the structure. Indeed, this is the most frequently used approach to the calculation of optical properties of graded index films[53,54], enabling application of the matrix formalism described previously. Attempts to calculate optical properties of inhomogeneous films with refractive index defined as a continuous linear function have been done[13,55,56]. However, it is not possible to calculate the optical performance of the system exactly in general, but only in few specific cases.

2.1.3. Effective medium theories

The dispersion models described previously (Chapter 2.1.1. Optical constants and dispersion models) consider that medium consists of only one kind of material and each point of the layer follows the same dispersion law. Of course, this is not the case for the films that are composed of two or more materials

presenting optical properties that are the mixture of the properties of the individual components. Therefore, it would be useful to define effective optical constants of the mixture that are related to the optical constants of the composing materials.

When considering material mixtures, it is assumed that the composing materials are in the mixture as phases of microstructure that is big enough to maintain the same optical properties as in a layer of a single material, but small in comparison to the wavelength of the incidence light. In this way the medium is microscopically heterogeneous, but macroscopically homogeneous. To satisfy this condition for the visible up to mid-infrared wavelengths, the microstructure should have dimensions typically 3-30 nm[57] (the shorter the wavelength, the lower the upper limit of the size).

The theories developed for description of properties of such effectively homogeneous media are called effective medium theories (EMTs)[58]. They are based on Claussius-Mossoti equation (Equation 14) that relates microscopic and macroscopic properties and that is possible to generalise to the case of different phases:

Equation 34
$$\frac{\varepsilon_{eff} - \varepsilon_h}{\varepsilon_{eff} + y\varepsilon_h} = \sum_j f_j \frac{\varepsilon_j - \varepsilon_h}{\varepsilon_j + y\varepsilon_h}.$$

Here ε_{eff} is complex dielectric function of the effective medium, ε_h of the host (the matrix of the mixed phases) and ε_j of the individual phase, f_j is volume fraction of the individual phase and y is screening factor that is related to the shape of microstructures that form the mixture[59]. If the microstructure consists of spherical particles $y = 2$.

The EMTs that are the most widely used are Maxwell-Garnett[18] (MG), Bruggeman[16] (BG) and Lorentz-Lorenz[17] (LL) effective medium theory. The first two assume that the mixing materials are in separated phases. MG considers the mixture that has separated two (or more) grain structure where particles of the first material are dispersed in the continuous host of the second material. On the other hand, BG assumes aggregate structure having a space filling random mixture of two (or more) material phases. In the limit of small volume fractions (f) the predictions of the two theories approach to each other. It is shown that in the case of higher filling factors, i.e. when volume fraction of one material is comparable to the volume fraction of another, the BG is valid up to the smaller particle radius than MG[57]. LL takes an average of molecular polarisability of the components. In this case no phase separation is considered as it is supposed that the mixture is realised at atomic/molecular scale. The host material is vacuum ($\varepsilon_h = 1$).

Additional simple model is linear model (LIN) that takes linear dependence of refractive index on the volume fractions of the constituents[19].

The relations for calculation of optical properties of two materials mixtures using described EMTs, where ε_L and ε_H are dielectric constants of lower and higher index components, respectively, and f_H is volume fraction of high index component, are:

Equation 35

$$\frac{\varepsilon_{eff} - \varepsilon_H}{\varepsilon_{eff} + 2\varepsilon_H} = (1 - f_H)\frac{\varepsilon_L - \varepsilon_H}{\varepsilon_L + 2\varepsilon_H} \qquad \text{MG}$$

$$f_H \frac{\varepsilon_H - \varepsilon_{eff}}{\varepsilon_H + 2\varepsilon_{eff}} + (1 - f_H)\frac{\varepsilon_L - \varepsilon_{eff}}{\varepsilon_L + 2\varepsilon_{eff}} = 0 \qquad \text{BG}$$

$$\frac{\varepsilon_{eff} - 1}{\varepsilon_{eff} + 2} = f_H \frac{\varepsilon_H - 1}{\varepsilon_H + 2} + (1 - f_H)\frac{\varepsilon_L - 1}{\varepsilon_L + 2} \qquad \text{LL}$$

$$\sqrt{\varepsilon_{eff}} = f_H \sqrt{\varepsilon_H} + (1 - f_H)\sqrt{\varepsilon_L} \qquad \text{LIN}$$

In the equation for MG it is assumed that the high index material is the host and therefore and $\varepsilon_H = \varepsilon_{host}$.

2.2. Spectrophotometry and ellipsometry

Spectrophotometry and ellipsometry are the most popular and developed experimental techniques for characterisation of optical properties of materials. Since these techniques have been used in characterisation of the samples in this work, they are briefly described in the following two subsections.

2.2.1. Spectrophotometry

Spectrophotometry measures reflectance and/or transmittance of a sample over a defined spectral range. The light beam from a source is reflected or transmitted through the sample and the ratio between the reflected/transmitted and incident beam intensities is determined. One type of spectrophotometers is dispersive, that measures in ultraviolet, visible and infrared range of light, typically 190-3000 nm. Another type is Fourier Transform Infrared (FTIR) spectroscopy that measures in the range typically 2-100 μm. The basic scheme of the dispersive spectrophotometer consists of a light source, a monochromator that selects the wavelength of the measurement, an optical system for adjustment of light beam that incidences to the sample and a system for light detection. FTIR spectrophotometers are based on Michelson's interferometer and detect the signal that corresponds to a

polychromatic light beam. The spectrum is obtained by applying Fourier transform to the measured signal.

To calibrate a spectrophotometer it is necessary to determine precisely the wavelength of the measurement, which is done by comparison with absorption lines of different reference materials. Resolution of the monochromators for commercial devices is generally less then 0.1 nm. However, the obtained beam has a certain spectral width (of the order 1-2 nm) that limits precision of the measurements. Another parameter critical for calibration is linearity of the response of the detector. The linearity can be checked by the use of different optical filters of appropriate transmittance.

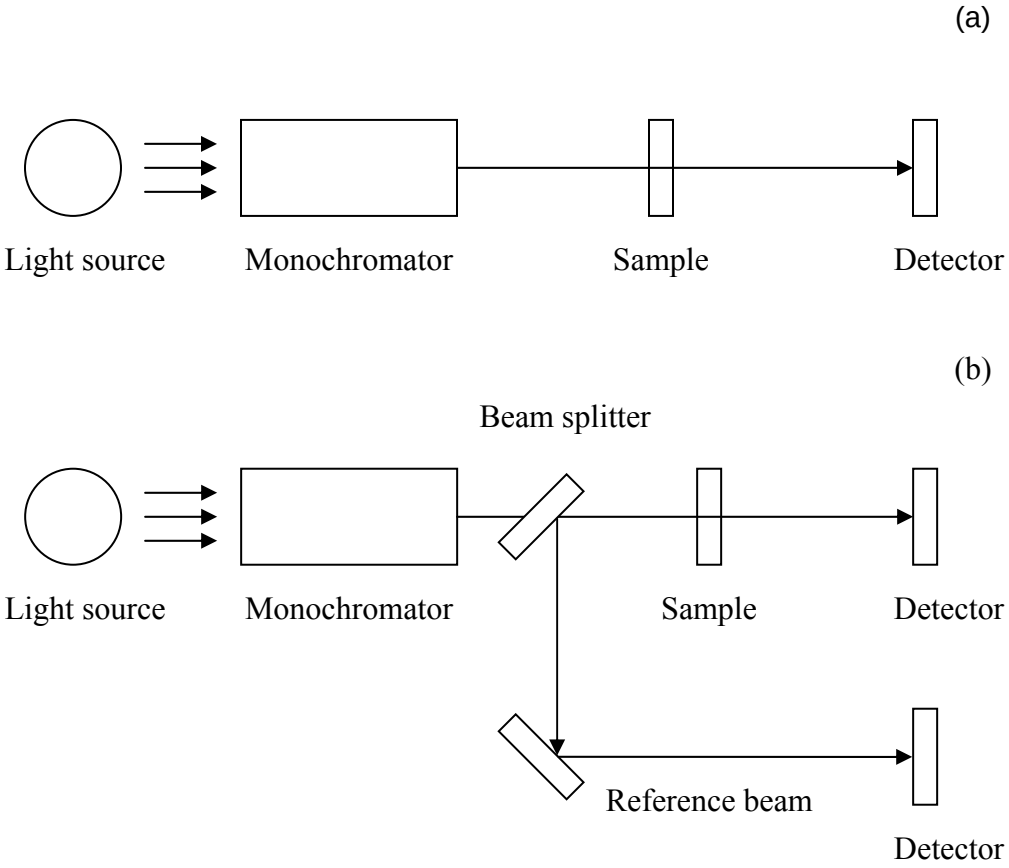

Figure 5. Schematic representation of a single beam (a) and double beam (b) spectrophotometer.

The range of detected intensities that correspond to 0% and 100% is determined from measurements of baseline. For this purpose a reference beam is necessary. There are single beam spectrophotometers (Figure 5a) with one reference beam in which reference measurements are done without the sample, and double beam spectrophotometers (Figure 5b) where reference is measured simultaneously with the measurement of the sample. Double beam spectrophotometers are more

reliable because the measurements are not affected by possible time variations of the beam and thus systematic errors are minimised.

The most accurate and simplest are measurements of transmittance at normal incidence. Reflectance measurements are more complex since for determination of baseline a sample with known reflectance is necessary. However, there are attachments for measurements of absolute reflectance, in so called VN configuration, where the beam comes to the sample twice and no reference sample is required. It is not possible to perform reflectance measurements at completely normal incidence, so special attachments are needed. Reflectance measurements are usually done at 6^{o} angle of incidence. This is taken as normal incidence because deviation from the spectra of real normal incidence is very small. Measurements at non-normal incidence (normally more than 15^{o}) are even more complex as polarisation of the beam should be controlled. These measurements are also less reliable since it is difficult to estimate the influence of multiple reflections from the back side of the substrate that arrive to the detector.

Typical value of experimental error in well calibrated commercial spectrophotometers, without systematic errors, is 0.15% for transmittance and 0.3% for reflectance at normal incidence.

Spectrophotometric measurements are basically applied for determination of refractive index and thickness of the layers. By simultaneous measurements of reflectance and transmittance it is possible to determine absorption of the sample, except in the case when sample absorbs so much so no light is transmitted.

2.2.2. Ellipsometry

Ellipsometry is based on measurements of polarisation states of beams incident and reflected by the sample. The measurements give ratio of coefficients of reflection of *s* and *p* polarisation (ρ):

Equation 36. $$\rho = \frac{r_p}{r_s} = tg\,\psi \cdot e^{i\Delta}.$$

Δ and Ψ are called ellipsometric angles. They determine the differential changes in amplitude (Ψ) and phase (Δ) experienced upon reflection by the component of the electric vector parallel and perpendicular to the plane of incidence.

Ellipsometers are basically measuring intensities and thus indirectly ellipsometric angles or their trigonometric functions. Ellipsometers consist of the light source, optical system for preparation

of light beam and a system for detection of light. Polarizers are especially important in the optical systems. They provide control over the state of polarisation of the beams and they are critical for determination of ellipsometric angles. They can be situated in the beam path before or after the sample. In the later case they are called analysers. Compensators are used for introduction of phase shift between *s* and *p* beam components.

There are several types of ellipsometers in use[60] and the most common are the following (Figure 6):

- Null ellipsometer[61] - angles are determined from measured minima of intensity. Before reaching the sample, the beam passes through linear polarizer and compensator and upon reflection at the surface of the sample through analyser. The angles are determined from angular positions of polarizer and analyser at the moment when minimum of intensity is detected. This setup enables very precise measurements and good control over systematic errors. However, since the measurements are very slow, this type of ellipsometer is not much in the commercial use, especially for spectral measurements.
- Ellipsometers with rotating elements[62] are based on periodical modulation of polarisation states of beam incident or reflected at the sample by mechanical rotation of some of the optical elements. Ellipsometers with rotating analyser or rotating polarizer can be distinguished. The signal is time dependent and upon Fourier analysis it is possible to determine ellipsometric angles. This type of ellipsometer performs measurements much faster compared with null ellipsometers. Drawback of this setup is necessity of very accurate calibration to avoid systematic errors.
- Phase modulation ellipsometers[63] don't need rotating elements. Before reaches the sample, the beam passes photoelastic modulator that vibrates with a defined frequency and introduces phase shift between components of electric field. The detected signal varies periodically and can be decomposed into the continuous signal, the signal that vibrates with frequency of modulator and the one that varies with double frequency of the modulator. Angles are determined from analysis of these signals. These set-ups are the most stable since they don't have mobile parts.

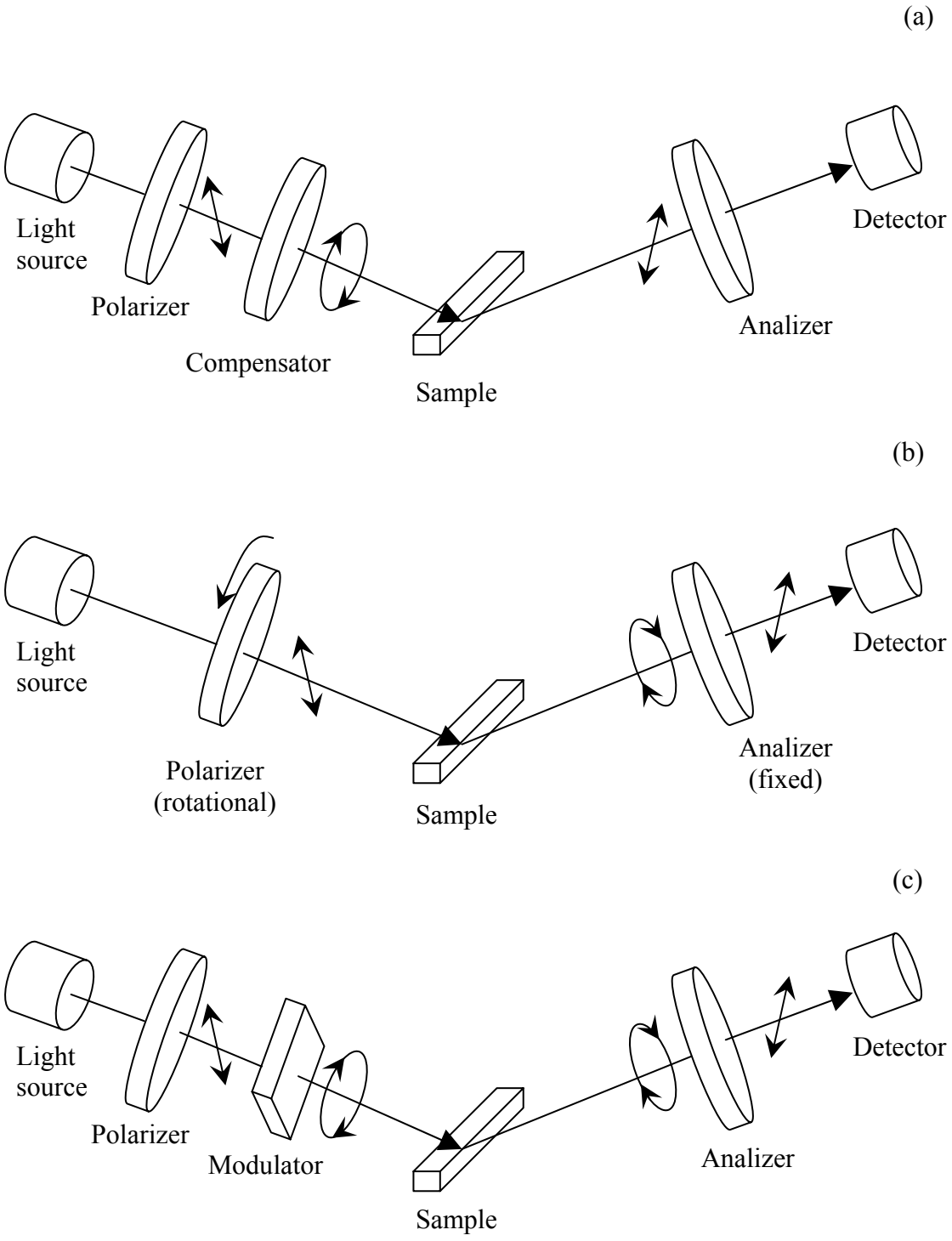

Figure 6. Schematic presentation of different types of ellipsometers: null ellipsometer (a), ellipsometer with rotating elements (b), phase modulation ellipsometer (c).

One of the main problems of ellipsometry is systematic errors. The required optics is pretty complex and it is necessary to make very precise calibration of the device to avoid errors in alignment of different optical elements[64].

Ellipsometric measurements are always done at large angles of incidence and therefore it is difficult to estimate the contribution from multiple reflections from the back side of the substrate. A great care should be taken to eliminate this contribution using incidence beam of micrometer diameter (microspot), absorbing substrates, substrates with sanded back side, thick substrates (~ 3 mm or more) or substrates with non-parallel surfaces. It is possible then to treat the sample as being deposited onto semi-infinite substrate.

For characterisation of materials at one wavelength variable angle ellipsometry is used, and in some spectral range spectroscopic ellipsometry. Single wavelength ellipsometry is used also for control of deposition processes. Variable angle spectroscopic ellipsometry is a very powerful and useful technique for accurate characterisation.

Ellipsometry is used in study of semiconductors in spectral regions of high absorption and metals, where spectrophotometry is not sufficient. This technique is very sensitive to the structure of the sample. Analysis of measured ellipsometric angles Ψ and Δ allows one to make conclusions about the character of a sample inhomogeneity. It has been shown that the ellipsometric angle Ψ is very sensitive to the bulk inhomogeneity[28,55,65]. At the other hand, Δ may be quite sensitive to the surface inhomogeneity i.e. surface micro roughness[66]. In this sense ellipsometry is a valuable technique for determination of refractive index profiles of inhomogeneous layers.

2.3. Rugate software and software for optical characterisation

In the next two sections softwares for design and optical characterisation of gradient index coatings will be presented. The first one was used in creating the antireflective and notch designs and the second in characterisation of all the deposited samples. Both of the softwares start from some initial refractive index profile which is then optimised by some numerical procedure until the discrepancy of its optical properties from the targeted properties is minimised. In the case of the software for design the targeted properties are in fact the required specifications and in the case of the software for optical characterisation it is data from experimental measurements. In both cases layers with gradient of refractive index are presented by division of the layer into sublayers of constant refractive index. The software for design calculates refractive index of the mixture via a general equation relating indices of pure materials and mixture by a coefficient having values 0-1. For the same purpose, the optical

characterisation software involves volume fractions of materials via effective medium theories. Also, it allows to the user more parameters in the optimisation, but in the same time better control over them.

Although the two softwares are conceptually similar, each of them presents some specific characteristics, like definition of the function to be minimised, that makes them appropriate for one or another purpose.

2.3.1. Rugate design software

The most common approach to synthesis of rugate filters (i.e. coatings having continuous variation of refractive index with thickness) is based on the inverse Fourier transform relation between a spectral function $Q(\lambda)$ and refractive index profile. The spectral function is, in fact, a function of the desired optical performance of the final system. One of the method's problems is that Q-function is not known exactly, but only its approximate values[3,14,15]. An alternative method in synthesis of rugate designs was followed using software specially developed for rugate systems[19,36] based on numerical optimisation technique. Here, spectral performance of the refractive index profile is calculated without approximation. The deviation of the performance of the model from the desired target values is optimised through the minimisation of a function of merit.

The refractive index profile of the design is considered and represented in the software as a polyline (Figure 7). The polyline is defined by a set of corner points $x_i(z_i, n_i)$ connected by straight lines representing segments of linear change of refractive index. All this points define a vector $X = \{x_i\}$. Here n_i is the refractive index of the layer with corresponding thickness z_i, at the reference wavelength λ_0 that is defined as

Equation 37. $$\lambda_0 = \sqrt{\lambda_m \lambda_M}\ .$$

λ_M and λ_m are the upper and the lower boundary of the spectral range where the target is defined. Thus, any continuous refractive index profile can be well approximated by increasing the number of corner points. For the calculation of the optical spectra of a sample defined in this way, the segments are divided into a number of sub-segments represented by homogeneous sublayers all having equal thickness and refractive indices equal to the mean index values of the individual sub-segment (Figure 8). The number of sublayers should be adequate for a reasonably good approximation of the gradient layers.

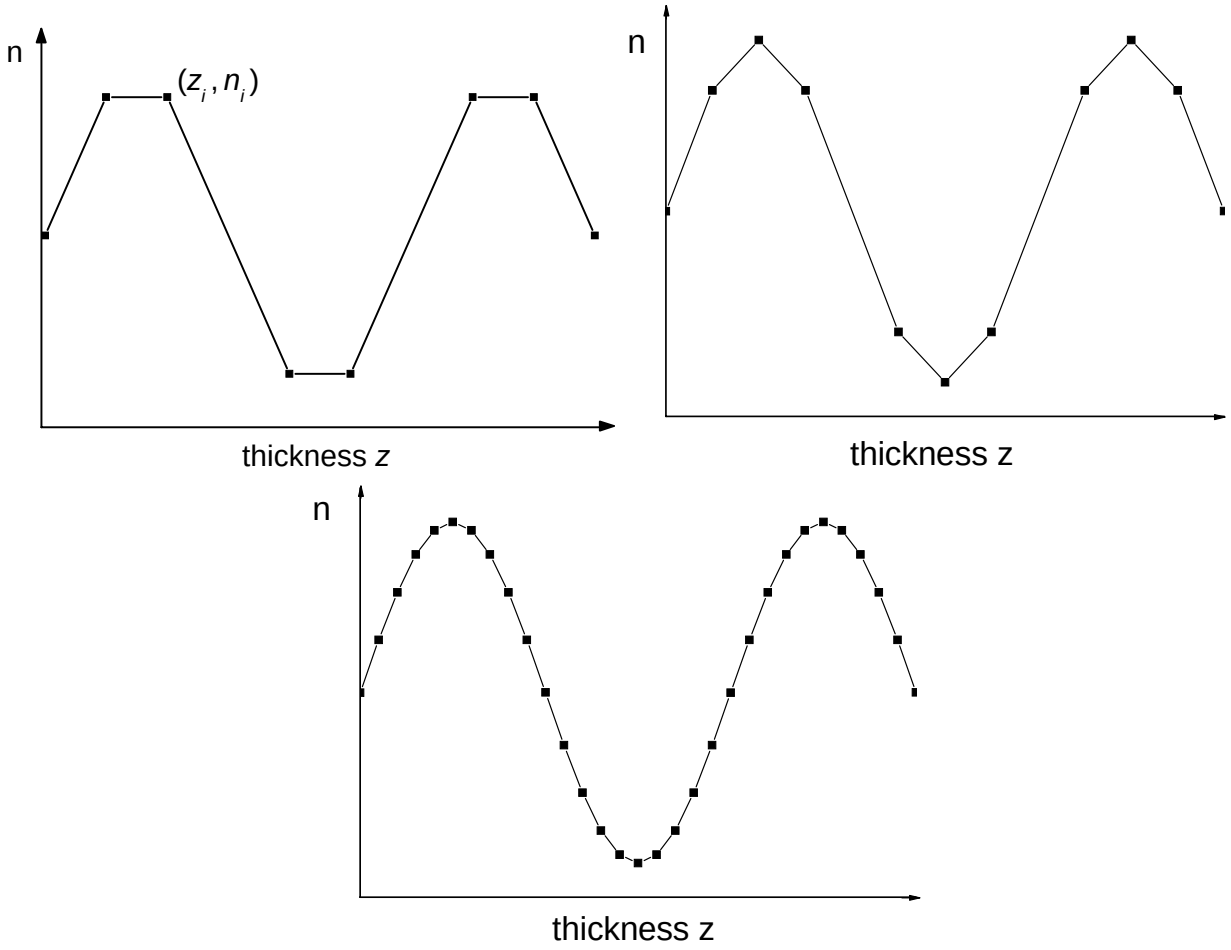

Figure 7. A sinusoidal refractive index profile, represented by polylines can be well approximated by increasing the number of corner points (z_i, n_i) (black squares).

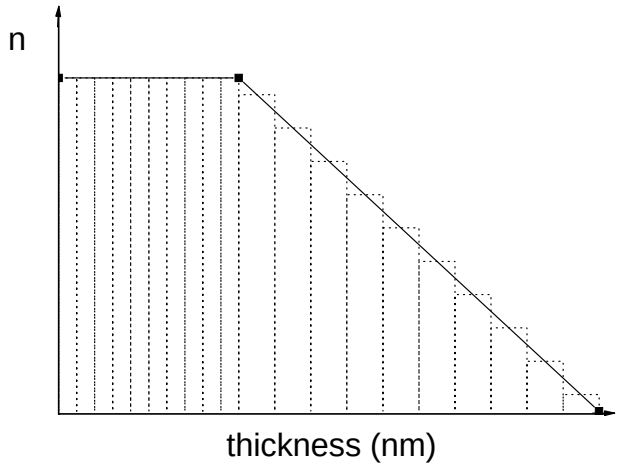

Figure 8. Division of segments into homogeneous sublayers of equal thickness and refractive indices equal to the mean values of the individual sublayer.

In the case of layers prepared by co-deposition of Nb_2O_5 and SiO_2 it is experimentally proven[67] that the dispersion of refractive index $n(\lambda)$ of the mixture may be approximated by

Equation 38. $$n(\lambda) = \mu n_H(\lambda) + (1-\mu) n_L(\lambda).$$

Here n_H and n_L stand for indices of pure materials, i.e. Nb_2O_5 and SiO_2 respectively, and μ is the parameter that can take value between 0 and 1. It is assumed that the same relation holds for the case of complex refractive index N ($N=n+ik$) if extinction coefficient k is much smaller than refractive index n, ($k << n$). Equation 38 relates the dispersion of refractive index of pure materials to the dispersion of their mixture. In this way both, dispersion and absorption are included into the calculation of the spectral performance of the model.

The software finds the design approaching targets by optimisation process. The function *M(X)*, which is minimised in process of optimisation, consists of three parts:

Equation 39. $$M(X) = \Phi(X) + P(X) + \alpha\Omega(X).$$

The first part of Equation 39 is a standard function of merit (FOM) *Φ(X)* that is a measure of closeness of spectral performance $R(X, \lambda_j)$ of the model to the desired target $R(\lambda_j)$:

Equation 40. $$\Phi(X) = \frac{1}{L}\sum_{j=1}^{L}\left[\frac{R(X,\lambda_j) - \tilde{R}\ (\lambda_j)}{\Delta_j}\right]^2,$$

where Δ_j are target tolerances and L is number of spectral points λ_j where the target is defined. If there are targets defined for transmittance, different polarisations or angles of incidence, then they should be taken into account in calculation of merit function. The second part is a penalty function *P(X)* that contains restrictions to maximum and minimum refractive index allowed. The third part is a stabilizing functional:

Equation 41. $$\Omega(X) = \sum_{i=1}^{N-1}\left(\frac{n_{i+1} - n_i}{z_{i+1} - z_i}\right)^2.$$

Here N is number of corner points. This part regulates smoothness of the refractive index profile: the steeper is the segment, the bigger is *Ω(X)*. In *M(X)* it is multiplied by a coefficient α that is its weighting factor. When α is set to 0 then abrupt changes in profile are allowed. A conjugate gradient method is used in minimisation[68].

2.3.2. Optical characterisation software

For the optical characterisation of the samples, general-purpose software[69] (NKDMatl) that allows determination of the optimal value of a set of parameters defining the sample by fitting experimental spectra has been used. Each sample has been represented as an in-depth inhomogeneous coating deposited onto a substrate with known optical constants. According to the design, some parts of the coating may have a constant composition making constant refractive index layers, while others present a linear variation of its composition, corresponding to the parts of constant refractive index gradients (ramps) in the design. Same as in the design software, the inhomogeneity of a ramp is taken into account by dividing it in a given number of sublayers, all with the same thickness. Each sublayer and each homogeneous layer have been modelled as a mixture of the two materials of high (n_H) and low refractive index (n_L) with volume fractions f_H and f_L, being $f_H + f_L = 1$. For each sublayer the volume fraction of the high index material is given by:

Equation 42.
$$f_{H-l} = f_{H-start} + \frac{f_{H-end} - f_{H-start}}{N_{sub}}\left(l - \frac{1}{2}\right).$$

Here f_{H-l} is the volume fraction of the material of high refractive index in the sublayer l ($l = 1,2,3,...N_{sub}$), $f_{H-start}$ and f_{H-end} are the values of the volume fractions of high index material at the beginning and at the end of the ramp and N_{sub} is the number of sublayers. It has been suggested[20] that an appropriate description of the optical constants of the mixture in our case is given by the Lorentz-Lorenz formula (Equation 35 LL). The optical constants of the high and low index materials can be used either from a data file or represented with a dispersion model.

In this way the sample is represented through a limited set of parameters: volume fraction and thickness for each layer and parameters defining the dispersion model for each material. The software enables fixing these parameters to a given value or to optimise them within some limits. Furthermore, it is possible to establish links between different parameters, allowing imposing the continuity of the volume fraction at the interface of different layers i.e. in corner points. The optimisation of the parameters is carried out by the minimisation of a merit function (MF) that is chi-square estimator χ^2:

Equation 43.
$$\chi^2 = \frac{1}{N - m - 1}\sum_{j=1}^{N_s}\sum_{k=1}^{N_j}\left(\frac{y_k^j - y^j\left(x_k; P_1, \cdots, P_m\right)}{\sigma_k^j}\right)^2$$

where N is the total number of experimental data points, N_s is the number of measured spectra, each one containing N_j experimental data points, y_k^j represents measured values at the wavelength x_k with

associated experimental error σ_k^j , $y_j(x_k;P_1,\ldots, P_m)$ is the corresponding value calculated using standard thin film computation algorithms[70] and $P_1, \ldots, P_m$ are the m parameters being optimised. It must be highlighted that this merit function permits considering different magnitudes simultaneously in the same optimisation procedure (like spectrophotometric and ellipsometric measurements) since the quantities being added are dimensionless. The minimisation of the merit function is carried out using the Downhill-Simplex algorithm[71].

Upon optimisation it is possible to evaluate the statistical uncertainties of the parameters. Uncertainties give estimation how precisely the parameters are determined according to experimental error of the used data. These uncertainties are given as confidence limits[71] that define a region in the parameter space which contains a certain percentage of the total probability distribution of the parameter, i.e. that there exists certain probability that the true value of the parameter is within this region. The uncertainties of the parameters (δP_i) are calculated as:

Equation 44
$$\delta P_i = \sqrt{\Delta\chi^2}\sqrt{C_{ii}}\,,$$

where $\Delta\chi^2$ defines the confidence region (we have chosen $\Delta\chi^2$=2.70 corresponding to 90% probability for the confidence region) and C_{ii} is diagonal element of the inverse of the curvature matrix α, with elements given by

Equation 45
$$\alpha_{ij} = \left(N - m - 1\right)\frac{\partial^2\chi^2}{\partial P_i \partial P_j}.$$

Thus, the curvature matrix is the matrix of the second derivatives of the merit function in respect to the parameters that are optimised. This matrix is numerically evaluated at the minimum of the merit function.

3. Designs

In this Chapter designs of hybrid broadband antireflective and notch optical system will be presented. They have been created taking into account the limitations posed by specific deposition techniques. The designs will be compared with corresponding classical HL stacks regarding optical performance and complexity of the systems.

The hybrid designs are intended to be produced by co-evaporation of Nb_2O_5 and SiO_2 using electron beam guns in a Leybold Syrus Pro 1100 deposition plant, where successful co-depositions have already been done[67]. The maximal and minimal refractive index of linear gradient layers of the design was limited by the technique of deposition and the difficulty to control precisely low rates of deposition, to the estimated values between 2.1 and 1.6 at a wavelength of 570 nm, which were determined from the achievable reproducible extremes of deposition rates identifying μ in the Equation 38 with volume fraction of Nb_2O_5. Besides this, it is not possible to obtain arbitrarily steep gradient of the mixture due to the technical reasons. Thus, the change in refractive index of 0.5 in 25 nm of thickness was the maximal allowed steepness of refractive index gradient in the design.

Each gradient layer has been divided into 8 homogeneous sublayers of equal thickness that has been shown to be a good approximation of the inhomogeneous layer in order to compute the theoretical performance of the design using the matrix method[72].

3.1. Antireflective design

Antireflective films are among the most frequently used coatings. They are applied in almost each optical system to improve intensity of transmitted light and prevent appearance of ghost images due to multiple reflections on intrinsic surfaces. The requirements are set on the spectral region and range of incidence angles where a low reflectivity is expected. As a conclusion from the maximum principle, two material based HL-systems will be the most efficient design for an antireflective coating for normal incidence. However, if performance at oblique incidence or, especially, broad angular range is necessary, the implementation of at least one additional material of intermediate refractive index is favourable[73]. The traditional dielectric multilayer antireflection stacks remain limited for this purposes by the choice of available materials having both, good mechanical and optical properties at the same time. In this case, the application of gradient index layers is preferable.

The ideal antireflective coating for a given spectral and angular range would be a gradient index structure having refractive index varying from the value of substrate, at substrate side, to the value of

incidence medium towards the surface[74,75,76]. This means that in the case of substrate/air interface, the coating should end with a refractive index of air or at least close to it. The problem is how to achieve such low values, since there are no suitable low index materials. Potential approaches to obtain gradients of low refractive index are moth's eye structures[77] or increased porosity of the film towards the incidence medium[78]. However, the main drawback is the mechanical resistance and cleaning of such surfaces.

In this work an alternative, hybrid, antireflective design is presented. It was optimised for the visible spectral region for BK7 glass substrate and commonly applied thin film materials Nb_2O_5 and SiO_2, keeping in mind the constraints due to limitations of the available electron beam evaporation deposition technology in Leybold Syrus Pro 1100 deposition plant where the coating was to be deposited. Two designs differing in the total thickness and complexity were generated and compared with a classical design obtained for the same purpose. Error analyses concerning thickness and refractive indices have been performed for the thinner design. In addition, the layer parameters most sensitive to errors have been detected. The thinner hybrid design was refined to the available materials of another two deposition techniques: ion beam sputtering and radio-frequency magnetron sputtering, to be able to evaluate the efficiency of different techniques. The material combinations used by these refined designs were TiO_2/SiO_2 and Ta_2O_5/SiO_2, respectively.

3.1.1. Specifications and design constraints

The required antireflection coating had to minimise reflectance R in the range 480-680 nm and for angles of incidence 0°-50°. Here R is an average of the reflectance at s polarisation R_s and p polarisation R_p, $R=(R_s+R_p)/2$. The additional requirement in synthesis was that at the same time the difference between R_s and R_p should be as low as possible for angle of incidence of 50° in the specified spectral region. The substrate was BK7, the low index material SiO_2 and Nb_2O_5 the high one. The intermediate refractive indices were calculated using the pure materials indices and their relative weight through parameter μ in the mixture according to the Equation 38.

3.1.2. Hybrid antireflective designs

As the first starting design for the hybrid AR system, a layer of constant refractive index of 1.85, 500 nm in thickness and 10 corner points has been defined. Also, another starting design has been tested, having double thickness and 15 corner points. During the optimisation the last two ramps have been replaced by layers of pure materials. As the result of the calculations two different designs have been

obtained consisting of 9 and 13 corner points. Their refractive index profiles at the wavelength of 570 nm and the corresponding reflectance for different angles of incidence together with that for uncoated substrate are shown in Figure 9 and Figure 10, respectively. The last four points (F, G and H, I) represent homogeneous layers of pure high and low index materials. The search in the literature shows similarity of the profiles to DeBell´s classical multilayer designs[74]. The corresponding total thickness of the hybrid designs are 526 nm (9 corner points) and 839 nm (13 corner points), respectively. The discrepancy from the specifications as expressed in terms of the function of merit (FOM) has 40% lower value in the case of the thicker design. However, both designs meet the target specifications well. Besides the quality of the optical performance, additional thickness and more corner points in the thicker one have to be taken into consideration. Because of the limitations of deposition process, a smooth transition between points D and F, i.e. continuous linear refractive index gradient, is not feasible. The approximation with an additional segment by inserting the point E does not spoil the quality of the performance (FOM) significantly.

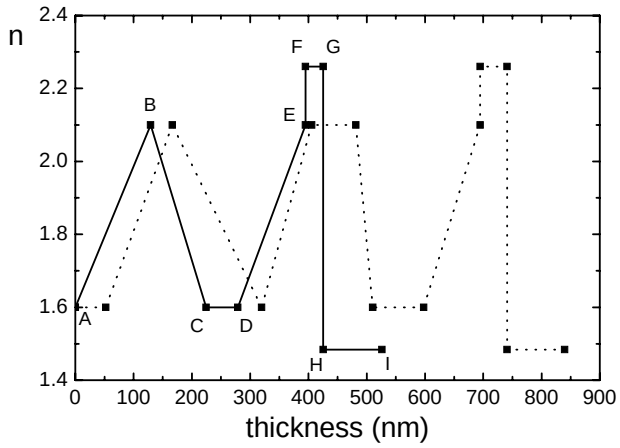

Figure 9. Refractive index profiles for the two hybrid designs (- thinner, ··· thicker) at 570 nm, capital letters stand for corner points.

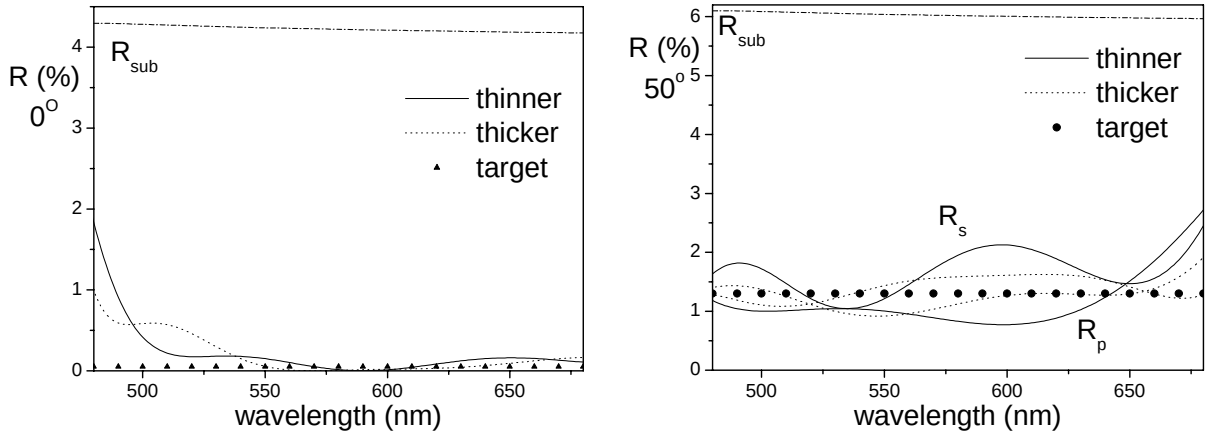

Figure 10. Optical performance of the thinner and thicker hybrid design for semi-infinite substrate (no back-side reflectance). Triangles and circles represent target reflectance at 0° incidence (left) and for *s* and *p* polarisation at the incidence angle of 50° (right).

Besides good optical performance and small physical thickness, the quality of hybrid AR designs is in their simplicity due to the small number of corner points forming the refractive index profile. The starting and the finishing points of the segments represent always the minimal and maximal allowed refractive indices of the mixtures. Thus, the refractive index values of only two mixtures have to be well controlled and repeatable. This minimises possibility of error in refractive indices at the corner points.

3.1.3. Comparison with a classical HL design

Defining the same specifications, substrate and materials, a classical high-low (HL) multilayer stack has been obtained by optimisation with Optilayer® software. It consists of 7 layers having the total thickness of 553 nm. The refractive index profile and the spectral performance compared with the thinner of the two hybrid designs, that is also thinner than the classical one, is shown in Figure 11 and Figure 12. The HL stack has 19% better FOM compared to the thinner hybrid. Its drawback is the first H layer which is only 4.6 nm thick that makes it sensitive for deposition. The similar HL design without so thin layer gives 10% worse FOM than the hybrid.

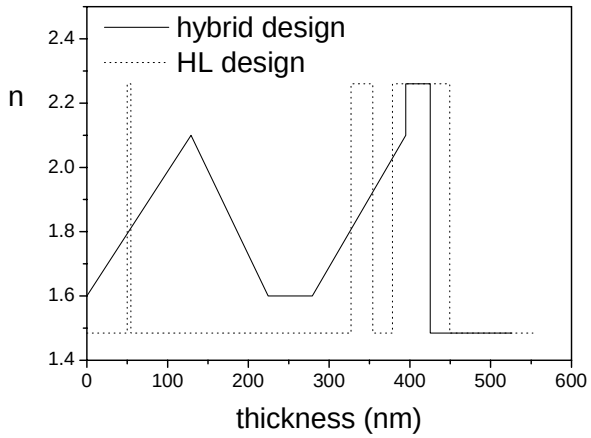

Figure 11. Comparison of refractive index profiles of the thinner hybrid design and the classical HL design.

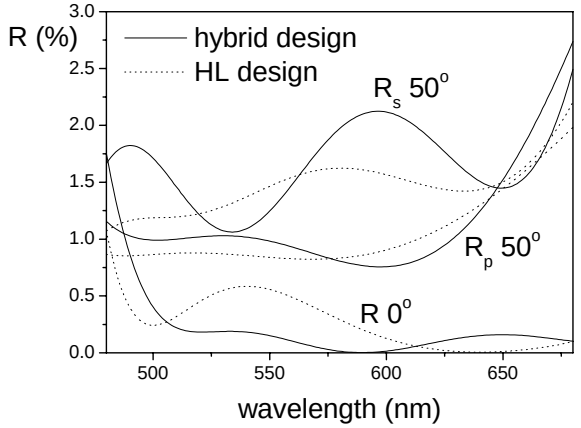

Figure 12. Comparison of reflectance spectra of the thinner hybrid and the classical HL design.

3.1.4. Sensitivity and error analysis

The sensitivity to fabrication errors and the knowledge where the most critical corner points are is very important for manufacturing of the proposed coatings. In order to detect which points are the most sensitive to errors, the coordinates (z_i , n_i) of each corner point of the thinner design have been varied individually by ±1% and the function of merit has been checked. The corresponding relative changes in FOM are presented in Table 1.

Table 1. Sensitivity of FOM of thinner hybrid design to errors in individual corner points defined in Figure 11

corner point	relative change in FOM / %			
	change in refractive index +1%	change in refractive index -1%	change in thickness +1%	change in thickness -1%
A	**2.7**	2.4	-	-
B	0.3	0.5	0.5	0.5
C	**4.3**	1.0	0.8	0.3
D	**7.4**	1.7	0.8	0.5
E	3.6	**6.7**	2.0	0.3
F	-	-	**2.0**	0.3
G	-	-	0.1	0.1
H	-	-	0.1	0.1
I	-	-	2.7	**7.0**

To check sensitivity of the designs to random fabrication errors the models of hybrid coatings, where each gradient index segment was divided into ten sublayers of constant refractive indices, were imported into Optilayer® software and the implemented error simulation procedure has been performed. A variation of 1% was permitted in both, thickness and refractive index. For the homogeneous layers of pure materials no error in refractive index was allowed. Number of designs with random errors has been generated, their spectra forming normal distribution. The average spectrum that can be expected as the outcome of the random trial is in fact mathematical expectation. The area in the normal distribution between a spectrum that is one standard deviation (here, standard deviation as a measure of the dispersion of a probability) below and a spectrum that is one standard deviation above the expectation is called corridor probability and is 0.6827 or 68.27%. This means that the probability of a single trial falling within one standard deviation of the expectation is 68.27%. The results of the calculations for the two hybrid systems and the corridor probability are presented in Figure 13 and for the HL-design in Figure 14.

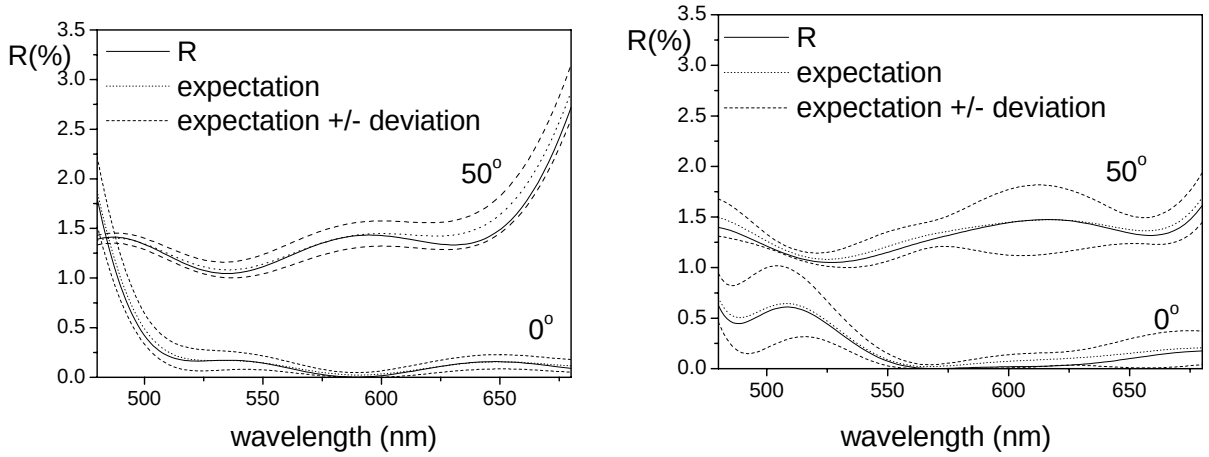

Figure 13. Reflectance variations of the thinner (left) and thicker (right) hybrid design caused by 1% random errors of thickness and refractive indices.

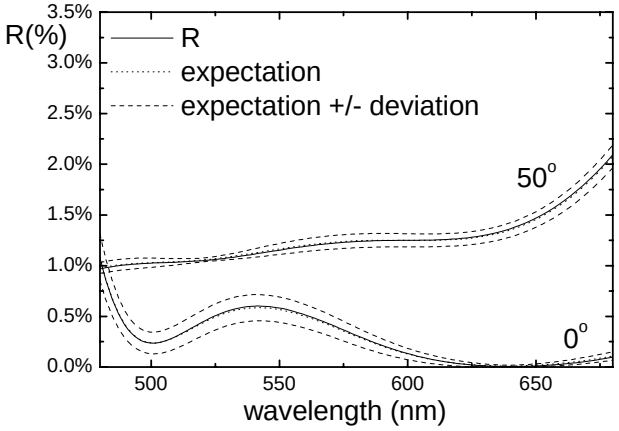

Figure 14. Reflectance variations of the HL-design caused by 1% random errors of thickness and refractive indices.

3.1.5. Refined designs

In order to compare success of different deposition techniques: electron beam deposition (EBE), radio-frequency magnetron sputtering (RFS) and ion beam sputtering (IBS), the thinner design presented in Figure 9 was refined according to the available materials (Ta_2O_5, TiO_2 and corresponding SiO_2). The obtained designs are presented in Figure 15 in conjunction with their corresponding reflectance values at 0^o and 50^o in Figure 16(a) and Figure 16(b), respectively. Absorption of materials used for the design was neglected. Some characteristics of the designs obtained for each applied deposition technique are presented in Table 2.

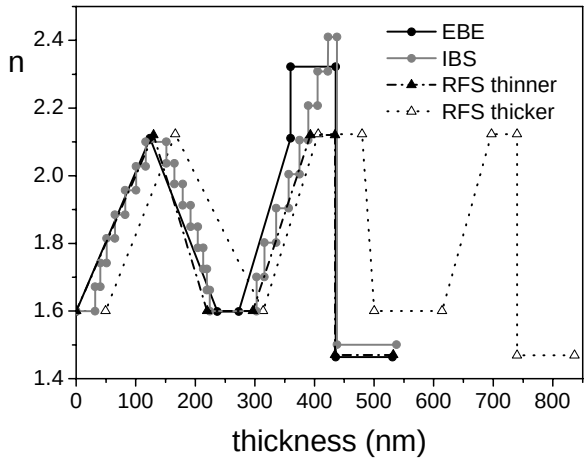

Figure 15. Designs proposed for each deposition technique. For RFS there are two designs proposed, the thinner and the thicker one, the last having lower deviation from the target, but being more demanding for deposition.

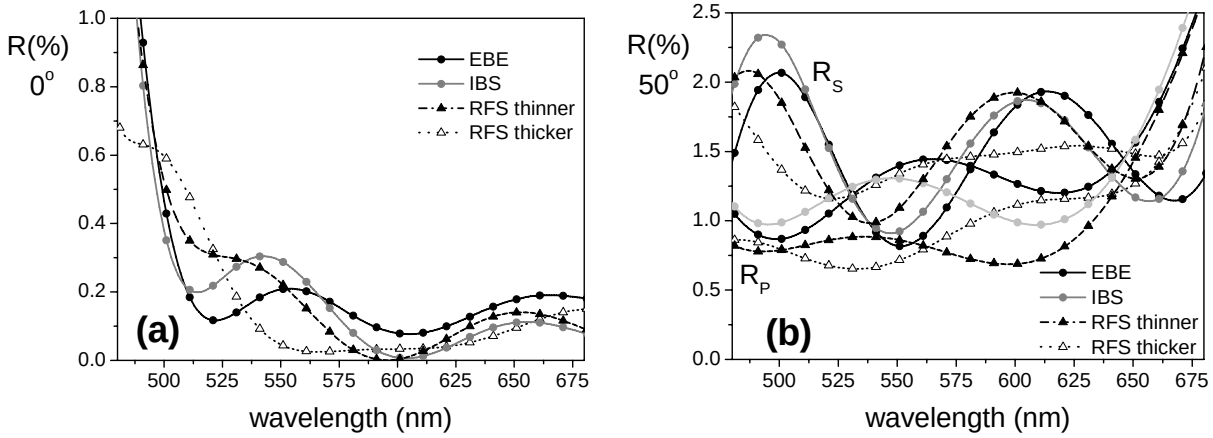

Figure 16. Theoretical reflectance spectra of a glass surface (no back side reflection) coated with the designs presented in Figure 15 for angles of incidence of 0^o (Figure 16(a)) and, as defined in specifications, 50^o (Figure 16(b)). One uncoated glass surface reflects 4% of light at 0^o angle of incidence in the presented spectral range.

Table 2. Refined designs

Design for technique	Material	n (570 nm)	Minimum (n_m) and maximum refractive index (n_M) at 570 nm	Total thickness (nm)	Deviation from the target (δ_{TH})
EBE	SiO_2	1.463	$n_m = 1.598$	531	0.0161
	Nb_2O_5	2.322	$n_M = 2.111$		
RFS	SiO_2	1.469	$n_m = 1.600$	532 (thinner)	0.0183 (thinner)
	Ta_2O_5	2.123	$n_M = 2.123$	837 (thicker)	0.0127 (thicker)
IBS	SiO_2	1.500	$n_m = 1.600$	537	0.0172
	TiO_2	2.409	$n_M = 2.308$		

The deviation was calculated according to:

Equation 46. $$\delta_{TH} = \sqrt{\frac{\sum_{i,j}\left[R_{i,TH}(\lambda_j) - R_{i,TAR}(\lambda_j)\right]^2}{N(N-1)}} \quad ,$$

where R_{TH} and R_{TAR} are theoretical and target reflectance values at the given wavelength λ_j. Index i denotes average polarisation for 0^o angle of incidence and s and p polarisation for 50^o angle of incidence. Target values of reflectance, for given polarisation and angle of incidence, were defined in the range of wavelength 480-680 nm, each 1 nm. N denotes the total number of points where target values have been defined.

3.2. Notch design

Notch filters, also known as minus or band stop filters, are optical components having very low transmittance in a narrow spectral range (the rejection or stop band) but a high transmittance elsewhere. They are mainly used in Raman and fluorescence spectroscopy, laser systems and as laser protective coatings. The ideal notch filter would have one hundred percent of reflectance in the required rejection band and zero reflectance outside of this region. The quality of the filters are estimated by the width of the stop band, the steepness of the transition between rejecting and transmitting region, the thickness of the coating and their optical density (OD) that is a measure of the strength of the reflectance peak and defined as negative logarithm of transmittance. For example, the optical density of an ideal notch filter equals 5 in the required rejection band and its reflectance would be zero outside this region.

It is well known that a quarter wave HL stack gives a fundamental stop band, i.e. region of high reflectance, as well as odd harmonic stop bands[51]. The fundamental stop band is positioned at the

wavelength that is equal to four times the layers optical thickness. The bandwidth of the stop band increases with the ratio of the minimal and maximal refractive indices used in the design. A smaller difference of these indices results in a narrower bandwidth, but also in a lower optical density at the same total thickness. Therefore, it is convenient to estimate how many pairs of HL layers of the given materials will be necessary to achieve the desired optical density.

The refractive index profile of a quarter wave stack can be understood as a square wave function and thus be represented by a Fourier series. Practically, this is transition from classical HL stacks to rugates. Each term of the series then generates a specific stop band of the transmittance spectrum[79]. The first term is a sine wave refractive index function that corresponds to the fundamental stop band. It gives the stop band at the same position as the quarter wave stack, but in this case there will be no harmonic stop bands since they are represented by other terms in the series.

The origin of sidelobes is in the mismatch of the equivalent refractive index of the coating and refractive index of the surrounding media. In order to eliminate sidelobes, an amplitude apodisation function is applied to the first Fourier term. Quintic (that is polynomial function of the 5^{th} order) or Gaussian apodisation were demonstrated to be excellent for this purpose[79,80]. Additionally, quintic apodised refractive index layers, alone or superimposed to the sine function, can be added to both ends of the structure to finally match its average refractive index to the one of the surrounding media[81]. However, the sidelobe suppression is very often improved at expense of reflectance in the stop band. Partial apodisation applied to only a number of end periods of the rugate can eliminate the sidelobes significantly, maintaining a good optical density. Another solution to preserve high reflectance would be increasing the number of periods in the filter, since OD increases about linearly with their number[82].

In this work the hybrid notch design is compared with a classical HL and rugate design, obtained from the same materials, specifications and restrictions. The advantages and drawbacks of each approach are discussed. The classical and the rugate design are based on the designs provided by courtesy of Mikroschicht Optik, Jena, Germany and Laser Zentrum Hannover, Germany, respectively.

3.2.1. Specifications

The performance of the required notch filter should satisfy the following demands under normal incidence: reflectance (no back side reflections from the substrate included) should be lower than 10% in the wavelength range 400-515 nm and 550-700 nm, transmittance in the range 530-534 nm should be lower then 0.01% and the total physical thickness of the design should not exceed 10 μm more then 10%. Three different approaches have been applied to model the filter and three different designs were

obtained. As substrate material BK7 glass was taken in all three cases. For the sake of clarity in the comparison of the designs, it is assumed that all the materials and the substrate are free of absorption.

3.2.2. Comparison of notch designs

In the classical HL notch design the original materials SiO_2 and Ta_2O_5 were replaced by SiO_2 and Nb_2O_5 having the same refractive indices as used in the design of hybrid antireflective coating. Thus changed design was refined to the specifications. The same was done with the original rugate design utilising the rugate numerical optimisation software. During the calculations each ramp, i.e. linear gradient layer, was divided into 9 sublayers of constant refractive index that was calculated as a mixture of SiO_2 and Nb_2O_5 materials.

The hybrid design was obtained utilising the rugate numerical optimisation software, starting from 45 periods of positive and negative refractive index gradient, with a refractive index ranging from 1.6 to 1.75 and total thickness around 7μm. The refractive indices and thickness of each ramp (i.e. gradient) were set to be optimised. Calculations lead to the apodised half-sinusoidal profile. The advantage of numerical optimisation is the possibility to control values of the design parameters, such as refractive index in individual points, thickness or steepness of ramps (due to the limitations of the available deposition technology). In the centre of the coating, the high refractive index value was fixed at 1.80 to reduce complexity for deposition. Adding new periods, followed by optimisation of the thickness and final introduction of a SiO_2 layer at the end of the design, in order to improve the transmission in the pass bands, the final design has been obtained.

The resulting HL design is presented in Figure 17. It has 106 layers and total physical thickness of 9627.98 nm. The individual sublayers range in thickness from 7.14 to 337.38 nm (Figure 18). The thickness of each of the layers was changed by the optimisation procedure but, corresponding to the original design approach, most of the thin layers are L layers and most of the thick ones are H layers.

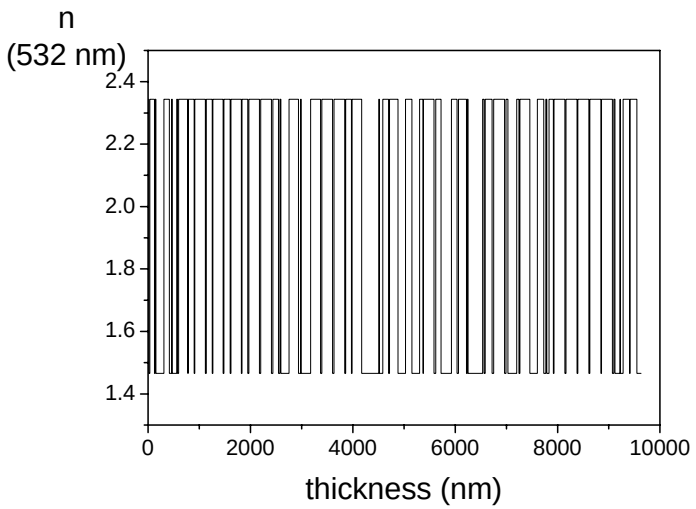

Figure 17. Refractive index profile of HL design.

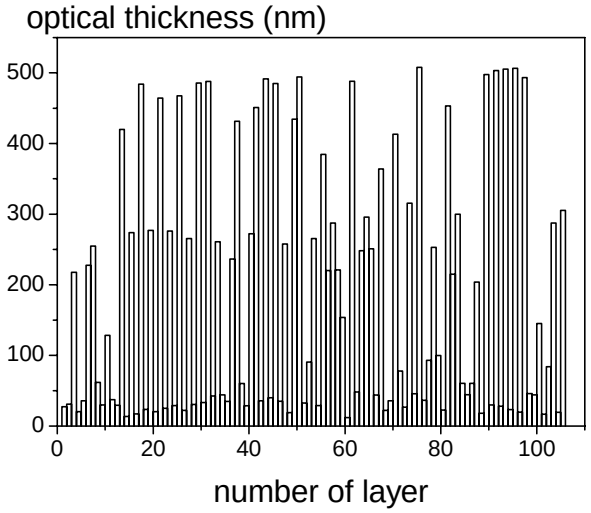

Figure 18. Optical thickness of layers through the HL design. The first layer is adjacent to the substrate.

The refractive index in the rugate design ranges from 1.582 to 1.958, at the wavelength of 532 nm. The refractive index profile is shown in Figure 19 and the corresponding reflectance in Figure 20. The performance illustrates the capacity of rugates to suppress completely sidelobes and ripples even in much wider wavelength range than required (400-700 nm). The reflectance out of the rejection band is around 5% at wavelengths shorter than the wavelength of the reflectance peak and 4% at longer wavelengths and fulfils the requirements ($R < 10\%$).

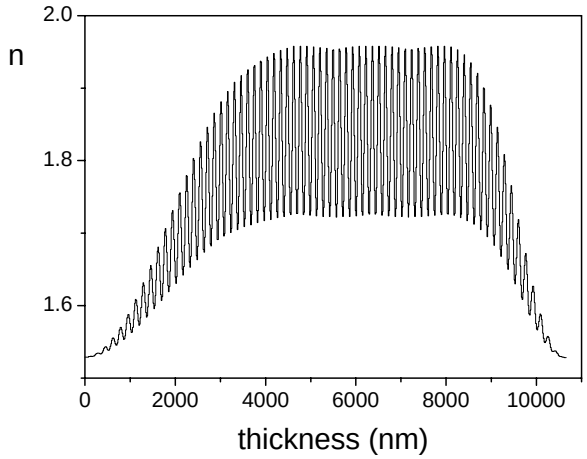

Figure 19. Refractive index profile of the rugate design.

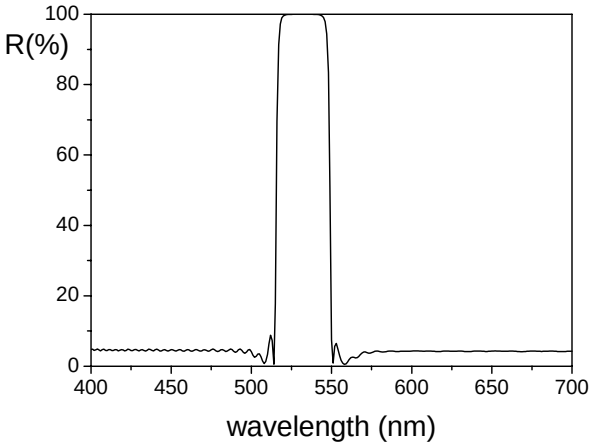

Figure 20. Performance of the rugate design presented in Figure 19.

In Figure 21, the apodised hybrid profile obtained after free optimisation of refractive indices is presented. The final design is shown in Figure 22. It should be noted that the peak value of refractive index in the hybrid design is often followed not by a ramp but by a layer of constant refractive index, which is the main characteristic of this kind of coatings. The total thickness is 10.667 μm. The minimum thickness of a homogeneous mixture layer is 8.78 nm and the minimal thickness of the ramp is 10 nm. Thus, the criteria of maximal change in refractive index of 0.5 in 25 nm of thickness was met in the design.

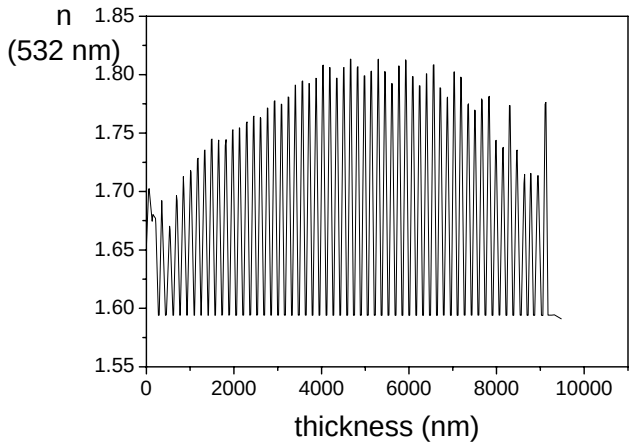

Figure 21. Apodised hybrid design obtained as a result of free optimisation of refractive indices, from an initial design whose indices were 1.6 and 1.75 at wavelength 532 nm.

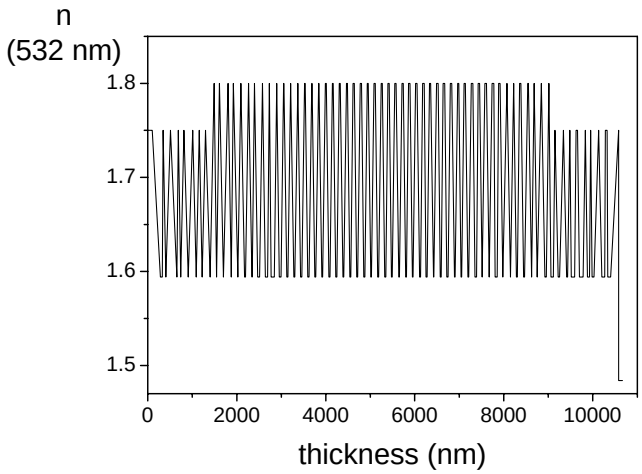

Figure 22. Final hybrid design, with added SiO_2 layer at the side towards the air.

As can be seen in Figure 23, all three designs show very similar reflectance. In order to evaluate and compare them, one should verify their thickness, optical density (OD), full width at half maximum (FWHM), etc. The results and comparison of presented notch designs are summarised in Table 3.

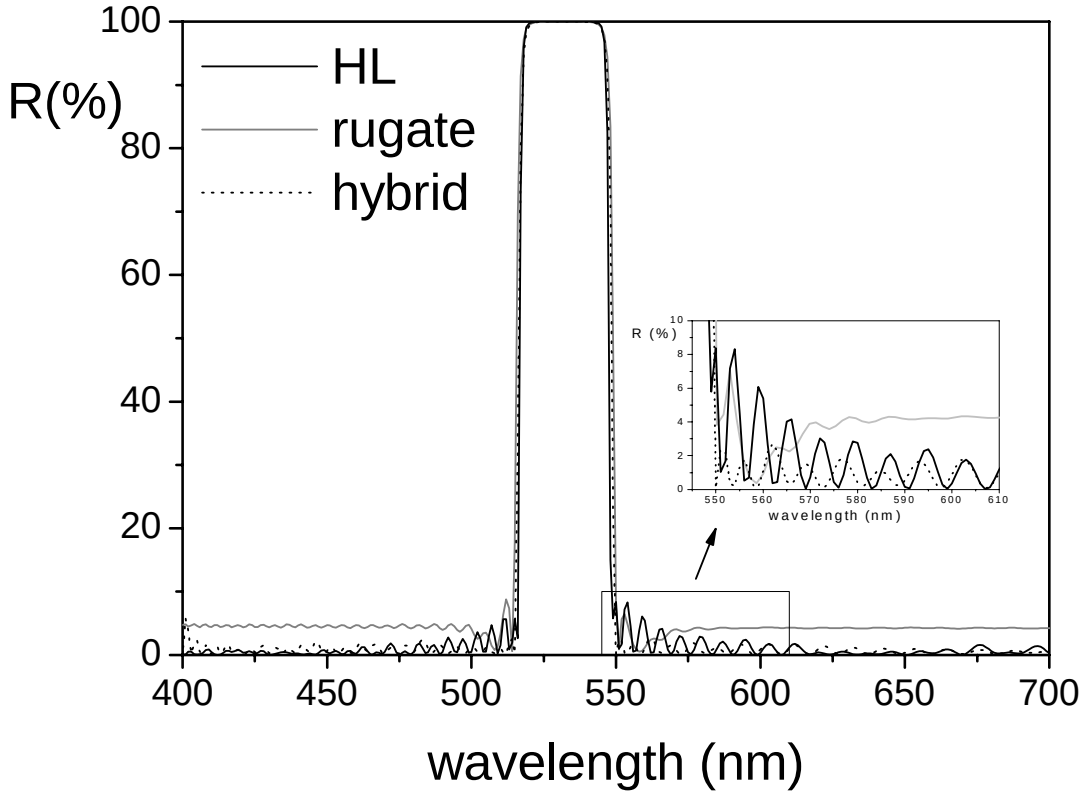

Figure 23. Comparison of the calculated reflectance spectra of the three notch designs.

Table 3. Comparison of the notch designs and their performances

	HL	rugate	hybrid
n_{max} / n_{min} @ 532 nm	2.343 / 1.465	1.958 / 1.528	1.800 / 1.594
T / R @ 532 nm (%)	0.0016 / 99.9984	0.0112 / 99.9888	0.0093 / 99.9907
FWHM (nm)	33	33	32
OD	4.45	3.93	4.01
number of periods	53	70	66
d_{total} / d_{min} (nm)	9627.98 / 7.14	10659.1 / 12.454	10666.67 / 8.78
$n_{average}$ @ 532 nm	2.055	1.743	1.685

4. Experimental

In this Chapter the experimental work carried out and its results are presented. Deposition techniques and parameters for production of samples are described. Optical performance of the deposited samples is compared with the targeted specifications and thus comparison between different deposition techniques is done. Optical characterisation is performed and the results are related to errors in deposition processes. The results of characterisation obtained using only spectrophotometry or combining it with ellipsometry are compared as well. Also, results of additional analysis of mixture layers are presented.

4.1. Deposition

In the following subsections deposition techniques applied in manufacturing the samples presented in this work will be described, followed by detail about the EBE processes in which they were made. Samples of single layers of pure materials, 10 periods of refractive index gradient, hybrid antireflective coatings and five material mixtures having constant refractive indices throughout the thickness have been deposited. Hybrid antireflective coatings manufactured by RFS and IBS were provided by Fraunhofer IST, Braunschweig and Laser Zentrum Hannover, respectively, in order to compare the efficiency of the applied techniques.

4.1.1. Deposition techniques

4.1.1.1. Electron beam evaporation

A Leybold Syrus Pro 1100 deposition system has been used previously with success for co-evaporation of Nb_2O_5/SiO_2 mixture coatings and gradient index films[67,33]. The chamber is equipped with two electron beam guns (EBG) and the Advanced Plasma Source (APS)[83]. LaB_6 cathode and anode of APS are placed within cylindrical magnetic coil producing magnetic field that gives spiral path to the electrons going out from the anode during their acceleration. Argon atoms are supplied to the cylinder. Argon ions and additional electrons are created by impacts between electrons and argon atoms. Electrons form discharge current I_D between cathode and anode. Number of electrons is accelerated out of the APS, along the magnetic field lines, thus leaving a positive charge causing bias voltage between APS and substrate holder that accelerates argon ions onto the substrate. Impact of ions with oxygen molecules create atomic oxygen necessary for a fast oxidation of the material being deposited to the

substrate. Impacts of argon ions contribute also to the energy of the particles that are being deposited increasing their packing density in the film and, consequently, increased refractive index of the coating, decreased porosity and thus water sorption into the coating and introduction of compressive stress to the film. The schematic presentation of APS and its operation is presented in Figure 24.

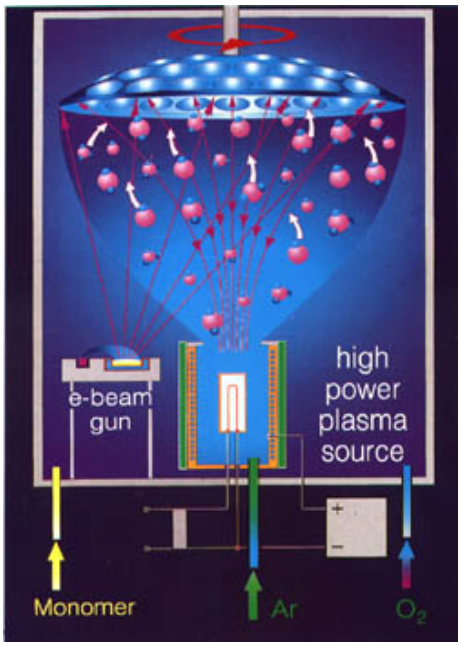

Figure 24. APS operation.

The deposition of the materials (Nb_2O_5 and SiO_2) was performed in an atmosphere of argon as working gas and, additionally, oxygen was employed as reactive gas to maintain the stoichiometry of the evaporated materials. Typical basic pressure before start of the deposition was $4 \cdot 10^{-7}$ mbar. Prior to the deposition the substrates were heated in the deposition chamber to the temperature of 150°C, which was also the working temperature. Substrates were cleaned first in ultrasound bath and additionally by 3 minutes of plasma etching in the deposition chamber. To insure uniformity of the film thickness across the substrate, the substrates were put to the calotte rotating with the speed of approximately 20 rpm. The material crucibles were set to rotation of 0.2 rpm to prevent deformation of the vapour cloud due to decreased quantity of material in the crucible during long processes. The deposition process is controlled by computer software that enables simultaneous automatic measurements and acquisition of parameters (rates, pressures, temperature, etc.) during the deposition. Photo of the evaporation chamber and its schematic presentation are shown in Figure 25 and Figure 26. Some specifications of the deposition process can be found in Table 4.

Figure 25. Evaporation chamber.

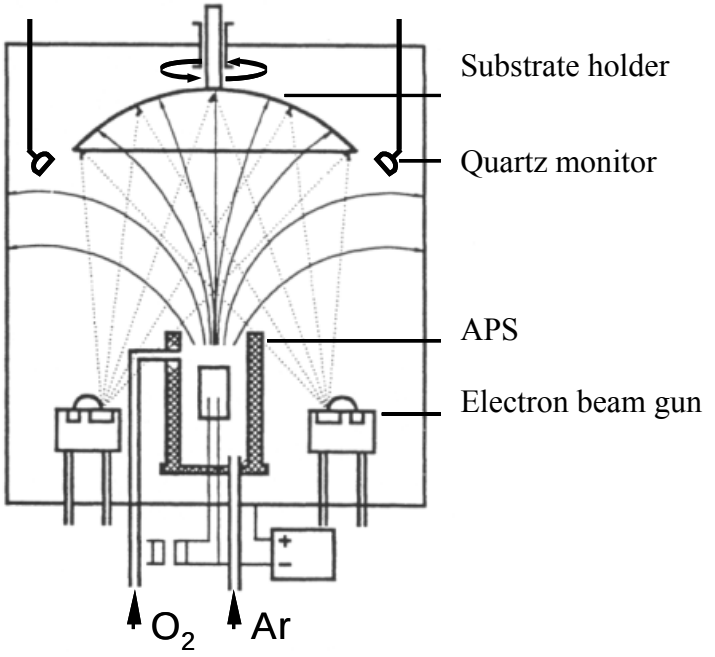

Figure 26. Schematic representation of the evaporation chamber.

Table 4. Some characteristics of the deposition process

		Nb_2O_5 deposition $\rho(Nb_2O_5) = 4.470$ g/cm^3	SiO_2 deposition $\rho(SiO_2) = 2.648$ g/cm^3	etching
	I_D	40A	40A	40A
APS	bias voltage	120V	120V	120V
	coil current	2A	2A	2A
O_2		40 sccm	40 sccm	0 sccm
EBG	$I_{emission}$	190-430 mA	75-950 mA	0 mA

The refractive index is changing due to varying concentrations of the deposited materials in the layer. This is achieved by a continuous linear modification in deposition rates r(t) of the individual materials via modification in emission current $I_{emission}$ of EBG. The inhomogeneous profile in the fabricated coating is, therefore, a real continuous change of the layer properties and not a succession of thin homogeneous layers, i.e. quasi-inhomogeneous coating. The range of available refractive indices feasible by the deposition system is restricted by the fact that it is impossible to achieve stable and reproducible arbitrarily low deposition rates for the given materials.

The rate of deposition for each material is computer controlled. In co-deposition process it is measured by two lateral quartz crystal monitors, one for each material. For thickness monitoring during deposition of single material layers the third monitor, in the centre of calotte is used. The sum of the rates of deposition of the two materials is kept constant during the deposition of the material mixtures. The crystal monitors were shielded from each other in order to minimise the influence of deposition of one material at the crystal monitor measuring another material (cross-talk). Efficiency of the shields was tested by evaporation of one material and checking how much thickness was measured at quartz monitor (QM) of the other material assuming density of this other material. The test was done with different rates of deposition to take into account the possible spatial changes in the shape of evaporated material cloud that would direct more or less particles towards QM. The test showed that QM of SiO_2 will count in average 7.9% thickness of Nb_2O_5 and QM of Nb_2O_5 will count 1.5% of SiO_2. The dependence on rate of deposition is shown in Table 5.

Table 5. Dependence of cross-talk on rate of deposition

r(nm/s) / QM	0.2	0.4	0.7	1	1.2
SiO_2	2.2%	1.6%	1.3%	1.4%	1%
Nb_2O_5	10.9%	7.7%	7.4%	7.1%	6.5%

Table 5. Read out of thickness at quartz monitor caused by material reaching it from the source of another material is presented in percents of the thickness of the actual material that was evaporated.

To take into account this cross-talk, set values for minimum (r_m) and maximum (r_M) rates of deposition for process where two materials will be co-deposited must be calculated. The rate of deposition read out at QM (r_i, $i=1$ for SiO_2, $i=2$ for Nb_2O_5) will be a sum of the real rate of deposition of the given material (r_{i0}) and the corresponding percent (A_i) of the real rate of another material:

Equation 47.
$$r_1 = r_{10} + A_1 r_{20}$$
$$r_2 = r_{20} + A_2 r_{10} .$$

If the real minimum and maximum rates are 1.2 nm/s and 0.2 nm/s, then in the case of depositing the mixture with the lowest refractive index n_m (r_{10}=1.2 nm/s, r_{20}=0.2 nm/s) read out values will be r_1=1.216 nm/s and r_2=0.218 nm/s. In the case of the maximal refractive index n_M (r_{10}=0.2 nm/s1.2 nm/s) read out values will be r_1=0.295 and r_2=1.203 nm/s. For the sake of simplicity and to keep the sum of the rates constant, the range of the rates was set to 0.3 nm/s to 1.2 nm/s, that, according to the Equation 47, gives real rates 0.205-1.178 nm/s for SiO_2 and 0.282-1.183 nm/s for Nb_2O_5. Therefore, the total rate during deposition of a ramp would vary between 1.382 nm/s and 1.472 nm/s that gives 1.427 nm/s for the complete ramp. The rates of deposition recorded during the process should be corrected to account for the range of the real rates for the given material.

According to the Lorentz-Lorenz formula, if the volume fractions are related to the rates of deposition as:

Equation 48.
$$f_{v1} = \frac{r_{10}}{r_{10} + r_{20}}, \; f_{v2} = \frac{r_{20}}{r_{10} + r_{20}},$$

with n(SiO_2) = 1.463 and n(Nb_2O_5) = 2.322 at 570 nm, the minimum and maximum refractive index that can be expected in a mixture are 1.589 and 2.15, respectively. Comparison with the refractive indices obtained using Bruggeman formula, or real rates ranging 0.3-1.2 nm/s, in the absence of cross-talk, is shown in Table 6.

Table 6. Comparison of expected minimum and maximum refractive indices of the mixtures, based on different models

	Lorentz-Lorenz	Bruggeman	no cross-talk, Lorentz-Lorenz
n_m	1.589	1.613	1.594
n_M	2.15	2.191	2.095

4.1.1.2. Radio frequency magnetron-sputtering

The radio frequency magnetron sputtering samples were produced using a laboratory coater designed and constructed at Fraunhofer IST, Braunschweig, Germany. The chamber can be equipped with up to five 4" magnetron round-sources (GENCOA, Ltd.) with three sources directed towards the substrate and allowing co-deposition from up to three target materials. For the coating experiments ceramic target materials were used (SiO_2 and Ta_2O_5). The desired material composition was achieved by variation of the power ratio of the two sources and thus the individual deposition rates of each component of the mixture. During the processes a constant total power of 800 W as well as constant gas flows (59 sccm for Ar and 4 sccm for O_2, with purities 99.998% for Ar and 99.995% for O_2) were maintained. The O_2-gas flow was necessary for the realisation of a stoichiometric Ta_2O_5 component of the mixture.

The calibration procedure used for the rates and refractive indices of the various material mixtures is quite comparable to the one described for EBE. Single thick layers were realised and analysed using variable angle spectroscopic ellipsometry. The data acquired using this analysis, together with process parameters (mainly gas flows and power ratio), were then compiled into a material database. The software controller of the deposition plant can use this database to generate a deposition recipe. For the presented depositions no *in-situ* monitoring of film properties or deposition rates was used.

4.1.1.3. Ion beam sputtering

The ion beam sputtering samples were produced by the rebuilt Varian 3125 deposition chamber in Laser Zentrum Hannover, Germany, which is equipped with a radio frequency ion source[84]. Argon ions are accelerated to energy values around 1.2 keV for reactive sputtering from metallic targets. In this setup the target materials silicon and titanium are arranged side by side on the cooling body and are mounted on a linear translation stage[85]. Thus, both materials can be sputtered simultaneously. The position of this zone target with respect to the ion beam defines the concentration of the oxide mixtures

of SiO_2 and TiO_2, as the individual sputter rates superpose. Since the gradient refractive index layers from the design are approximated with thin sublayers of constant refractive index for the purpose of deposition by this technique, the target in not moving in continuous, but in step mode. The resulting coatings are, in fact, quasi-rugates.

The reactive process for film growth is operated at a pressure of $3x10^{-4}$ mbar. In this way an arbitrary refractive index from pure SiO_2 to pure TiO_2 can be realised with deposition rates between 0.06 and 0.02 nm/s and sufficient homogeneity on substrates with diameter up to 25 mm. A shutter is protecting the substrates, when the target is preconditioned with the ion beam.

The implemented *in-situ* broad band CCD-monitoring system[86] records calibrated transmittance spectra directly on the rotating substrate. The corresponding spectra in a range from 475nm to 950 nm are processed to continuously calculate the actual layer thickness and thus the layer termination points.

4.1.2. Deposited samples

In order to determine the refractive index and rate of deposition r at every moment of the film growth, it was necessary to perform characterisation of $n(\lambda)$ and calibration of rates for individual materials prior to the deposition of the coating by EBE. A thick single layer of each material has been fabricated for this purpose, varying deposition rates linearly and periodically between 0.2 nm/s and 1.2 nm/s during the deposition. After characterisation of refractive indices and rates of deposition, tooling factors for quartz monitors were determined and thus calibration of rates was performed.

Sample with twenty successively increasing and decreasing volume fraction of Nb_2O_5 ($f_v(Nb_2O_5)$), i.e. with ten periods, has been deposited to check the operation of the evaporation plant for co-deposition of two materials and check if the refractive indices at the beginnings and ends of ramps, same as thickness of ramps, correspond to the expected values. By the optical performance, this sample should behave as a mirror due to its structure that is similar to the classical HL quarter wave mirrors.

After the refinement of the deposition parameters (tooling factors of lateral quartz monitors and time for each ramp in the design), hybrid antireflective coating has been deposited. The n_M and n_m in the design have been transferred to deposition parameters by identifying μ in the Equation 38 with $f_v(Nb_2O_5)$, related with rates of deposition by Equation 46. In this way linear effective medium theory has been applied as connection between design and deposition. The refractive indices in the intermediate points were to be produced by varying $f_v(Nb_2O_5)$ linearly since only linear variation of deposition rates is possible in the deposition plant that was used.

The spectral performance of thus obtained hybrid antireflective coating has been compared with the performance of the samples deposited by the other two techniques. The material combinations used by these techniques were Nb_2O_5/SiO_2, TiO_2/SiO_2 and Ta_2O_5/SiO_2, respectively. Spectral performances of one-side and both-side coated samples have been compared to the corresponding theoretical spectra of the designed profile. For radiofrequency magnetron-sputtering an additional, thicker design, having even better performance, has been prepared as well. To check the real benefits of this more complex coating, once when it had been fabricated, its performance has been compared to the sample with the simpler (thinner) coating. Also, the reproducibility of results for each process has been verified.

Finally, five mixture samples of constant refractive index through the layer, with different concentration of SiO_2 were deposited in order to check experimentally the effective medium theory that best describes Nb_2O_5 – SiO_2 mixtures.

In each EBE deposition process typically 3 kinds of substrates have been used: BK7 glass, Suprasil and silicon wafer chunk.

4.1.2.1. Nb_2O_5 and SiO_2

Layers of Nb_2O_5 and SiO_2 have been deposited with constant rates of deposition and used for determination of refractive index of pure materials that would later be used in optical characterisation of deposited rugate and hybrid systems. They were also used for determination of tooling factors for the third quartz monitor, positioned at the centre of calotte, which was controlling the thickness of pure (non mixed) layers. The recorded rates of deposition during growth of these two samples are presented at Figure 27. The difference in stability of the rates for the two materials is obvious. As mentioned before, SiO_2 is the material that sublimes erratically when evaporated by electron beam.

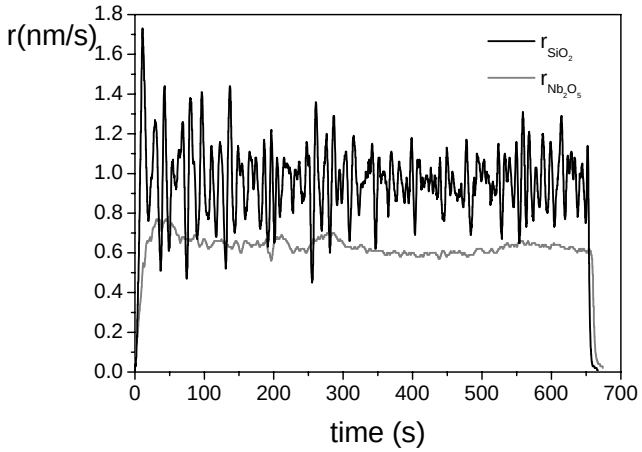

Figure 27. The rates of deposition of Nb_2O_5 and SiO_2 during growth of pure material layers. The data were recorded each 0.2 s.

4.1.2.2. Sample with ten periods

A sample consisting of ten periods of increasing and decreasing refractive index is deposited to check the performance of system for deposition and optical properties of the grown rugate. The time of deposition for single ramp was 55 s. The recorded rates of deposition during growth of this sample are presented at Figure 28.

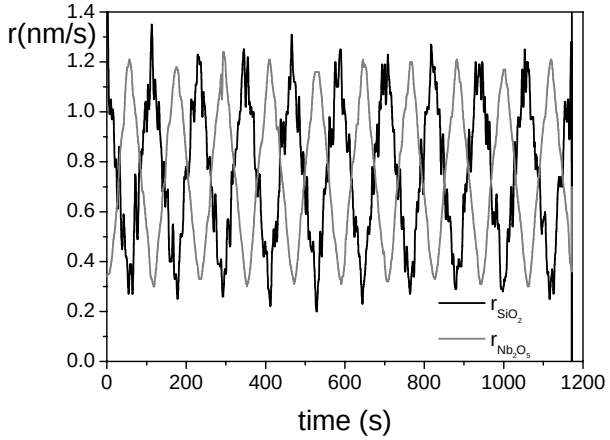

Figure 28. The rates of deposition of Nb2O5 and SiO_2 during growth of the sample with 10 periods. The data were recorded each 0.2 s.

4.1.2.3. Hybrid AR coating

The deposition parameters corresponding to the hybrid antireflective design are given in Table 7. The rates of deposition of individual materials recorded during the process are presented in Figure 29.

Table 7. The parameters for deposition of hybrid AR coating

Layer	Thickness (nm)	Deposition time (s)
A	-	78
B	-	70
C	-	23
D	-	55
E(Nb_2O_5)	75.48 (central QM)	
F(SiO_2)	95.55 (central QM)	

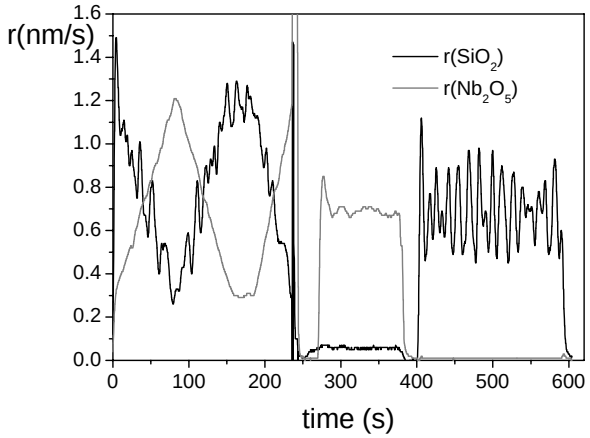

Figure 29. The rates of deposition of Nb2O5 and SiO_2 during growth of the hybrid antireflective sample. The data were recorded each 0.2 s.

4.1.2.4. Comparison of samples prepared by different techniques

Samples with the thinner design (Figure 15) are deposited with all three techniques, one side and both side coated. The quality of their performance can be compared by evaluating standard deviation values of the measured spectra from the theoretical data, defined in the similar way as in Equation 46, only, the target values of reflectance are replaced by experimental values in the range of wavelength 480-680 nm, measured in steps of 2 nm and angles of incidence are here 0^o and 45^o.

Selected deposition parameters for the fabricated hybrid antireflection samples are presented in Table 8. The coating was deposited on BK7 glass substrates on one and on both sides, respectively. *Ex-*

*sit*u transmittance and reflectance measurements were taken at 0^o, as well as *s* and *p* polarisations at 45^o angle of incidence. More details about the optical measurements are given later.

Table 8. Characteristics of the deposition techniques

Deposition technique	Deposition rate (nm/s)	Deposition time (min)	Thickness control	Optical monitoring	Estimated thickness deviation	Estimated refractive index deviation
EBE	1.4 nm/s	9	time	no	6 %	0.6 %
RFS	0.14 nm/s	89 (thinner) 114 (thicker)	time	no	1.5 %	0.25%
IBS	0.035 nm/s	260	optical thickness determination	yes	2%	0.2%

Table 8. Estimated deviations in thickness and in refractive indices correspond to mixture layers.

Reflectance spectra of samples with hybrid antireflection coating deposited at one and both sides of the substrate are presented in Figure 30 and Figure 31, respectively. Theoretical curves of the corresponding designs obtained with the design software are also shown for comparison. Good matching of the theoretical and experimental curves for angle of incidence 45^o indicates also that the specification for 50^o angle of incidence ($R_s = R_p$) is well met. Calculated values of deviations of measured spectra from the theoretical data for both sets of samples (one-side and both-side coated) are shown in Table 9.

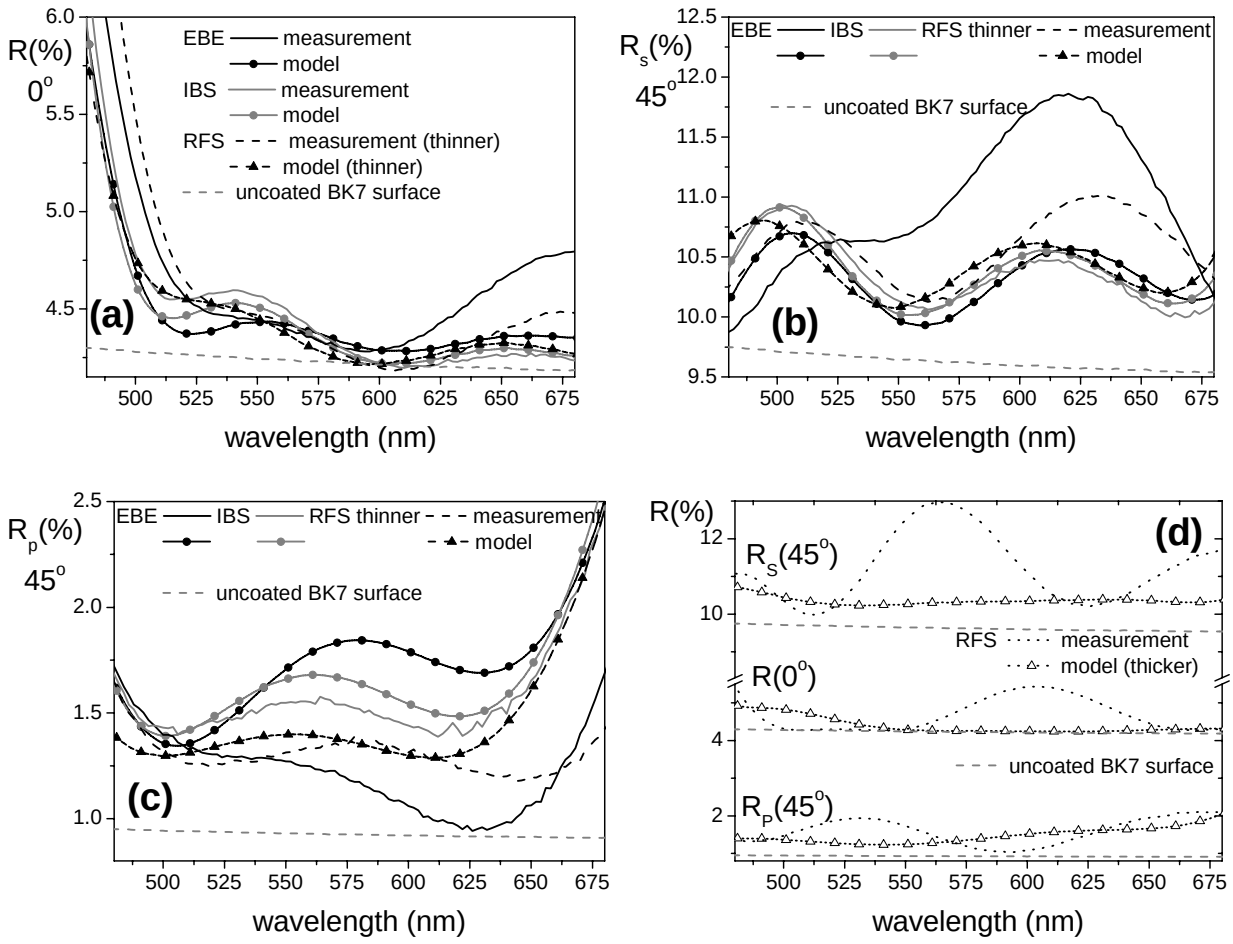

Figure 30. Experimental and theoretical reflectance spectra of one-side coated samples. Figure 30 (a), (b) and (c) are showing spectra of the thinner coatings and designs, at 0^o and *s* and *p* polarisation at 45^o angle of incidence, respectively. Reflectance of one uncoated glass surface is also shown for comparison. On Figure 30(d) corresponding spectra for the thicker RFS coating and design are presented.

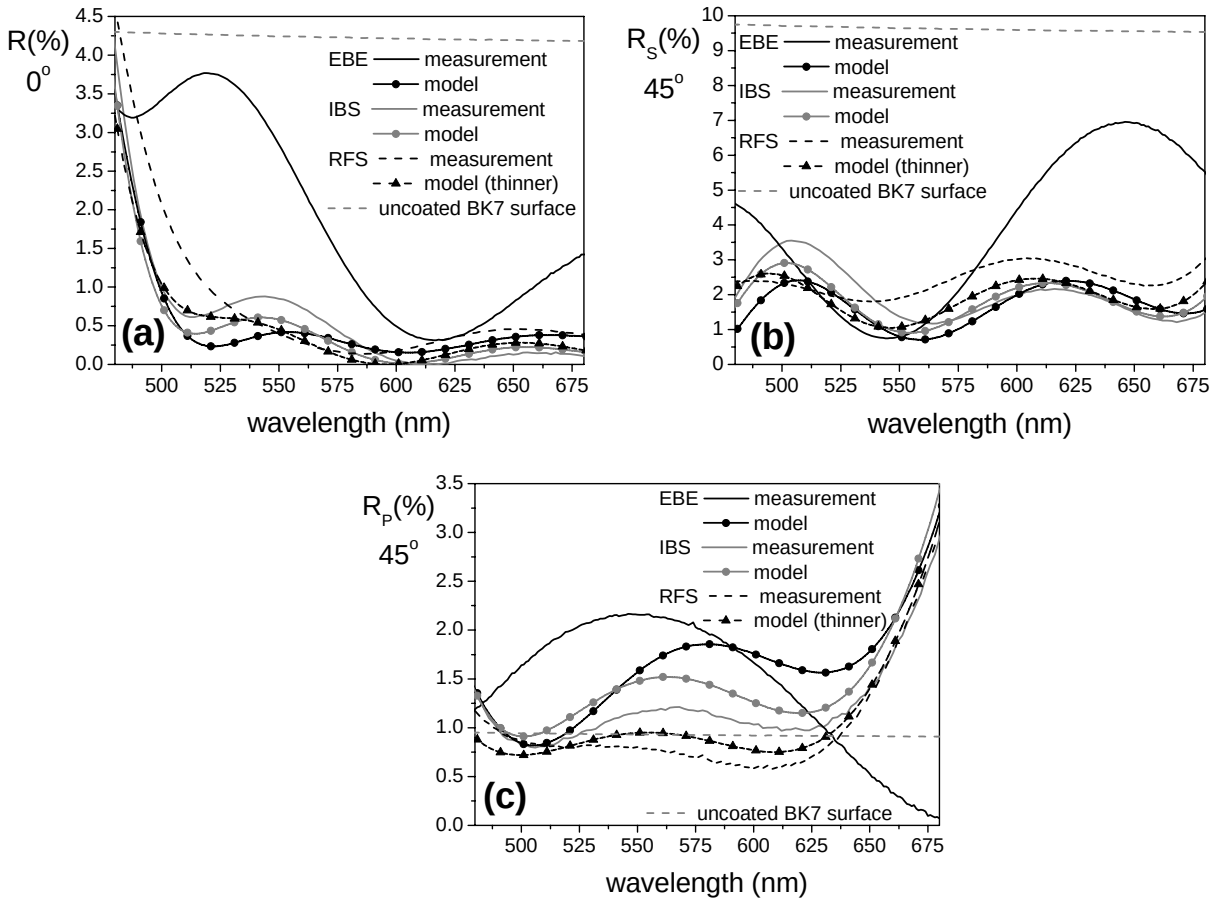

Figure 31. Experimental and theoretical reflectance spectra of both-side coated samples. Figure 31 (a), (b) and (c) are showing spectra of the thinner coatings and designs, at 0° and *s* and *p* polarisation at 45° angle of incidence, respectively. Reflectance of one uncoated glass surface is also shown for comparison. Note higher discrepancy between model and reflectance for EBE both-sides coated sample (most clearly seen at Figure 31 (a)) compared to the discrepancy for EBE one-side coated sample (Figure 30 (a)) that originates from accumulation of error (errors in second coating added to the errors in first coating). (See also Figure 32).

To check the reproducibility of the results for each technique, reflectance spectra of the samples coated with the identical design, but made in different runs were compared. They are represented in Figure 32 and deviations of one from the other, δ_{1+1}, are shown in Table 9. IBS samples show much better reproducibility then the others.

Table 9. Comparison with theory and reproducibility

Technique		$\delta_{1\ exp}$	$\delta_{2\ exp}$	$\delta_{1+1\ exp}$
EBE		0.107	0.253	0.047
RFS	thinner	0.064	0.079	-
	thicker	0.132	-	0.138
IBS		0.015	0.051	0.006

Table 9. $\delta_{1\ exp}$ stands for deviation of the reflectance of the best one-side coated sample for a given technique from corresponding theoretical reflectance of the model (presented in Figure 30). $\delta_{2\ exp}$ denominates the corresponding parameter for samples coated on both-sides (presented in Figure 31). $\delta_{1+1\ exp}$ is the deviation between performances of two samples coated on one side but in different runs (presented in Figure 32). $\delta_{1\ exp}$ and $\delta_{2\ exp}$ are calculated in the range 480-680 nm and $\delta_{1+1\ exp}$ in the range 400-950 nm. The high deviations of the RFS thicker samples may be attributed to spectral shifts (see Figure 32) induced by the different thickness of the coatings.

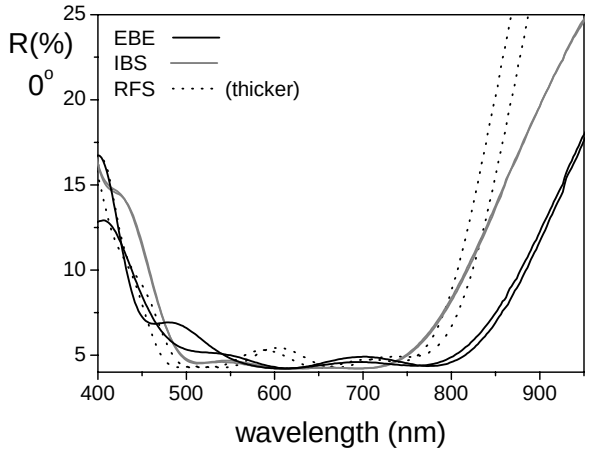

Figure 32. Reproducibility of the results: comparison of spectra of two one-side coated samples produced with the same technique but in two different runs; presented for each of the techniques.

4.1.2.5. Mixture layers

Mixture layers of constant composition through thickness, differing in ratio of SiO_2 to Nb_2O_5 were deposited to verify which EMT is the best for characterisation of Nb_2O_5 – SiO_2 mixtures. For this purpose five coatings have been manufactured with $f_v(SiO_2)$ ranging from approximately 0.2 to 0.8 in more or less equal steps. Deposition rates for the sample with maximum (n_M), a bit lower than maximum (n_{M-x}), medium (n_{MED}), a bit higher than minimum (n_{m+x}) and minimum (n_m) content of Nb_2O_5 are shown in Table 10. In the same Table is presented $f_v(SiO_2)$ calculated from deposition rates

recorded during the deposition and cross-talk corrected. The expected thickness was calculated in the same way. Deposition time for all the samples was 310 s.

Table 10. Set rates of deposition, $f_v(SiO_2)$ and thickness d of the mixture samples calculated from cross-talk corrected recorded rates of deposition

Sample	$r_{set}(Nb_2O_5)/r_{set}(SiO_2)$ (nm/s)	$f_v(SiO_2)$ from $r(t)$	d from $r(t)$ (nm)
n_M	1.2/0.3	0.1967	446.91
n_{M-x}	0.95/0.35	0.3570	439.63
n_{MED}	0.75/0.75	0.4855	439.76
n_{m+x}	0.55/0.95	0.6151	428.10
n_m	0.3/1.2	0.7839	429.02

4.2. Spectroscopic optical characterisation

Spectrophotometric and ellipsometric measurements under different angles of incidence were performed for optical characterisation of the deposited samples. Optical characterisation has always started from the simplest initial model, parameters were introduced and set independent gradually and limits to their values were set whenever possible.

Different effective medium theories for material mixtures have been tested in optimisation. Finally, it was shown that the lowest values of merit function were obtained when LL model is applied. Thus, it was shown that the starting assumption for relating design and deposition, that linear variation of volume fractions gives linear variation of refractive index, is wrong. The presented models are using LL EMT.

The model obtained from optical characterisation of EBE antireflective sample using reflectance, transmittance and ellipsometric measurements was compared with the one obtained using only spectrophotometric measurements and the one obtained from secondary ion mass spectrometry based initial design to test the limitations in choice of experimental data and initial designs.

The concavity of the curve representing dependence of refractive index with volume fraction that corresponds to LL model has been experimentally proven for the combination of Nb_2O_5 and SiO_2 from optical characterisation of the five mixture samples.

4.2.1. Transmittance, reflectance and ellipsometric measurements

Spectrophotometric measurements were performed with a Perkin Elmer Lambda 900 spectrophotometer. A VN-attachment allowing absolute measurement of reflectance without moving the sample after the transmittance measurement has been used. Reflectance and transmittance were measured in steps of 2 nm: average R and T measured at angle of incidence of 6 degrees and R_s, R_p, T_s and T_p at 45 degrees. Errors in R and T measurements at normal incidence were 0.2%, and for measurements at 45 degrees 0.5%. Ellipsometry was used for the hybrid AR samples. Measurements of spectra of ellipsometric Δ and Ψ functions were performed with a standard SENTECH SE800 null ellipsometer with microspot (200μm). Usage of microspot, together with thickness of the glass (2mm) results in measurements without the contribution of reflection from the back side of the substrate. Ellipsometric measurements were done in the spectral range 400-850 nm at the angles of 50^o, 55^o and 60^o, in 575 wavelength points per angle. These angles were chosen for the ellipsometric functions to present maximum amplitude of their interferential fringes. In the optimisation process $cos\Delta$ and $cos2\Psi$ were considered. The error of these ellipsometric quantities was estimated to be 0.0018 for $cos\Delta$ and 0.0072 for $cos2\Psi$.

4.2.2. Substrates: BK7 and Suprasil

The dispersion of the real part of refractive index for BK7 and Suprasil, determined from spectrophotometric measurements, is shown in Figure 33.

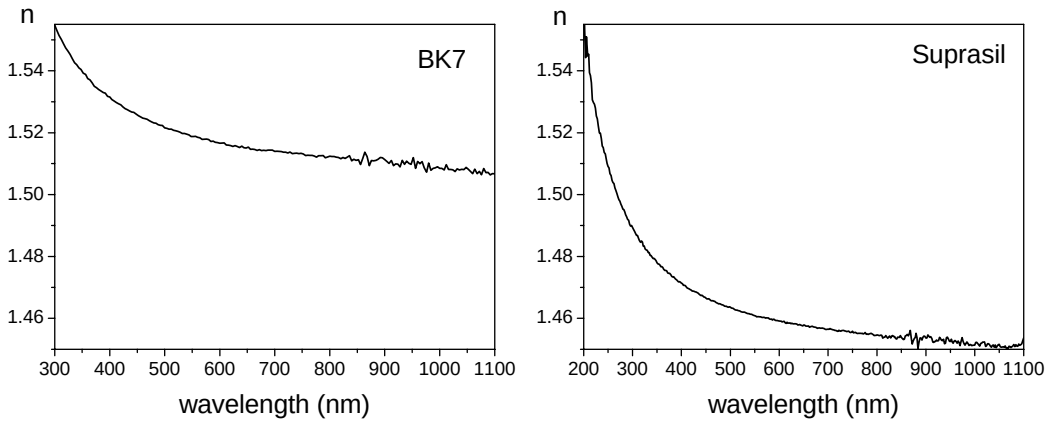

Figure 33. Refractive index for substrate materials BK7 and Suprasil.

BK7 and Suprasil substrates used for sample deposition were round, both side polished, 1 inch in diameter. BK7 substrates were 2 mm and Suprasil 1 mm thick. Thickness of silicon chunks was 0.4 mm.

4.2.3. Characterisation of the deposited samples

4.2.3.1. Nb_2O_5 and SiO_2

Measurements of reflectance and transmittance under normal incidence in the range 350-950 nm, each 2 nm, were used for optical characterisation of these samples. The samples deposited at Suprasil were measured. The obtained refractive index parameters and thicknesses are presented in Table 11. The thicknesses that are obtained from rates of deposition are 416.2 nm for Nb_2O_5 and 627.2 nm for SiO_2. The results of optical characterisation suggest that the real average rates of deposition were 0.675 nm/s for Nb_2O_5 and 0.775 nm/s for SiO_2 (see Figure 27). The measurements, together with fittings and optical constants, are presented in Figure 34 and Figure 35.

Table 11. Results of optical characterisation for Nb_2O_5 and SiO_2

Material	Thickness (nm)	$\Delta n/\overline{n}$ (%)	Parameters	n (at 570 nm)
SiO_2	507.3	-1.022	$A = 1.454$	1.4667
			$B = 4127$ nm^2	
			$C = 625.8$ nm^4	
Nb_2O_5	450.3	-2.707	$E_g = 3.302$ eV	2.2838
			$E_o = 4.75$ eV	
			$A = 115.7$ eV	
			$C = 1.085$ eV	
			$\varepsilon_\infty = 2.66$	

Table 11. The dispersion model used for Nb_2O_5 is Tauc–Lorentz and for SiO_2 Cauchy. $\Delta n/\overline{n}$ is degree of inhomogeneity of a layer defined by ratio of the difference of refractive index next to the air and the one next to the substrate and mean refractive index of the whole layer, given in percents.

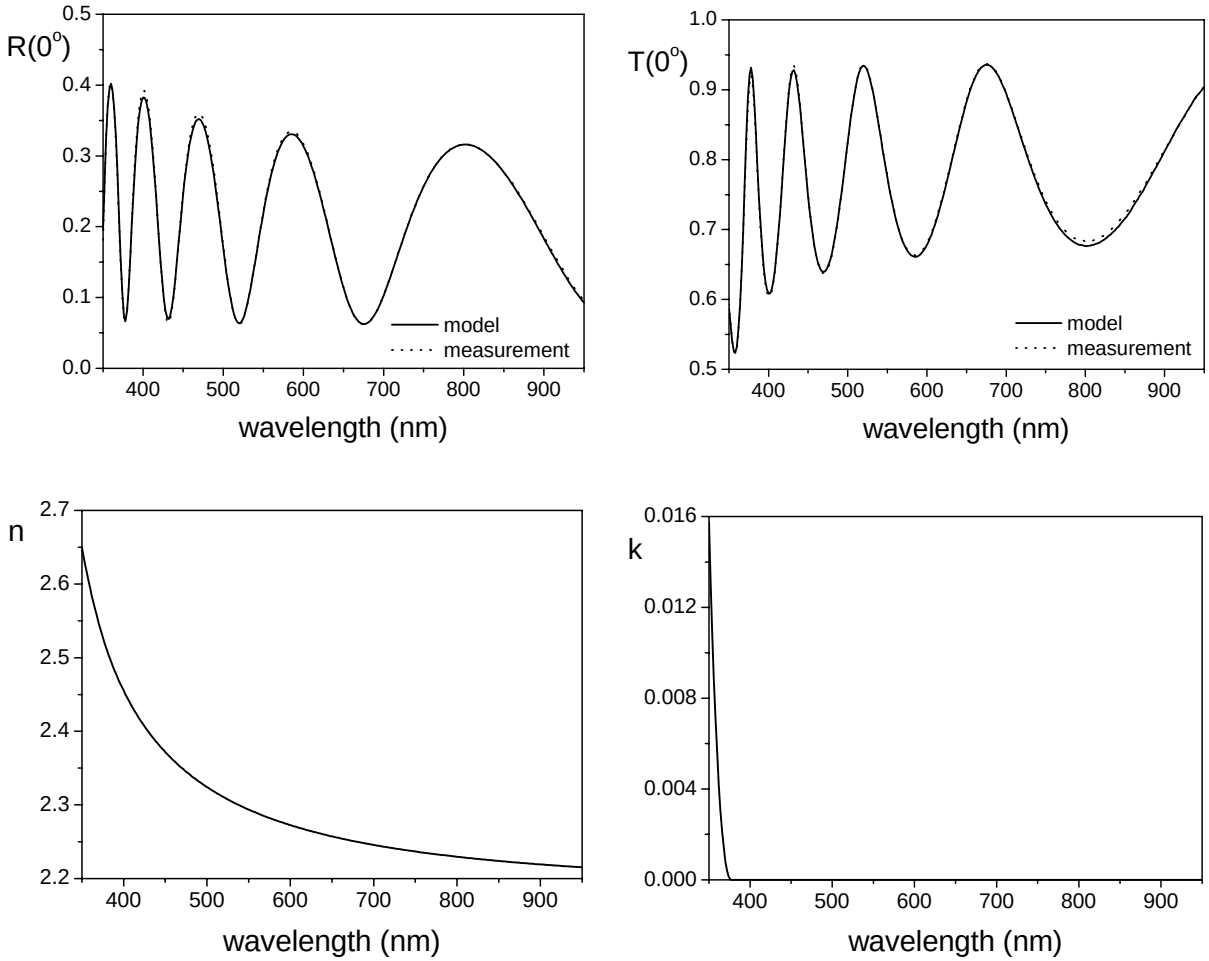

Figure 34. Measurements, fits and dispersion of refractive index and extinction coefficient of Nb_2O_5 layer.

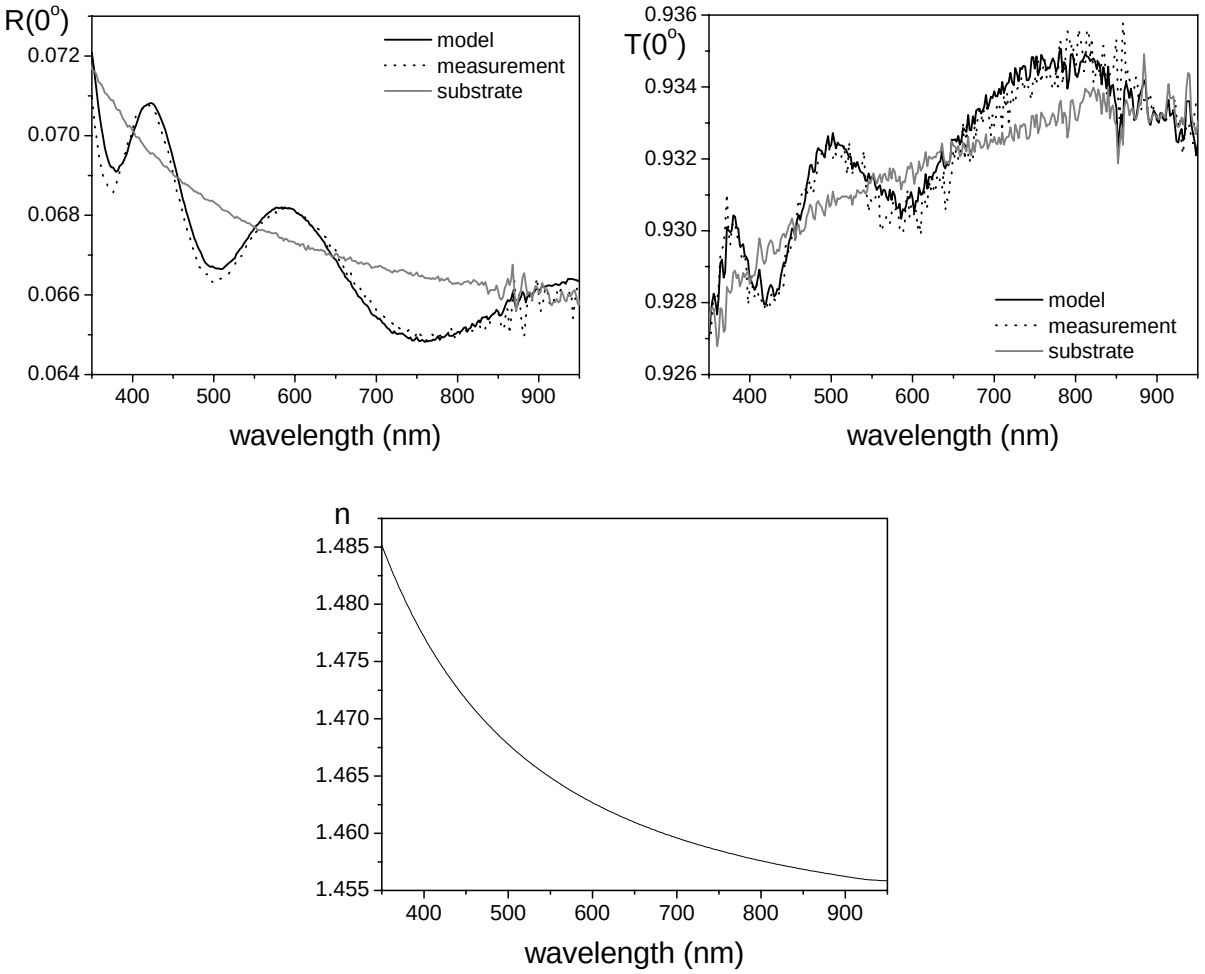

Figure 35. Measurements, fits and dispersion of refractive index of SiO_2 layer.

4.2.3.2. Sample with ten periods

Measurements of reflectance and transmittance under normal incidence, same as *s* and *p* polarisation of reflectance and transmittance at incidence of 45° in the range 400-900 nm, each 2 nm, were used for optical characterisation of this sample. The sample deposited at Suprasil was measured. Refractive indices obtained from pure material layers and expected refractive index profile (thickness of each ramp 78.5 nm, n_m = 1.5747 and n_M = 2.1481, according to LL model with cross-talk correction and results for refractive indices obtained from the samples of pure materials) are used as initial solution. Ramps were divided into 5 sublayers. At first, thicknesses, n_{m} and n_M of all the ramps, except the first and the last due to the instabilities in deposition rates, were linked to maintain the same value during the optimisation, but later they were set free independently to obtain satisfying results. Thus merit function has decreased 30%. The obtained total thickness of the coating is 1591.72 nm. The thicknesses

of each ramp vary in the range 69.4 - 92.5 nm, while n_m and n_M vary in the range 1.6129 – 1.6284 (1.4851 at the beginning of the first ramp) and 2.2554 – 2.27595 respectively. The comparison of the expected profile (design), the one obtained from optical characterisation (model) and the refractive index profile obtained from rates of deposition after cross-talk correction is presented in Figure 36. In Figure 37 measurements and corresponding fittings are shown. The discrepancies of parameters of model and the profile obtained from rates of deposition from the values expected by design, presented as errors in percent, are shown in Table 12.

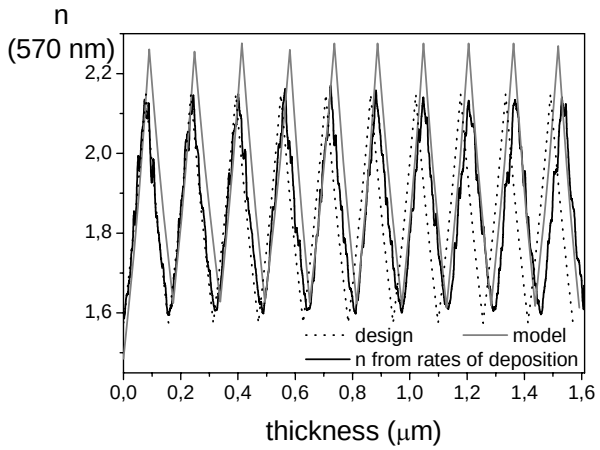

Figure 36. Refractive index profiles of the sample with ten periods: expected, modelled and calculated from rates of deposition after cross-talk correction.

Table 12. Discrepancies of the obtained profiles from the design

	Error(d) %	Error(n_M) %	Error(n_m) %
Model	1.40	5.67	2.94
Profile from *r(t)*	2.43	0.33	1.67

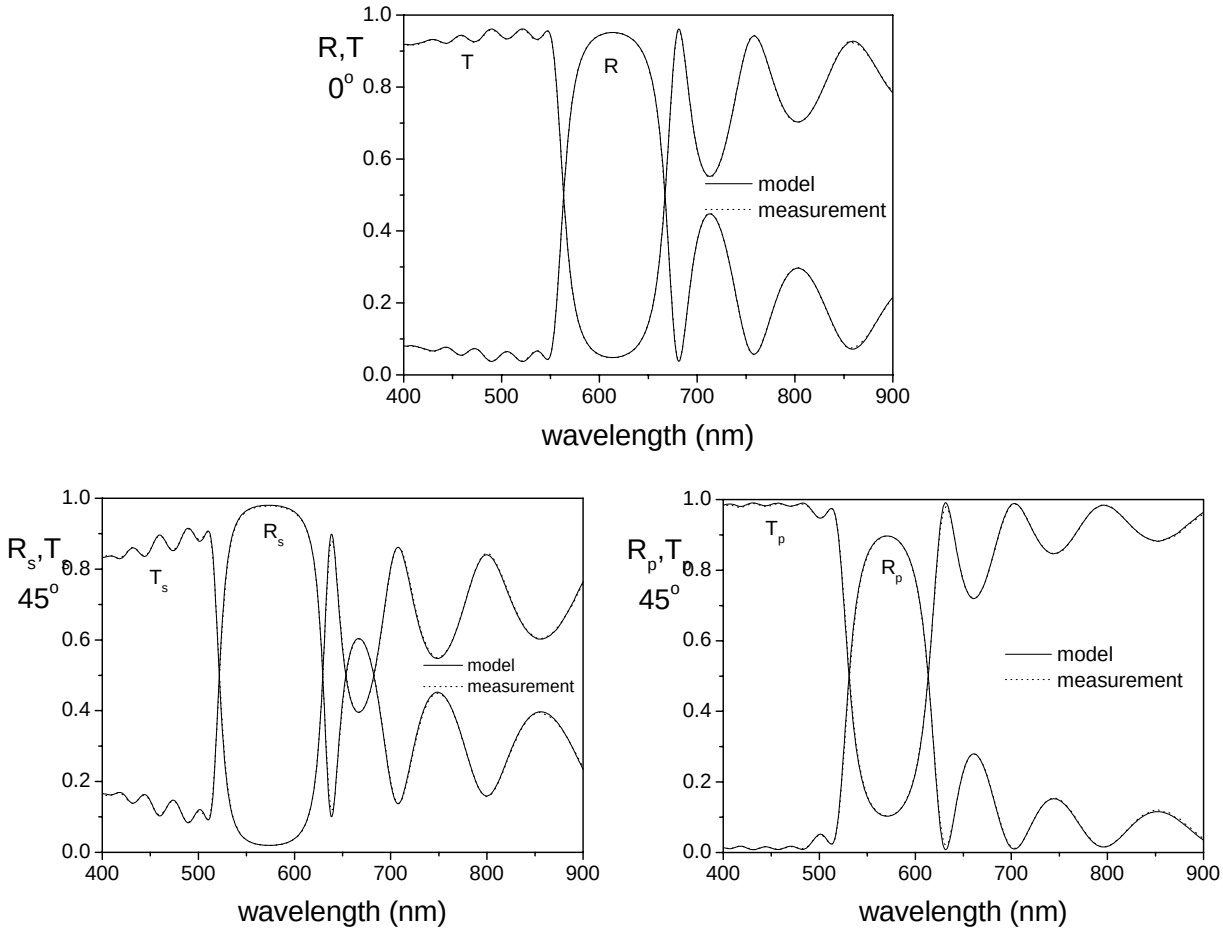

Figure 37. Measurements and fits of the rugate sample with 10 periods.

4.2.3.3. Hybrid AR samples

For optical characterisation of hybrid AR samples reflectance and transmittance measurements (normal incidence, *s* and *p* components at 45°) were combined with ellipsometry.

The original targeted designs have been taken as starting designs for optical characterisation defining the initial values of the parameters to be optimised. Each ramp in EBE and RFS sample was divided into 8 sublayers. In this way, only starting and ending volume fractions of one material, same as the thickness of the ramp, were optimised. Initially, at the beginning of the optimisation procedure, thickness limits of RFS and IBS samples were set to 3% and of EBE to 6% of the design's thickness, that correspond to the estimated deviation in thickness for each technique of deposition (Table 8). In the case of EBE sample, higher errors are expected due to the fact that rates of deposition were controlled by quartz monitor only, because of high deposition rates compared with the other two

techniques and because of instabilities of these rates[33] due to the non-uniform evaporation of the materials from the rotating crucible. Refractive indices of the pure materials (pure, in the sense that they were not mixtures of materials prepared in a process of co-deposition) obtained previously from the optical characterisation of the single material layers were used. In the next step, in order to improve the data fits, the optimisation of the optical constants of the materials by using dispersion formulas was allowed. For the case of the RFS sample, spectrophotometric measurements indicated the presence of losses (R+T<1). Since in RFS high index material data file absorption was neglected, it was included in optimisation by a dispersion formula for the extinction coefficient. Finally, the effect of removing the thickness limits of individual layers (one at the time) to improvement of quality of the fit was studied.

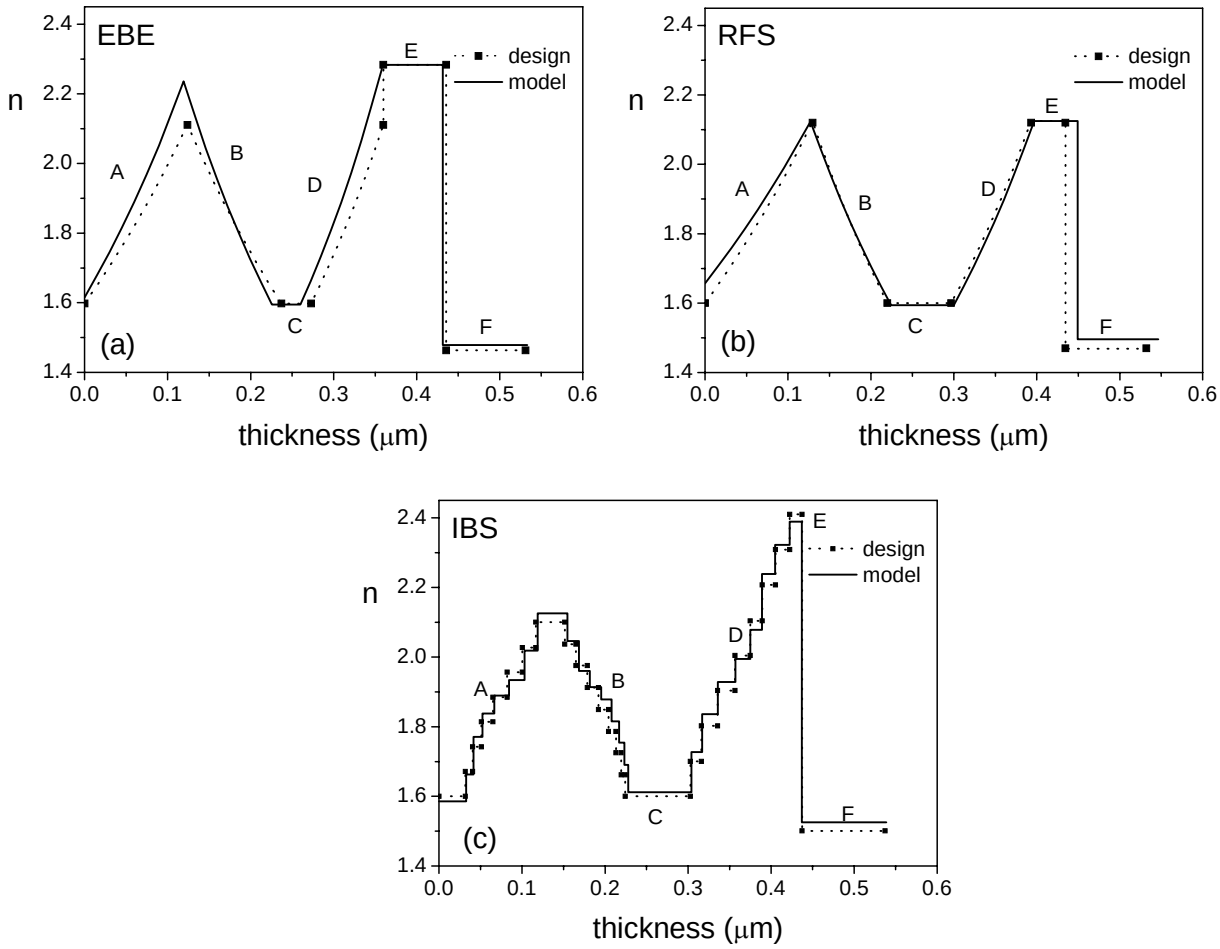

Figure 38. The optimised models of refractive index profiles and the original designs that were used as starting models.

For the purpose of detection of deposition errors from comparison of optical characterisation results with the design, spectral performance of the design has been recalculated taking into account Lorentz-Lorenz model in calculation of intermediate refractive indices in the ramps. The corner points remain the same since maximum and minimum volume fractions have been calculated to give the n_m and n_M values of the original design (i.e. n of each step in IBS design). The difference in the spectral performance of the models originates, in fact, from the different values of intermediate refractive indices. Instead of linear ramps of refractive index LL model gives slightly concave shape[87]. Recalculation of spectral performance of design using LL model ensures that the discrepancies with the performance of model originate not from the wrong initial assumption of validity of linear model, but really only from deposition errors or limitations of the model to describe the real sample as well as possible.

The optimised models of refractive index profiles that are obtained in the process of optical characterisation, together with the original designs that were used as starting models, are shown in Figure 38 for all three samples. In Table 13 numerical values of materials Cauchy parameters and refractive indices are presented.

Table 13. Dispersion parameters and material refractive indices

material	A	B(nm^2)	k_A	k_B(nm)	n(570nm)	k(570nm)
Nb_2O_5	data file determined from single layer				2.2838	0
Ta_2O_5	data file determined from single layer		0.00093	0.013	2.1249	9.3e-4 ±0.9e-4
TiO_2	data file determined from single layer				2.4078	0
SiO_2 EBE	1.4703	2790	0	0	1.4789 ±0.0009	0
SiO_2 RFS	1.4852	3520	0	0	1.496 ±0.001	0
SiO_2 IBS	data file determined from single layer				1.4992	0

Table 13. The dispersion formula for the refractive index was $n(\lambda)=A+B/\lambda^2$ and for the extinction coefficient $k(\lambda)=k_A \cdot exp(k_B/\lambda)$ (Equation 17 and Equation 20).

The spectral characteristics of the models, compared with the measured spectra, are given in Figure 39, Figure 40 and Figure 41.

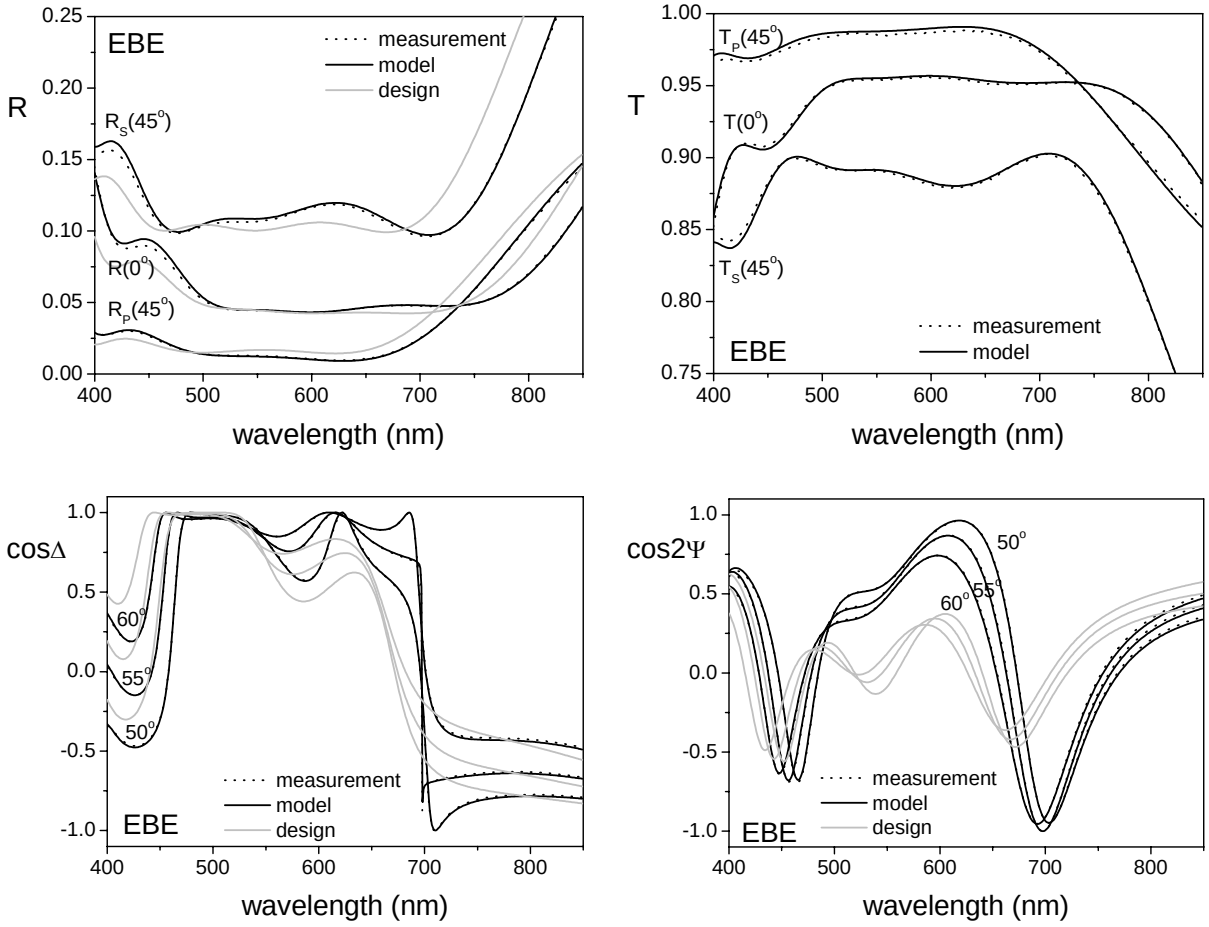

Figure 39. The spectral characteristics of the models compared with the measured spectra of the sample deposited by electron beam evaporation. Spectra of the design have been added for comparison. The back side of the substrate remained uncoated.

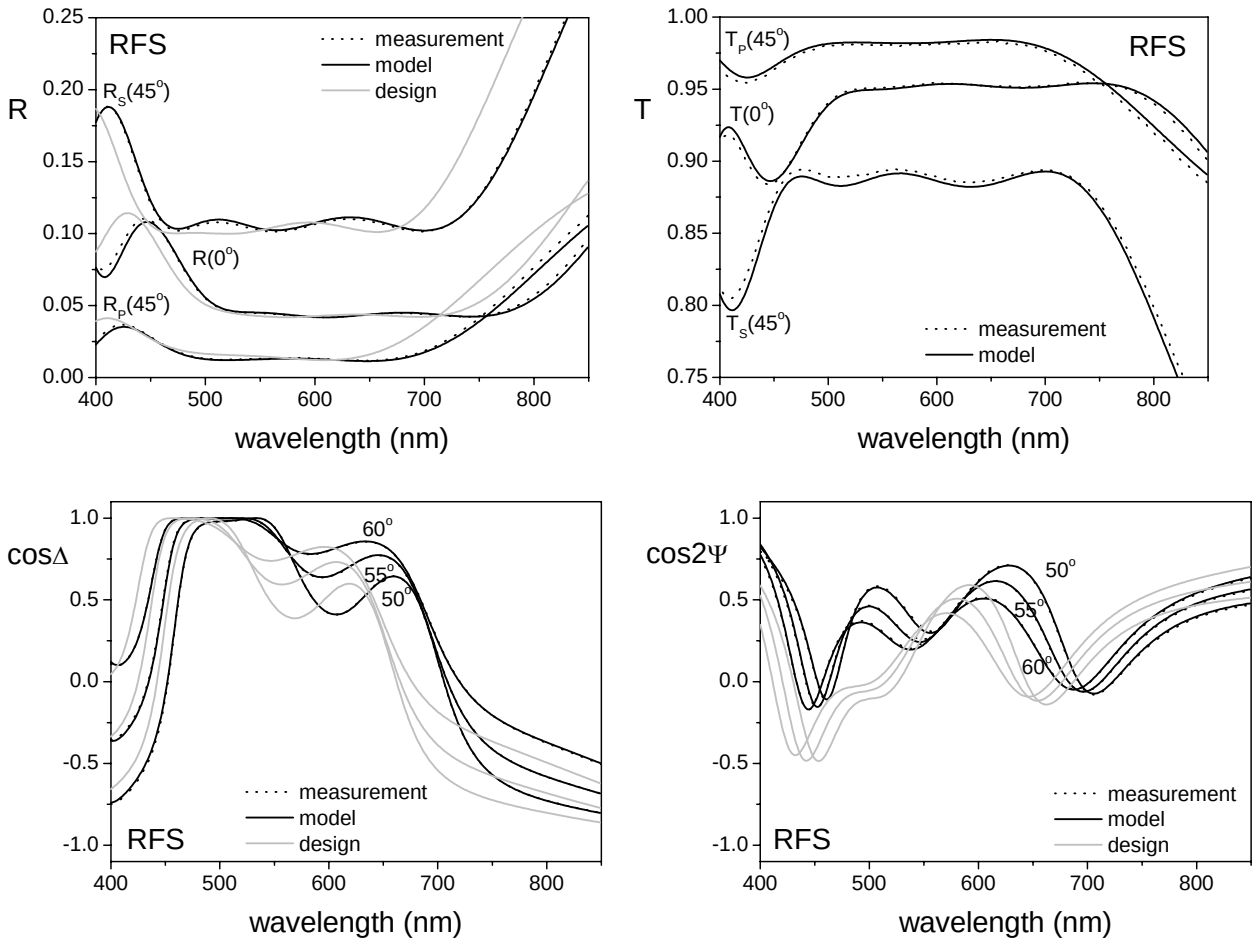

Figure 40. Spectral characteristics of the models compared with the measured spectra of the sample deposited by radio-frequency sputtering. Spectra of the design have been added for comparison. The back side of the substrate remained uncoated.

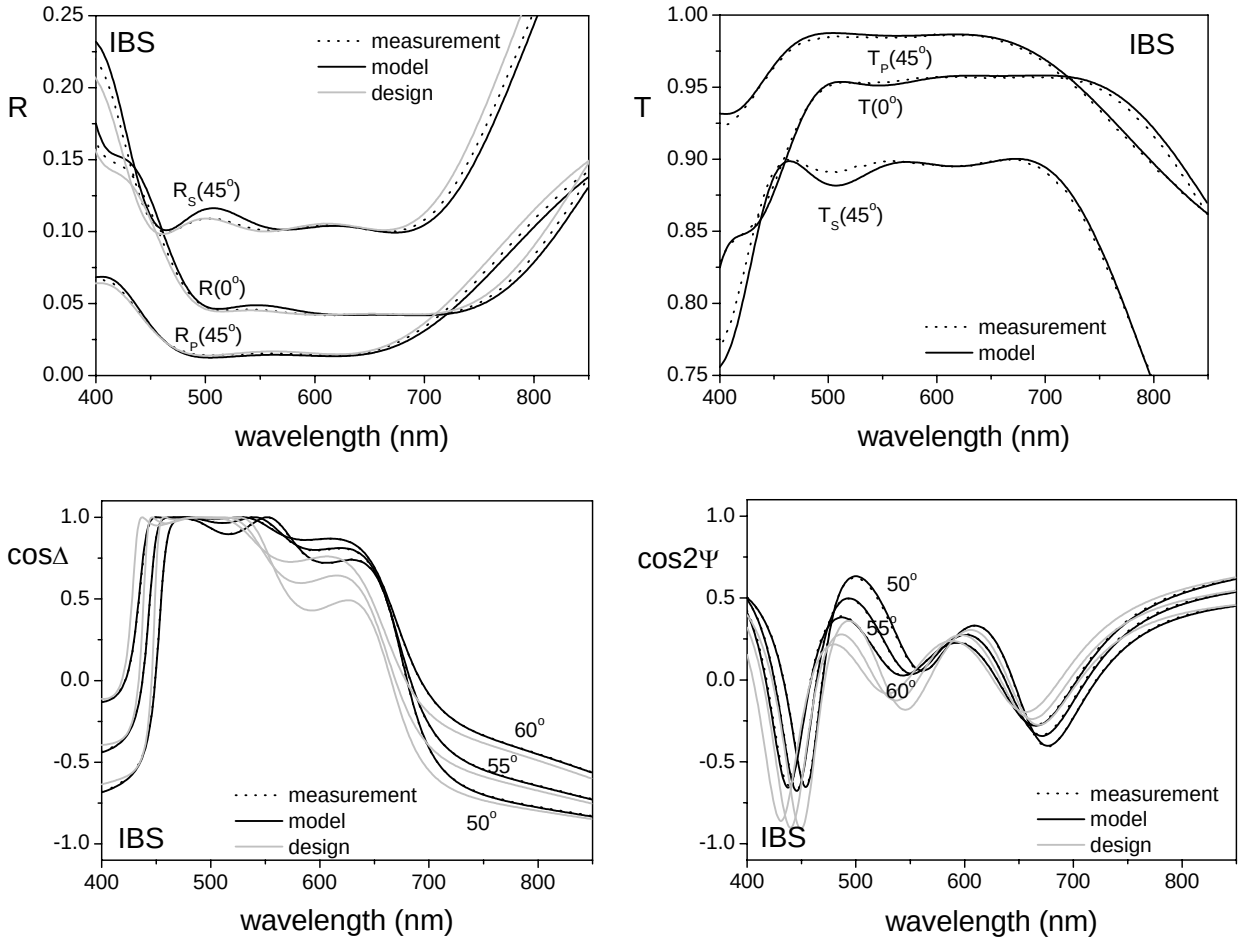

Figure 41. Spectral characteristics of the models compared with the measured spectra of the sample deposited ion beam sputtering. Spectra of the design have been added for comparison. The back side of the substrate remained uncoated.

Table 14, Table 15 and Table 16 show the comparison of designs and models, in the sense of discrepancies of thicknesses and refractive indices. Errors are calculated as the absolute value of difference of the parameter value in model and design divided by the parameter value in the design. Errors are given in percents.

Table 14. EBE discrepancies from the design (err_d, err_n)

layer	d_{design} (nm)	d_{model} (nm)	err_d (%)	n_{design} at 570nm	n_{model} at 570nm	err_n (%) at 570nm
A	124.05	118.68±0.16	4.33	1.5980	1.6153±0.0014	1.07
B	112.89	106.2±0.4	5.95	2.1110	2.236±0.003	6.00
C	35.91	34±4	6.00	1.5980	1.595±0.002	0.21
D	87.15	96.7±1.0	10.98	2.1110	2.273±0.011	7.67
E (Nb_2O_5)	75.46	72.9±1.1	3.38	2.2840	2.2840	0.00
F (SiO_2)	95.55	101.00±0.06	5.70	1.4630	1.4789±0.0009	1.06

Table 14. Refractive indices correspond to the starting refractive index of the layers. Only the thickness d_{model} of the third ramp (D) is more then 6% higher then the thickness of the original design d_{design}. Average error in refractive index is 2.7%. Error of Nb_2O_5 refractive index is 0 because it was fixed. When allowed to optimise, the quality of the fit did not improve.

Table 15. RFS discrepancies from the design (err_d, err_n)

layer	d_{design} (nm)	d_{model} (nm)	err_d (%)	n_{design} at 570nm	n_{model} at 570nm	err_n (%) at 570nm
A	129.72	126.97±0.08	2.12	1.6000	1.6568±0.0007	3.55
B	90.05	97.3±0.4	8.03	2.1250	2.125±0.002	0.00
C	76.97	76±4	1.51	1.6000	1.594±0.002	0.21
D	96.39	96.4±0.6	0.04	1.6000	1.594±0.002	0.21
E (Ta_2O_5)	41.44	52.7±0.4	27.08	2.1250	2.1250	0.00
F (S_iO_2)	97.45	97.50±0.09	0.06	1.4690	1.496±0.001	1.84

Table 15. Refractive indices correspond to the starting refractive index of the layers. The thickness of the second ramp B d_{model} is 8% higher then the thickness of the original design d_{design} and the thickness of the Ta2O5 layer is 27% higher (11 nm). Thicknesses of the other layers are within 3% of error to the starting thickness. Average error in refractive index is 2.2%. Error of Ta_2O_5 refractive index is 0 because it was fixed. When allowed to optimise, the quality of the fit did not improve.

Table 16. IBS discrepancies from the design (err_d, err_n)

layer	d_{design} (nm)	d_{model} (nm)	err_d (%)	n_{design} at 570nm	n_{model} at 570nm	err_n (%) at 570nm
A1	31.84	32.7±0.7	2.61	1.5997	1.5857±0.0002	0.90
A2	8.61	8.8±0.7	2.21	1.6715	1.6631±0.0005	0.49
A3	10.61	10.82±0.15	1.98	1.7421	1.7709±0.0017	1.65
A4	13.90	14.32±0.13	3.00	1.8144	1.838±0.003	1.34
A5	17.22	17.74±0.14	3.00	1.8849	1.889±0.004	0.26
A6	18.27	18.71±0.12	2.41	1.9570	1.934±0.004	1.16
A7	16.29	15.8±0.6	3.00	2.0276	2.019±0.005	0.42
B1	34.72	35.8±0.4	3.00	2.1005	2.126±0.003	1.21
B2	13.57	13.84±0.18	1.99	2.0367	2.0466±0.0009	0.47
B3	13.70	13.3±0.9	3.00	1.9752	1.961±0.004	0.76
B4	13.34	13.7±0.5	3.00	1.9122	1.914±0.002	0.09
B5	12.12	12.25±0.17	1.07	1.8496	1.8788±0.0011	1.60
B6	8.94	9.13±0.14	2.13	1.7868	1.8155±0.0008	1.64
B7	6.43	6.50±0.12	1.09	1.7247	1.7548±0.0014	1.74
B8	4.70	4.56±0.11	3.00	1.6618	1.6909±0.0017	1.75
C	78.47	76.1±1.6	3.00	1.5997	1.612±0.002	0.74
D1	13.39	13±1	2.99	1.7005	1.728±0.006	1.61
D2	19.54	18.9±1.4	3.00	1.8026	1.836±0.011	1.87
D3	21.00	21.1±0.6	0.71	1.9039	1.928±0.005	1.27
D4	18.12	17.7±0.5	2.21	2.0046	1.995±0.010	0.48
D5	14.63	14.3±0.6	2.39	2.1048	2.078±0.009	1.23
D6	15.88	15.6±0.5	1.7	2.2070	2.239±0.006	1.42
D7	17.49	17.56±0.17	2.09	2.3085	2.322±0.006	0.60
E (TiO2)	14.84	14.8±0.8	0.13	2.4096	2.389±0.010	0.87
F (SiO2)	99.86	101.7±0.2	1.85	1.5003	1.5252±0.0011	1.64

Table 16. Thickness of each layer is within 3% of error. Thicknesses of 10 layers have reached their minimum/maximum allowed value. There was no improvement of the fit when absorption was introduced. Average error of refractive index is 1.1%.

4.2.3.4. Optical characterisation of EBE hybrid AR sample based on initial profile from SIMS

The electron beam deposited hybrid antireflection sample has been in-depth characterised by secondary ion mass spectrometry (SIMS) at Fraunhofer IST, Braunschweig, Germany. It is the process of ion formation by bombarding the surface of the sample with a highly collimated beam of primary ions. In the sputtering process the surface emits material, a fraction of which is in the form of secondary ions. These secondary ions are measured with a mass spectrometer to determine the quantitative elemental composition of the sputtered material. A plot of the intensity of a given mass signal as a function of time is a direct reflection of the concentration of elements with depth bellow the surface.

In the Figure 42 atomic concentration through the depth of the layer is presented. The measurements were taken at each 7-8 nm of depth.

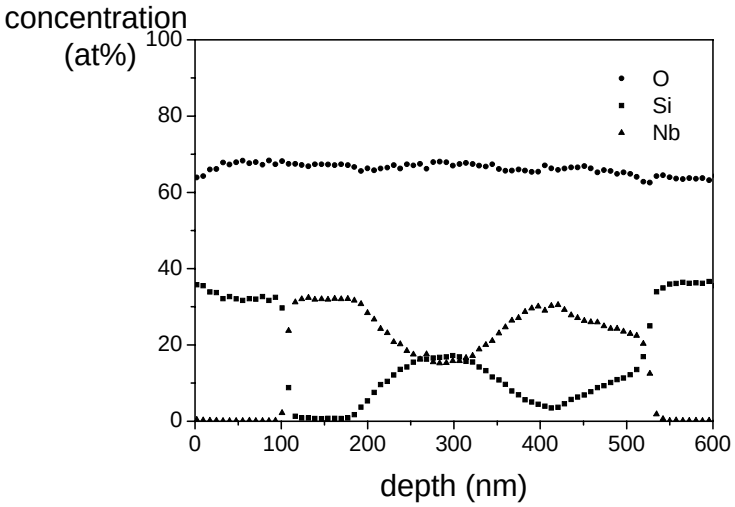

Figure 42. Concentration profile of EBE hybrid AR sample obtained by SIMS technique.

Volume fraction of Nb_2O_5 is calculated from the measured atomic concentration using

Equation 49
$$f_v(Nb_2O_5) = \frac{\frac{at\%(Nb)}{2}\frac{M(Nb_2O_5)}{\rho(Nb_2O_5)}}{\frac{at\%(Nb)}{2}\frac{M(Nb_2O_5)}{\rho(Nb_2O_5)} + \frac{at\%(Si)}{2}\frac{M(SiO_2)}{\rho(SiO_2)}},$$

where *at%* is atomic concentration given in percent, M is molar mass and ρ is density (4470 kg/m^3 for Nb_2O_5 and 2648 kg/m^3 for SiO_2). Using refractive indices from the model found from previous optical characterisation of this sample and Lorentz-Lorenz model, SIMS refractive index profile is obtained. It is compared with the design and previously found model in Figure 43.

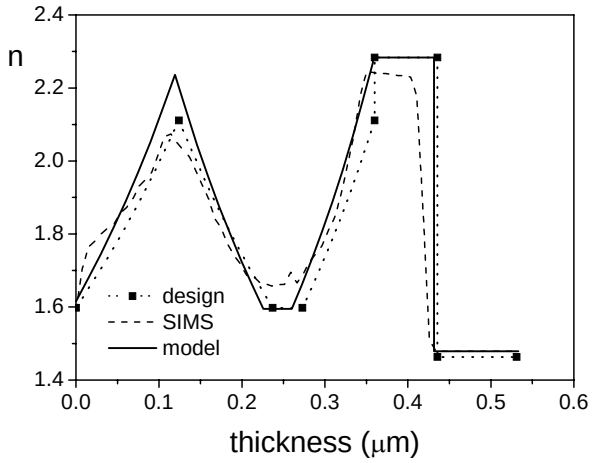

Figure 43. Comparison of SIMS profile with design and model obtained by previous optical characterisation.

The refractive index profile obtained from SIMS was used for a SIMS based initial design (Table 17) for optical characterisation of the sample. The result of optical characterisation that was performed in the same way as previously, except some limits have been broadened, is shown in Figure 44 and Table 17.

Table 17. SIMS based initial design and resulting model

	initial design		resulting model	
layer	d (nm)	n	d (nm)	n
A	98.91	1.712	119.52	1.612
B	114.13	2.050	108.76	2.236
C	22.83	1.632	30.09	1.576
D	98.88	2.236	96.36	2.241
E	83.70	2.284	76.71	2.284
F	93.33	1.479	101.90	1.478

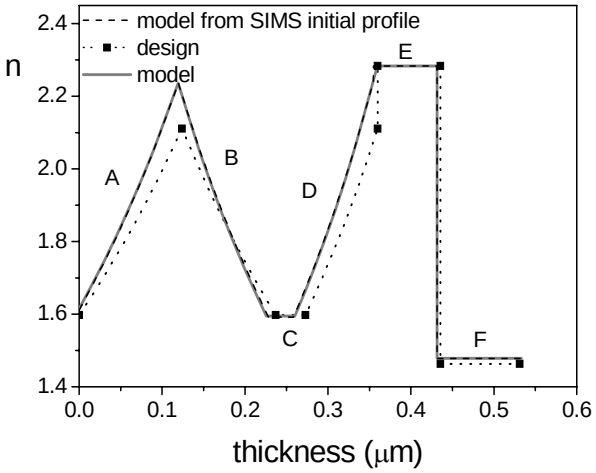

Figure 44. Model obtained from optical characterisation and SIMS based initial design, compared with the targeted design and model obtained previously.

4.2.3.5. Comparison of optical characterisation results obtained with and without ellipsometry

The ellipsometric measurements were included into the characterisation in order to define optical properties of the sample better and help the optimisation process to avoid multiplicity of solutions. In this Section justification of inclusion of this additional data will be checked via comparison of the EBE antireflection model obtained previously and the one obtained in the same way, but using only reflectance and transmittance data (measured at 0^o and 45^o).

The new model obtained in this way, compared with the previous one, is shown in Figure 45 and its parameters in Table 18. The optical performance of the two models is shown in Figure 46.

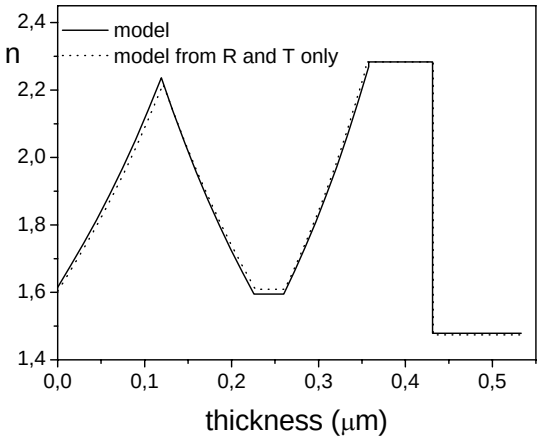

Figure 45. Refractive index profile of the EBE antireflective model obtained using reflectance and transmittance measurements only, compared to the previous one when also ellipsometry functions were included into the optimisation.

Table 18. Parameters of the refractive index profile of the model obtained using reflectance and transmittance measurements only

layer	d (nm)	n at 570nm
A	121.5	1.603
B	106.17	2.217
C	33.96	1.593
D	93.34	2.264
E (Nb_2O_5)	77.22	2.284
F (SiO_2)	101.81	1.474

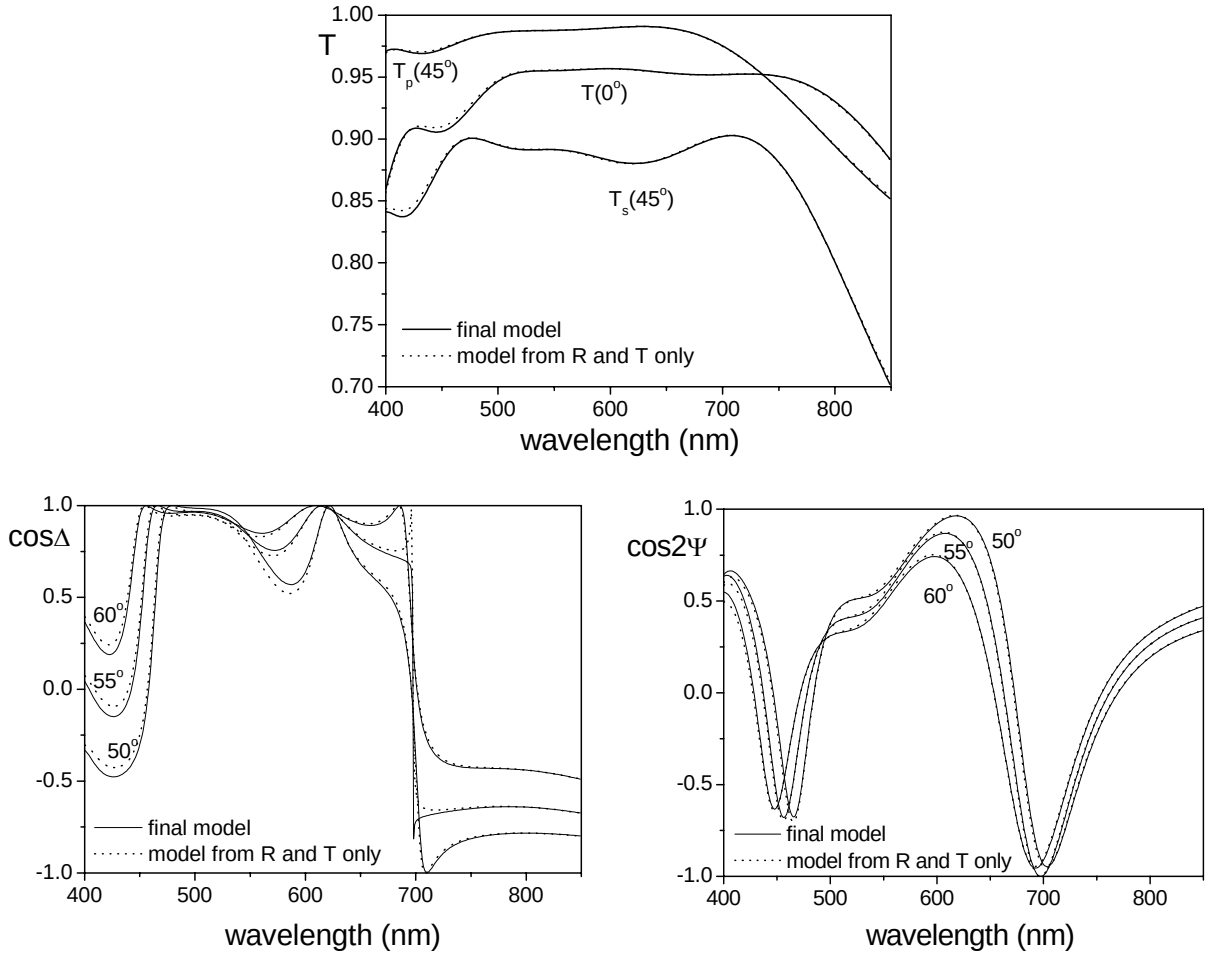

Figure 46. Optical performance of the model obtained using reflectance and transmittance measurements only compared to the previous one when also ellipsometry functions were included into the optimisation.

In order to distinguish the two models better, the evaluation of statistical uncertainties of the optimisation parameters has been performed and the results are shown in Table 19.

Table 19. Statistical uncertainties of optimisation parameters

Parameter	Uncertainty (%), optimisation including ellipsometry	Uncertainty (%),optimisation with R and T only
A (Cauchy)	0.06	0.14
B (Cauchy)	6.03	9.85
C (Cauchy)	1019.98	3332.13
d(A)	0.14	0.54
d(B)	0.37	0.21
d(C)	1.53	2.99
d(D)	1.04	1.98
d(E)	1.58	3.09
d(F)	1.06	0.15
f_v(A)	1	3.29
f_v(B)	0.30	1.06
f_v(C)	1.71	4.08
f_v(D)	0.98	2.04

4.2.3.6. Optical characterisation of the mixture layers

Mixture layers of constant composition through thickness, differing in ratio of SiO_2 to Nb_2O_5 were deposited to check which EMT is the best for characterisation of mixtures of these materials. From the results of optical characterisation of the previous samples, it is LL. Appropriateness of the EMTs is related to the structure of the mixtures, so in this case it is indicated that phases are well mixed. In order to verify the correlation of the structure with the result of optical characterisation that shows preference to LL, annealing of the mixture samples has been performed. It can be expected that upon thermal treatment phases will be separated and instead LL the optical properties will follow BG or MG law, which are more appropriate for this kind of mixtures.

The five mixture layers deposited on Suprasil and Si chunks were measured as deposited (AD) and after five hours of annealing in air at 500°C and 750°C. Reflectance and transmittance measurements at 6° incidence in the range 350-950 nm, in 1 nm steps were used in optical characterisation. The sample with pure Nb_2O_5 layer has been treated in the same way, while the sample with pure SiO_2 layer has not been annealed since structural changes in this material are expected only at higher temperatures. Upon annealing at 750°C Nb_2O_5 sample checked by naked eye showed milky reflection typical for high scattering and indicating crystallisation in the layer. Therefore, scattering measurements have been performed for Nb_2O_5 and other high content Nb_2O_5 annealed samples by Perkin Elmer Lambda 19 spectrometer with Ulbricht integrating sphere. No significant scattering has been detected at any of the samples annealed at 500°C. Scattering spectra for samples annealed at 750°C are presented in Figure 47. Peaks in spectra of Nb_2O_5 and n_M samples (Figure 47 a)) correspond to peaks in reflectance spectra (compare with Figure 34): the more light reflected, the more is scattered. The results of optical characterisation, using Tauc-Lorentz model or Cauchy model with exponential absorption, are shown in Table 20. The samples showing scattering have been rotated 90° and their reflectance measured again. No anisotropy has been found in this way.

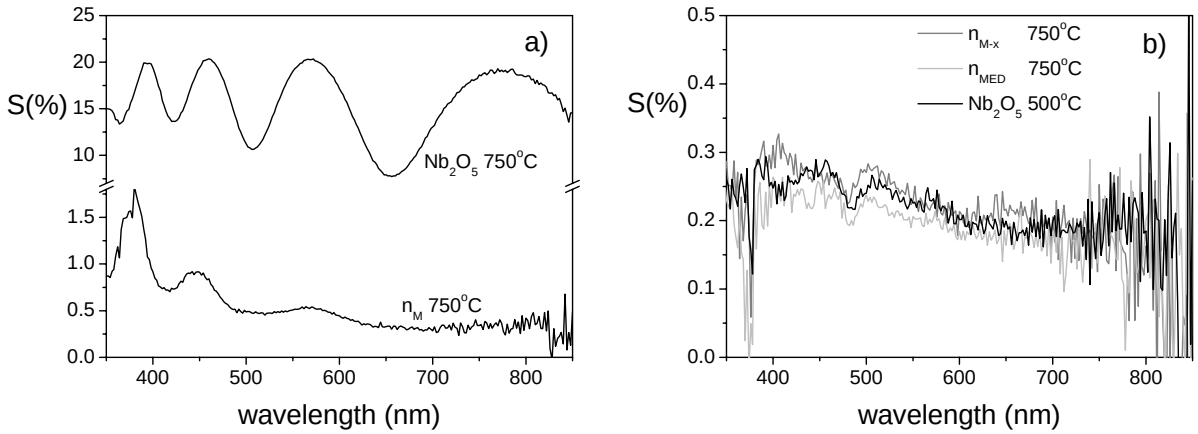

Figure 47. Scattering of the annealed samples with high content of Nb_2O_5.

Table 20. Results of optical characterisation of as deposited and annealed mixture samples

		n at 570 nm	*d* (nm)	*Δn/n*	TL model C model	E_g (eV) *A*	E_0 (eV) *B* (nm^2)	*A* (eV) *C* (nm^4)	*C* (eV) k_A	ε_0 k_B (nm)
Nb_2O_5	AD	2.2838	450.3	-2.71	TL	3.302	4.750	115.7	1.085	2.660
	500°C	2.3126	436.7	-1.42	TL	3.282	4.724	110.9	0.7642	2.801
	750°C	too high scattering for optical characterisation								
n_M	AD	2.0857	449.6	4.46	TL	3.368	4.880	88.39	1.025	2.402
	500°C	2.1035	433.5	5.05	TL	3.698	4.692	173.9	1.022	2.229
	750°C	2.1856	404.2	3.70	C	2.131	2312	5.017E9	7.50E-4	674.3
n_{M-x}	AD	1.9032	506.8	1.60	C	1.820	2.709E4	3418	3.50E-5	894.5
	500°C	1.9195	481.2	2.62	C	1.825	3.070E4	4235	1.42E-19	1.27E4
	750°C	1.9928	442.9	0.84	C	1.89	3.340E4	2.100E4	3.61E-7	3377
n_{MED}	AD	1.8389	464.0	2.48	C	1.766	2.370E4	1.963E5	4.22E-21	1.44E4
	500°C	1.8404	441.1	3.26	C	1.794	1.049E4	1.558E9	3.53E-28	1.99E4
	750°C	1.8924	415.3	3.04	C	1.847	7532	2.349E9	7.36E-16	1.05E4
n_{m+x}	AD	1.7065	500.6	0.71	C	1.676	6405	1.143E9	1.30E-4	1.75E-5
	500°C	1.7138	473.9	1.85	C	1.679	7638	1.194E9	3.05E-9	4542
	750°C	1.7463	430.0	1.67	C	1.724	0.019	2.354E9	7.17E-15	9519
n_m	AD	1.6000	471.7	0.07	C	1.568	1.043E4	4.851E4	5.38E-5	9.91E-6
	500°C	1.5970	453.8	1.19	C	1.562	1.136E4	6550	1.91E-7	2146
	750°C	1.5992	421.6	0.60	C	1.557	1.360E4	1.386	1.78E-7	3029
SiO_2	AD	1.4667	507.3	-1.02	C	1.454	4127	625.8	0	0

The dispersions of the refractive indices are presented in Figure 48.

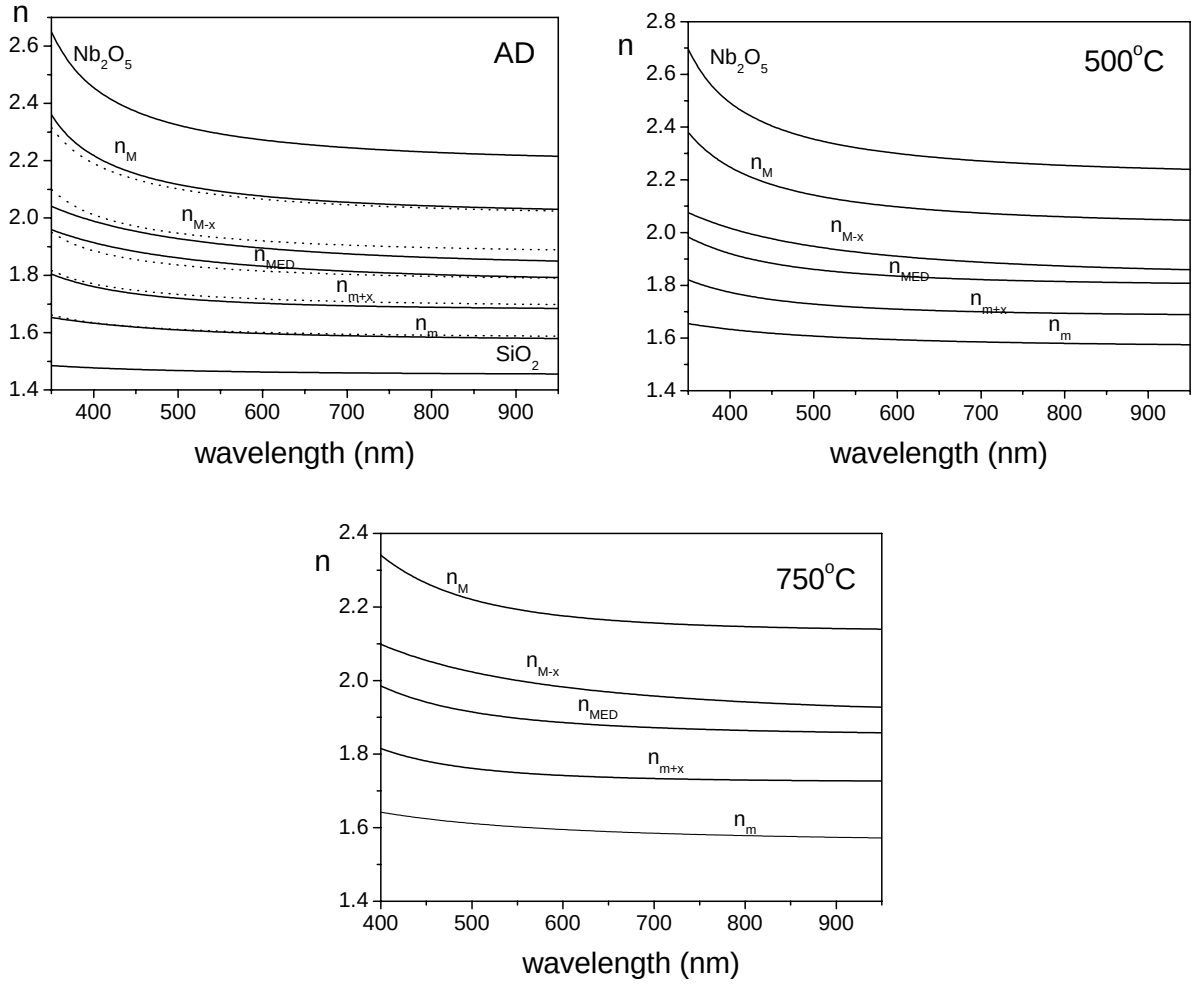

Figure 48. Refractive index dispersions of the mixture samples. Theoretical LL dispersion curves for corresponding AD samples are presented with dots.

4.3. Structure of the mixture layers

In this Section additional measurement techniques for analysis of structure of the mixture layers and their results will be presented. The idea is to relate the structure of the mixtures with the EMT law that the best describes their refractive indices as function of ratio of compounds. Thus, the FTIR (Fourier Transform Infrared) measurements will show if absorption band related to Si-O-Nb bonds are present, indicating the level of mixing of the two phases. They will also show the dependence of intensity of this band on concentration of Nb_2O_5 and the annealing temperature. It is expected that with thermal

treatment this band will decrease in intensity, while the one associated with Si-O-Si bonds will increase. This would be an indication of separation into phases.

XRD (X-ray Diffraction) technique should also show the level of mixing of SiO_2 and Nb_2O_5. If no diffraction peaks are detected it would mean that the mixture is amorphous or crystallites are very small (less than 2-3 nm)[88]. In this case the phases cannot be distinguished. Presence of diffraction peaks would indicate crystallinity in the coating and separation of materials into phases. This is expected for samples with higher content of Nb_2O_5 after annealing.

AFM (Atomic Force Microscopy) can detect crystalline grains eventually formed on the surface of the layer after thermal treatment.

TEM (Transmission Electron Microscopy) diffractograms are expected to confirm level of crystallisation found by XRD. TEM, high resolution electron microscopy and Z-contrast images can show structure of the layer in sense of distribution of materials and grains demonstrating again restructuring of the materials and separation in phases.

4.3.1. Additional measurement techniques

XRD is a technique used to determine the arrangement of atoms within a crystal. It measures the density of electrons within the crystal, from which the atomic positions can be inferred. The periodicity of the electron density is used to diffract X-rays with manageable measurement error. The technique involves the scattering of X-rays of a single wavelength from a crystal. This scattering produces a diffraction pattern, a set of intense spots (also called reflections) on a screen behind it. The spots can be related to the density of electrons in the crystal via Fourier transform. The reflections vary in intensity and by gradual rotating of the crystal and recording the intensity of the spots it is possible to determine magnitude of Fourier transform of electron density within the crystal. By using data on related molecules, or by recording several sets of data with specific changes in the scattering, the phases corresponding to these magnitudes may be computed. Combining the phases and magnitudes yields the full Fourier transform of the electron density, which may be inverted to obtain the electron density in terms of position within the crystal. XRD is used to characterise the crystallographic structure, grain size and preferred orientation in polycrystalline powdered solid samples. It is also a common method for determining strains in crystalline materials.

AFM is a high resolution type of scanning probe microscopy. The device consists of a microscale cantilever with a sharp tip (probe) at its end that is used to scan the specimen surface. The tip radius of curvature is on the order of nanometers. When the tip is brought into proximity of a

sample surface, forces between the tip and the sample lead to a deflection of the cantilever according to Hooke's law. Typically, the deflection is measured using a laser spot reflected from the top of the cantilever into an array of photodiodes. Other methods that are used include optical interferometry, capacitive sensing or piezoresistive AFM cantilevers. These cantilevers are fabricated with piezoresistive elements that act as a strain gage. Using a Wheatstone bridge, strain in the AFM cantilever due to deflection can be measured, but this method is not as sensitive as laser deflection or interferometry.

TEM is an imaging technique whereby a beam of electrons is transmitted through a sample, then an image is formed, magnified and directed to appear either on a fluorescent screen or photographic film, or to be detected by a sensor such as a CCD camera. Electrons are generated by thermionic discharge or by field emission. They are then accelerated by an electric field and focused by electrical and magnetic fields onto the sample. The electrons can be focused onto the sample providing a resolution far better than is possible with light microscopes, and with improved depth of vision. Z-contrast imaging allows distinguishing different elements by difference in atomic number *Z*, as the intensity shown is approximately proportional to Z^2. In the most powerful diffraction contrast TEM instruments, crystal structure can also be investigated by High Resolution Transmission Electron Microscopy (HRTEM), also known as phase contrast imaging as the images are formed due to differences in phase of electron waves scattered through a thin specimen.

4.3.2. Results of additional measurements of mixture samples

FTIR measurements were done by BIO-RAD FTIR spectrometer model FTS 175. XRD was performed by Dr. S. Yulin at Fraunhofer IOF, Jena, by Burker D505 diffractometer using Cu-Kα radiation at 0.154 nm, applying large angle X-ray diffraction method. AFM was done also at Fraunhofer IOF, Jena, by Dr. M. Flemming, at different scan sizes (1 μm X 1 μm and 10 μm X 10 μm). TEM was performed by S. Grözinger (sample preparation) and A. Chuvilin (TEM study and report) at Universität Ulm, Germany.

4.3.2.1. FTIR

The FTIR spectra are taken in order to compare the absorption bands of SiO_2 in mixture samples as a function of Nb_2O_5/SiO_2 composition and temperature of thermal treatment. The spectra were measured in the wavenumber range 400-7000 cm^{-1} (wavenumber is defined as $1/\lambda$). Before each measurement a spectrum of a reference Si substrate has been taken as a background, so the data presented at Figure 49,

Figure 50 and Figure 51 are solely spectra of the deposited layers. Figure 49 shows absorption curves of AD and annealed samples in the range where Si-O-Si, Nb-O and Nb-O-Si bands are expected. Figure 50 presents the evolution of the spectra with annealing temperature for three samples with different $f_v(SiO_2)$. In Figure 51 are FTIR spectra of the range where water absorption band is expected[89]. Transmission T spectra have been calculated from as $T = T_{sub}*10^{-\mathcal{A}}$, where $T_{sub}=10^{-\mathcal{A}_{sub}}$. Absorbance $\mathcal{A}$ is obtained from measurement of the sample and $\mathcal{A}_{sub}$ from measurement of the reference bare Si substrate. The measurements were taken 7 days after deposition. The area under water peak transmission of each sample has been calculated and normalised to thickness found from optical characterisation. The obtained values are presented in Table 21. Also, relative change of thickness after annealing is given.

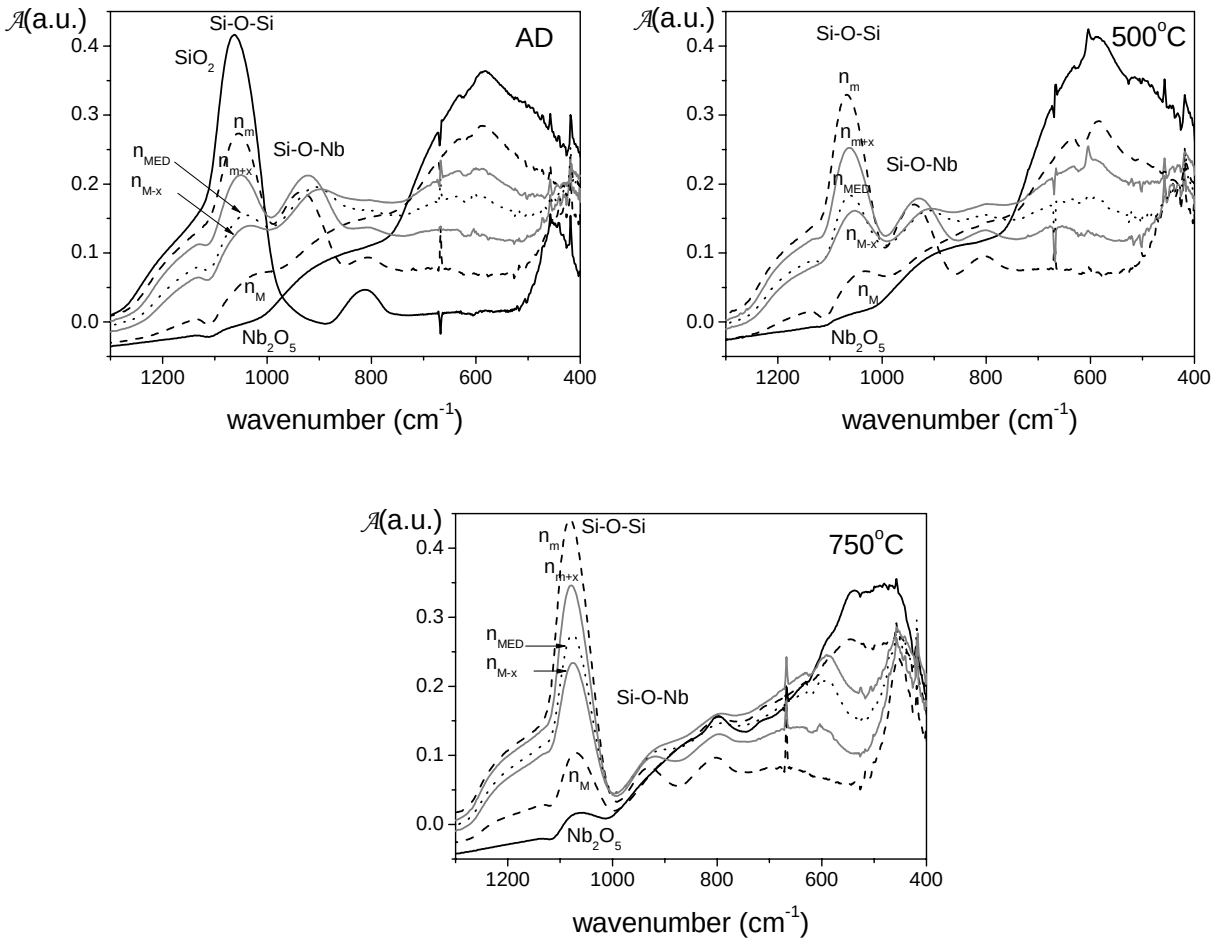

Figure 49. FTIR spectra of AD and annealed mixture samples.

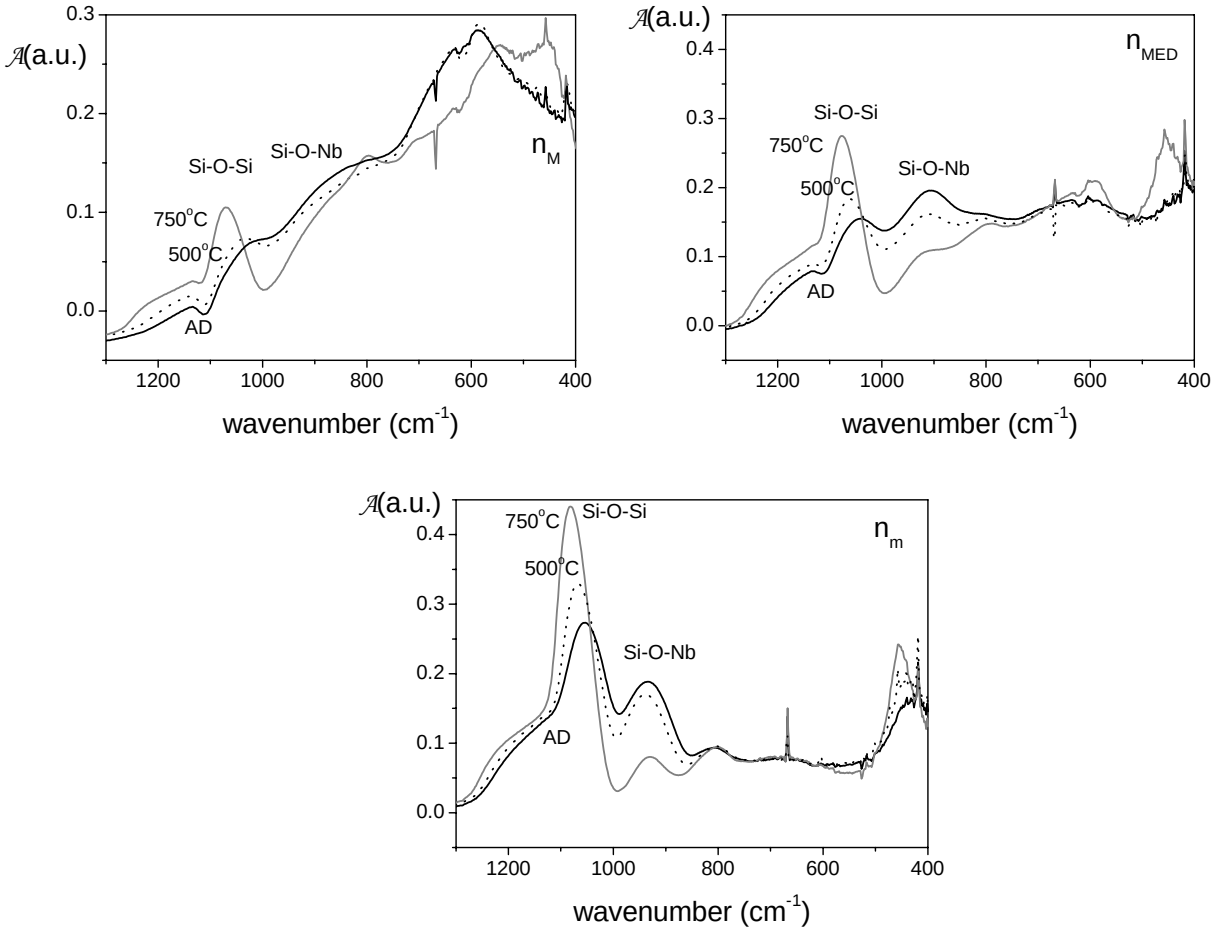

Figure 50. Evolution of the FTIR spectra with annealing temperature.

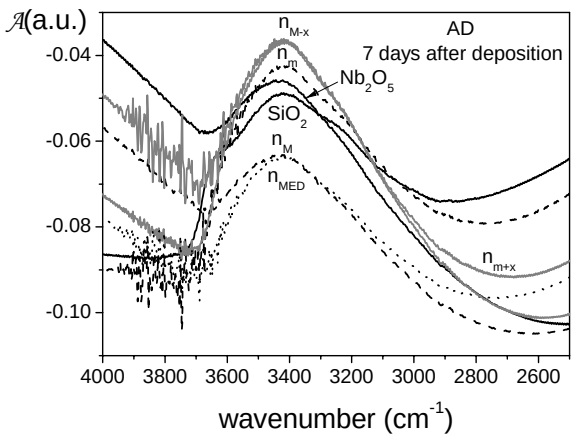

Figure 51. Water absorption band of the mixture samples.

Table 21. Area under water peak normalised to thickness of mixture layers related to annealing temperature and relative change in thickness

	Area under water peak normalised to thickness (nm^{-1})		Relative change in area (%)	Relative change in thickness (%)	
	AD	500°C	$\Delta_{AD\text{-}500^{o}C}$	$\Delta d_{AD\text{-}500^{o}C}$	$\Delta d_{AD\text{-}750^{o}C}$
Nb_2O_5	0.03120	0	-100	-3.02	-
n_M	0.03396	0	-100	-3.58	-10.10
$n_{M\text{-}x}$	0.06085	0.01070	-82.42	-5.05	-12.61
n_{MED}	0.04894	0	-100	-4.94	-10.50
n_{m+x}	0.08296	0.03530	-57.45	-5.33	-14.10
n_m	0.09018	0.03230	-64.18	-3.79	-10.62
SiO_2	0.05000	not annealed			

4.3.2.2. XRD

The samples deposited on Suprasil substrates were subjected to XRD analysis. The measurements have been performed in the range of angles 7.5° - 30°. The measurements are shown in Figure 52. The peaks correspond to hexagonal and orthorhombic crystalline structure of Nb_2O_5. The values of root mean square (RMS) roughness obtained from these measurements, same as density of the samples, have been presented in Table 22. Also, the density of the layers has been determined from the top approximately 100 nm of thickness.

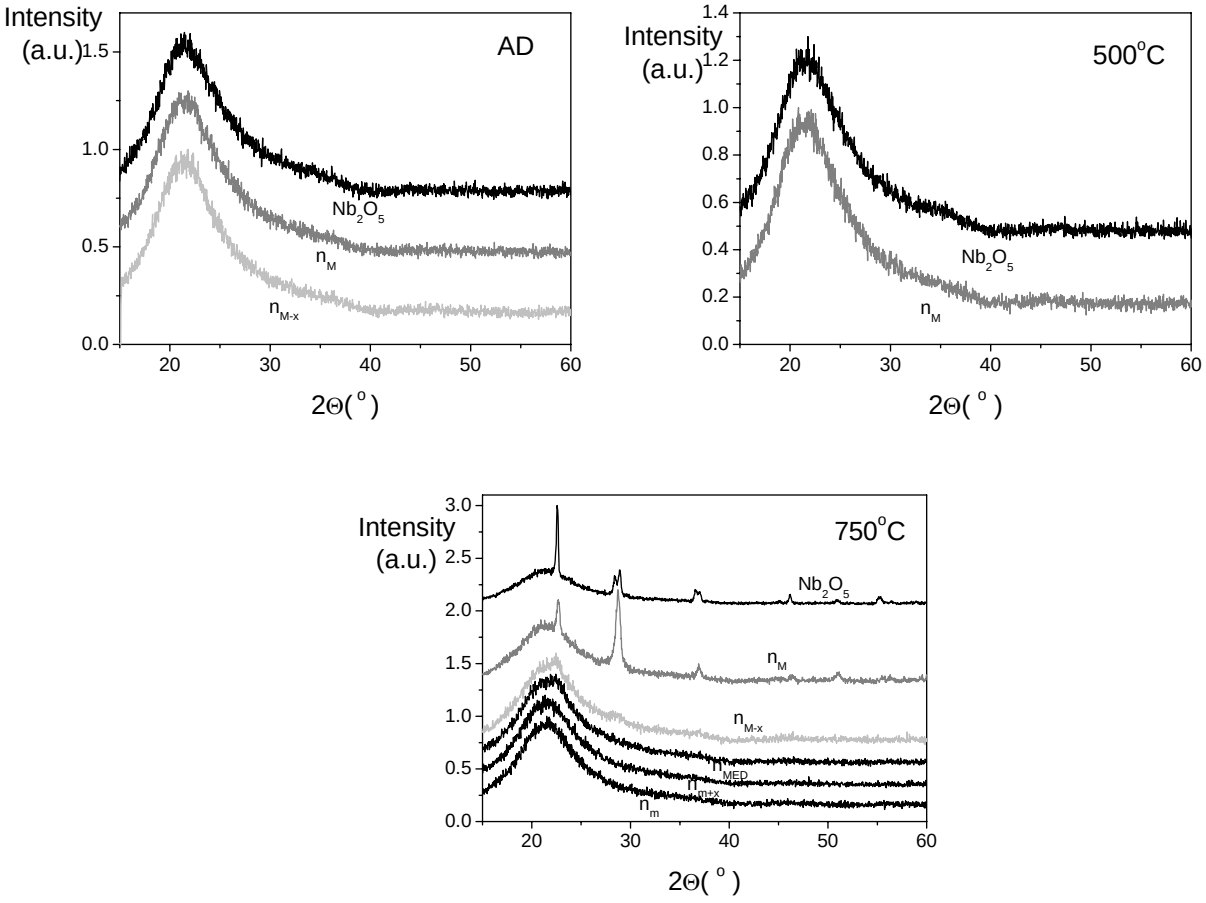

Figure 52. XRD spectra show crystallinity only for the three samples with highest content of Nb_2O_5 annealed at 750°C.

4.3.2.3. AFM

The AFM topographs of AD and annealed Nb_2O_5, n_M and n_m layers deposited on Suprasil are shown in Figure 53, Figure 54 and Figure 55. The average roughness values obtained from several AFM measurements are given in Table 22 and compared with values obtained from XRD.

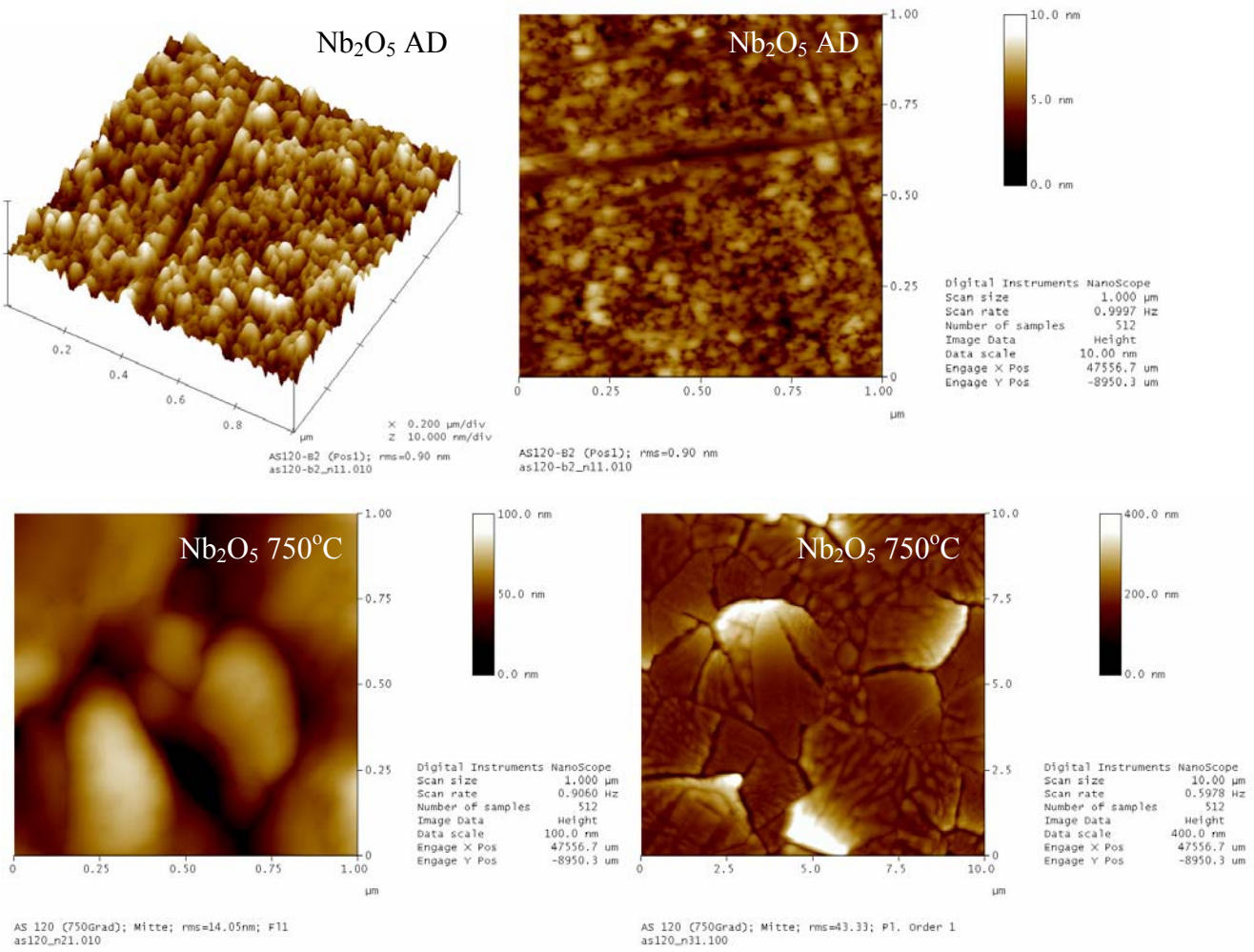

Figure 53. AFM pictures of Nb_2O_5 sample AD and annealed at 750°C. Note different roughness values of annealed sample depending on the scale of measurement.

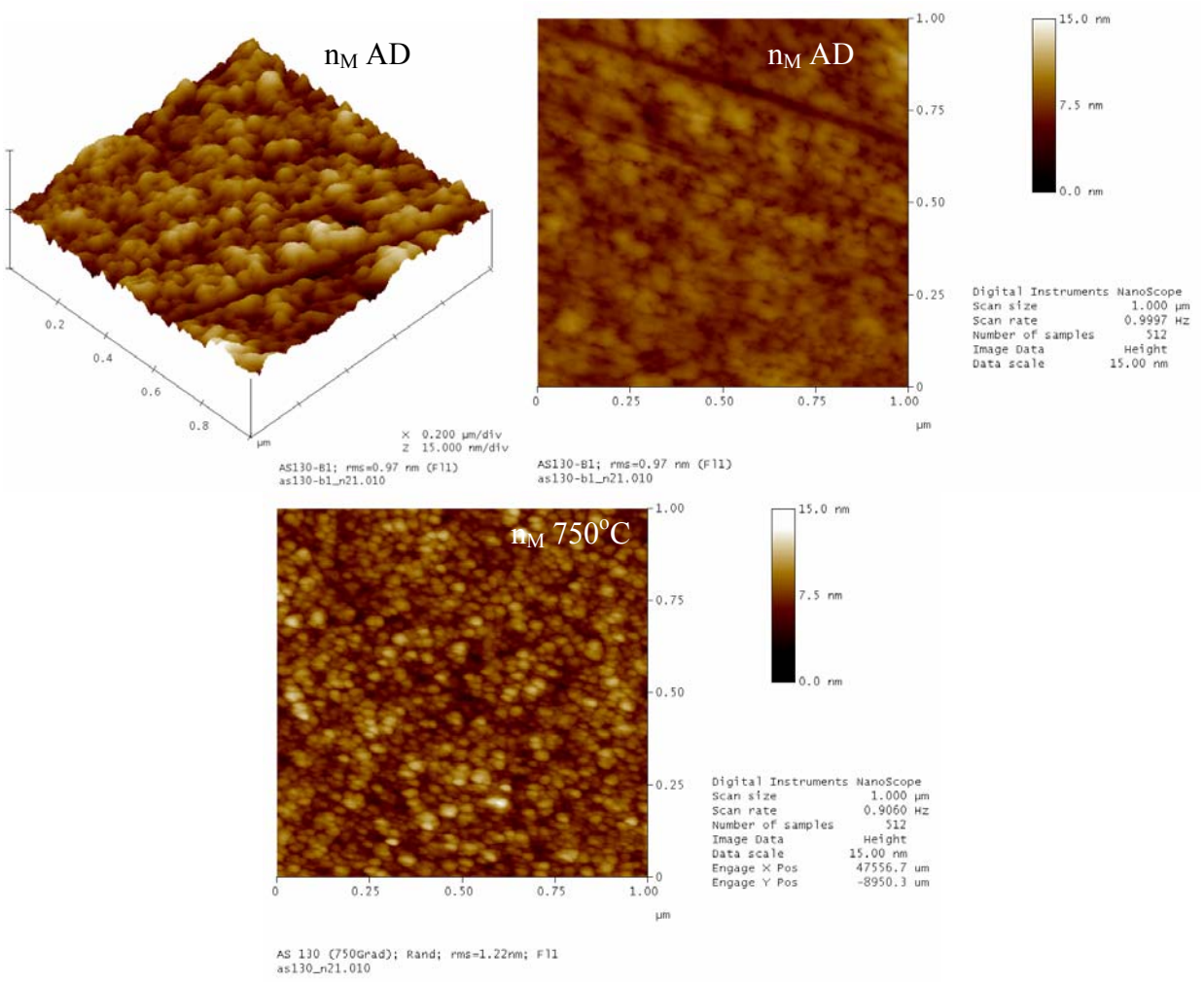

Figure 54. AFM pictures of n_M sample AD and annealed at 750°C.

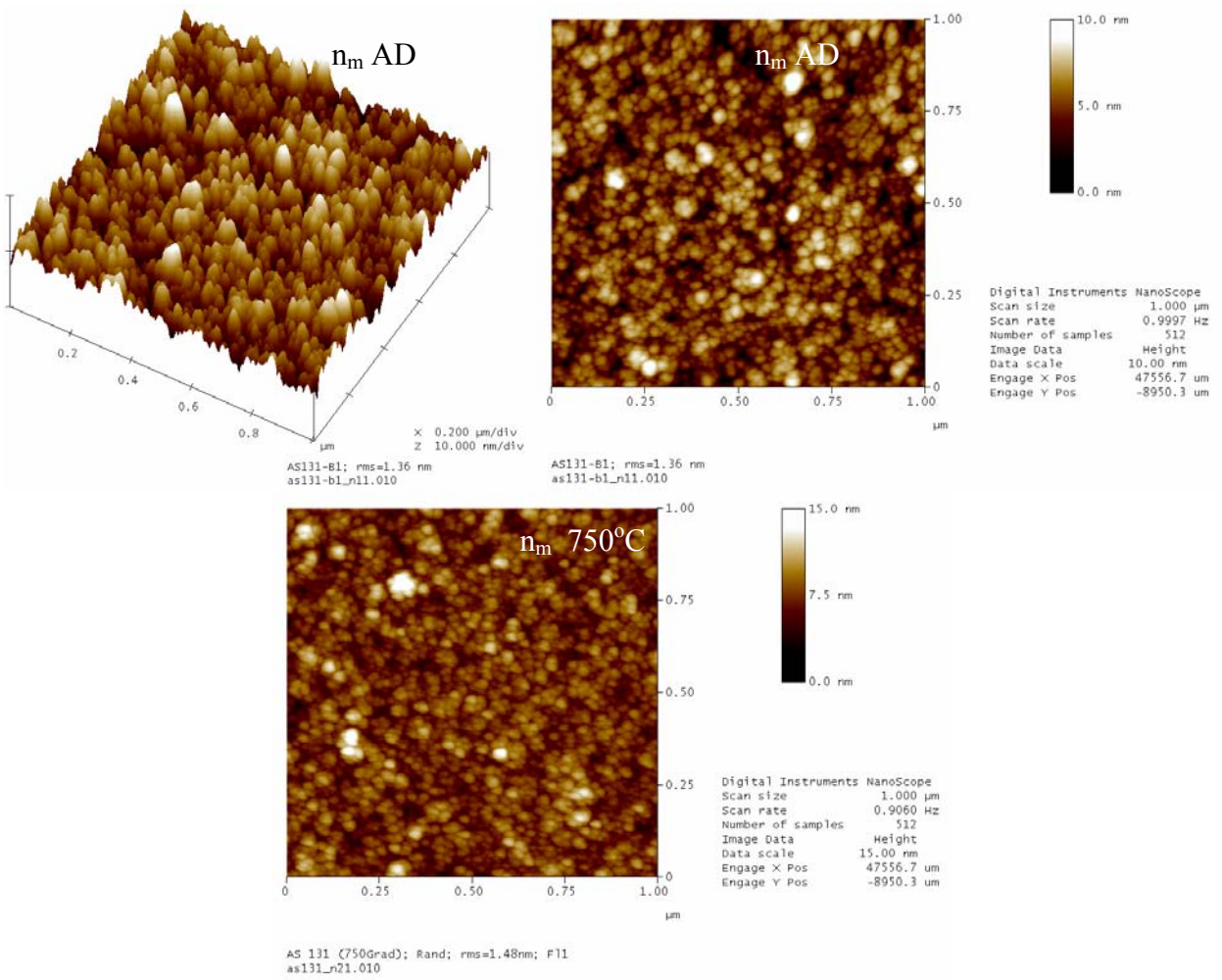

Figure 55. AFM pictures of n_m sample AD and annealed at 750°C.

Table 22. Comparison of roughness values obtained from AFM and XRD, density of the layers obtained from XRD analysis

Sample	roughness AFM (nm)		roughness XRD (nm)		ρ XRD (g/cm^3)	
	AD	750°C	AD	750°C	AD	750°C
Nb_2O_5	0.94	47.59	1.7	3.3	4.5	4.5
n_M	1.40	1.24	1.8	1.6	4.3	4.4
n_{M-x}	-	-	2.0	1.3	3.65	4.0
n_{MED}	1.05	1.22	-	-	-	-
n_{m+x}	-	1.44	-	-	-	-
n_m	1.36	1.47	-	-	-	-
SiO_2	1.82	-	-	-	-	-

4.3.2.4. TEM

TEM images of AD Nb_2O_5 sample and n_M AD and annealed at 750°C, deposited on Si are shown in Figure 56, Figure 57 and Figure 58, respectively. For the n_M sample also Z-contrast image is presented.

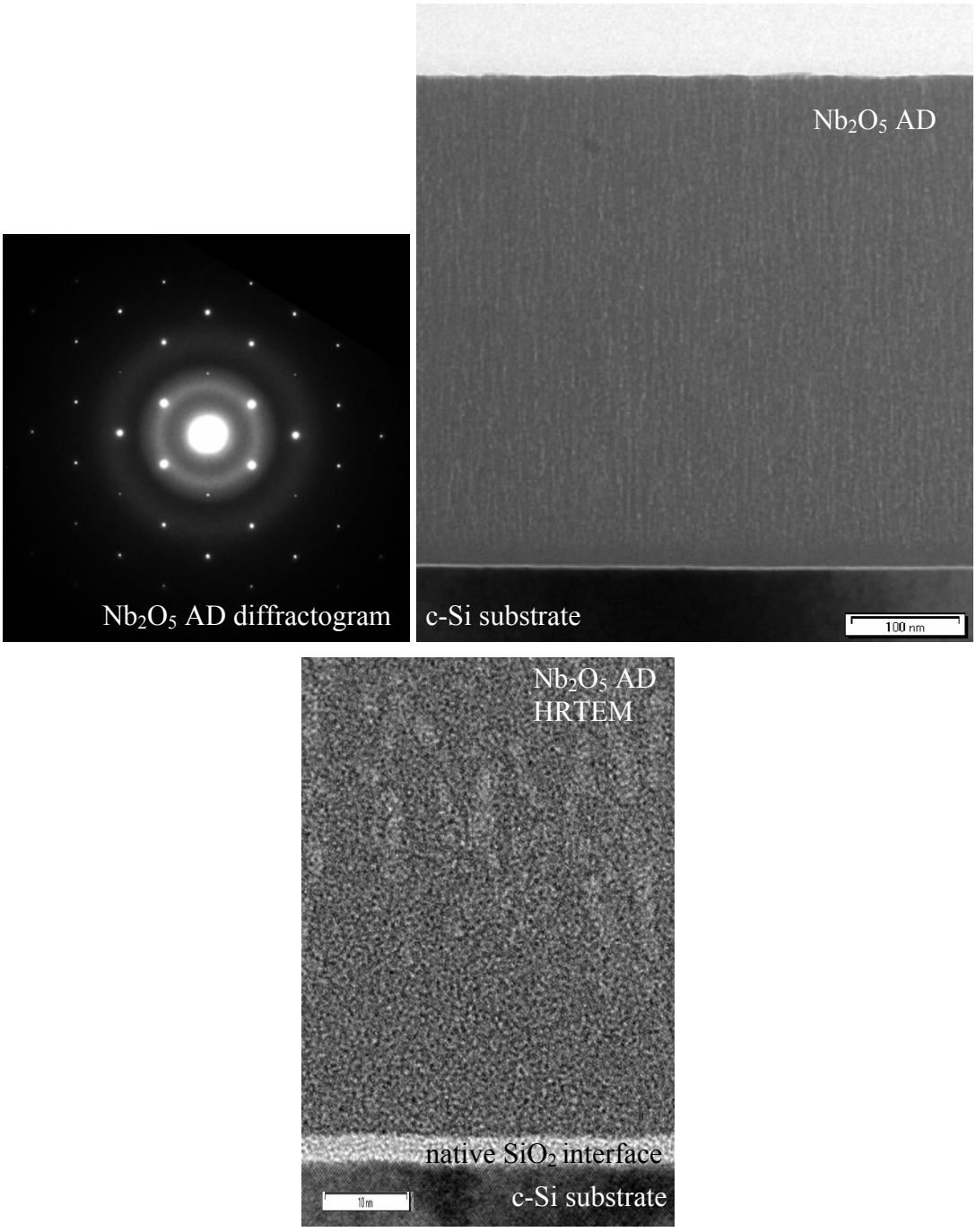

Figure 56. TEM images of AD Nb_2O_5 sample.

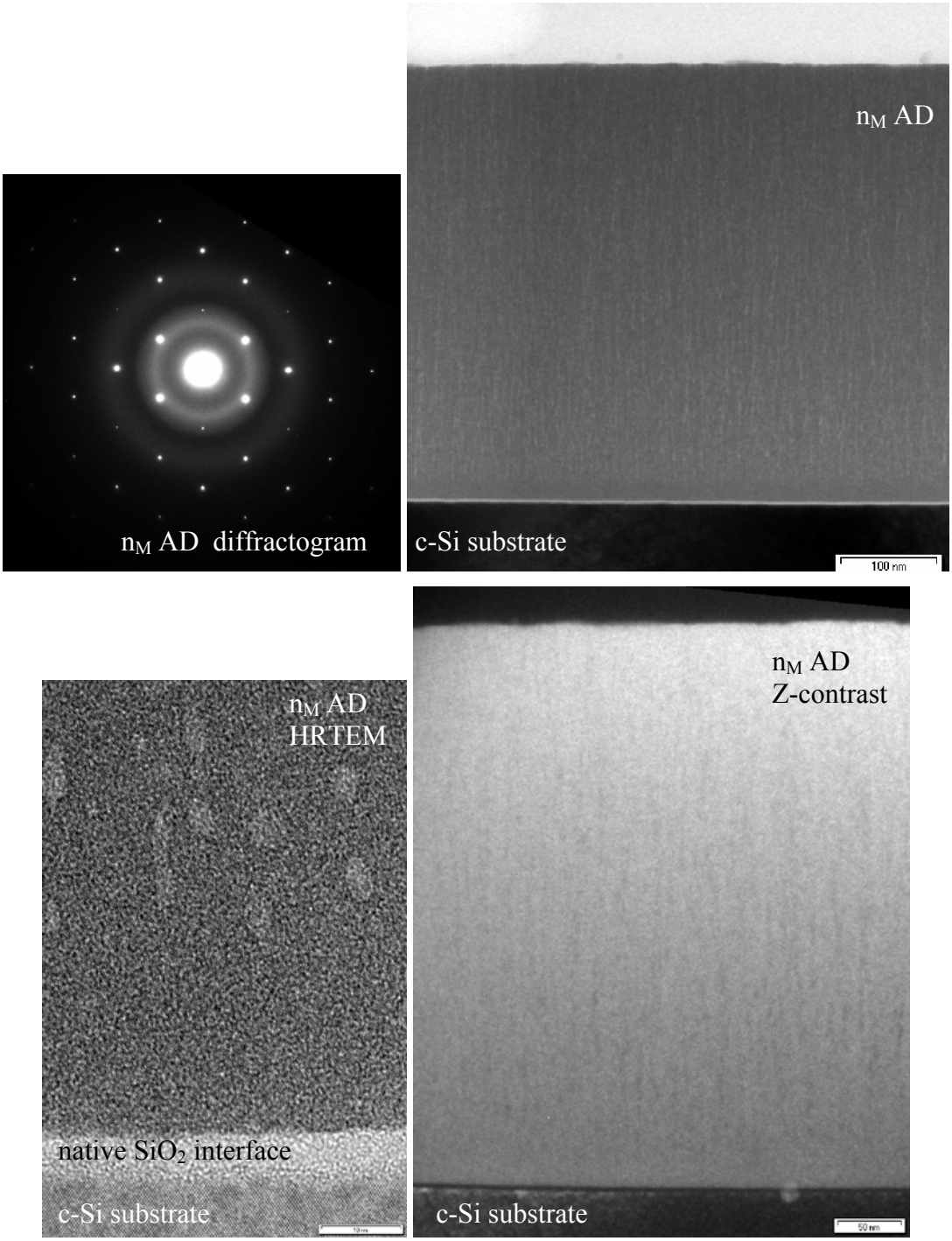

Figure 57. TEM images of AD n_M sample.

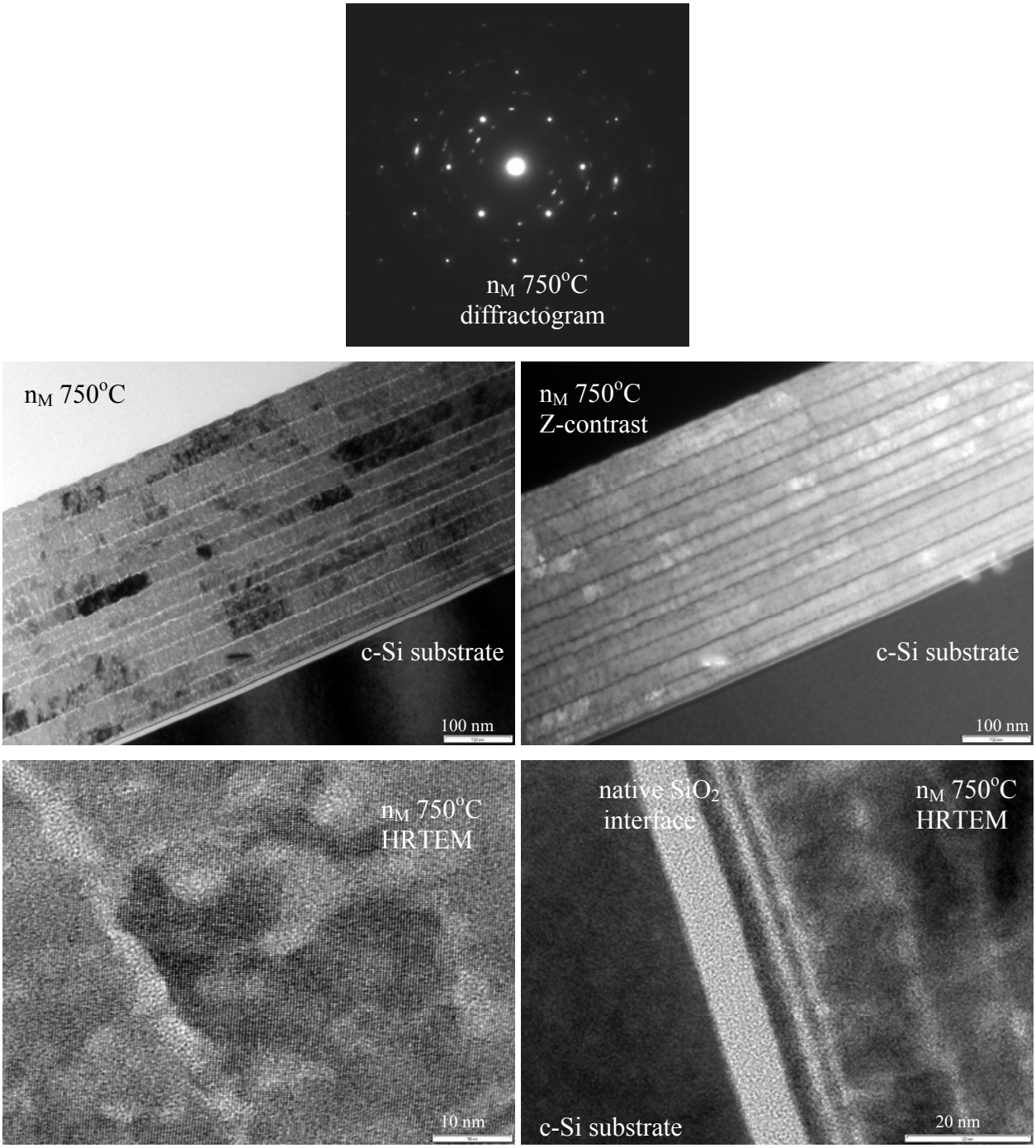

Figure 58. TEM images of n_M sample annealed at 750°C.

5. Discussion

In this Chapter the discussion of the results described in the previous chapters, regarding hybrid designs and their properties compared to classical and rugate systems, deposition of samples, their optical characterisation and structural properties of mixed samples will be presented.

5.1. Antireflective design

It is shown (Figure 10) that both antireflective hybrid designs (thinner and thicker) meet the requirements well, i.e. they predict very good reflection suppression and satisfy specifications for 0^o and 50^o. Even for angles up to 60^o the reflectance of the coated substrate is expected to be lower than of the uncoated BK7 glass at 0^o (Figure 59). The thicker design has FOM 40% lower than the thinner one, due to more advanced refractive index profile, i.e. more complex structure.

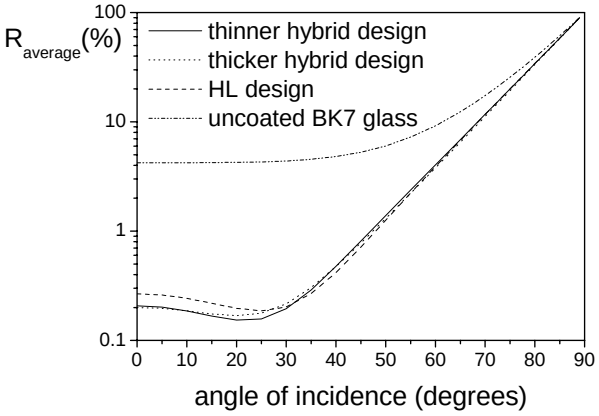

Figure 59. Reflectance averaged over the spectral range of interest and polarisation as a function of angle of incidence.

Compared to the equivalent HL AR design, the two hybrids have similar or even better spectral and angular performance than the classical one, which is related with the maximum principle that HL systems are not any more preferable in the case of non-normal incidence. The total thickness of the thinner hybrid is a bit lower than of the HL coating.

The analysis of individual corner point sensitivity to errors in deposition of the thinner design shows that the worst performance of the coating was obtained in the case of increased refractive index at the end of constant refractive index mixture layer (point D, Figure 9), decreased thickness of the SiO_2 layer (point I) and decreased refractive index at the end of the last ramp before the pure material

layers (point E) (Table 1). In this analysis errors in refractive index of pure material layers were not taken into account.

Width of corridor probability is related to the discrepancy of the spectral performance of the design from the expected performance, caused by random errors in parameters of design. The corridor is broader for thicker hybrid AR system that results from higher number of parameters. It is an indication that the thicker design is more sensitive for deposition due to its complexity. The corridor of the thinner design is about as small as the one of the HL stack, although the last varies more along the wavelength scale at normal incidence. At 50^o the classical design is clearly less sensitive (Figure 13 and Figure 14).

Comparing designs obtained by refinement of the thinner hybrid design for the purpose of deposition with other techniques, one can see (Table 2) that designs and their quality are almost the same, which can be seen from comparison of n_m and n_M of the mixtures used in the design, total thickness and deviations from the targeted specifications.

5.2. Notch design

The classical notch HL design (Table 3) has achieved the best OD in the reflectance peak region (530-534 nm) and thus the best transmittance at the central wavelength of 532 nm. At the same time it has the lowest number of periods and the lowest thickness, compared with the other two designs. Gradient index designs require more thickness than the classical HL stack to achieve the optical thickness necessary for the same quality of the performance. Steepness of the transition between pass and rejection band is around 1 nm for the change from 20% to 80 %, while *FWHM* is around 33 nm, for all three models. Comparing the rugate and the hybrid design one can notice wider pass band in the case of the first (Figure 60) and slightly better OD in the case of the second. Both of these models show better sidelobes and ripples suppression than the classical one. Due to the simpler refractive index profile, i.e. linear ramps and constant amplitude of the periods, the hybrid design is perhaps less demanding for implementation and production in a deposition system than the rugate design.

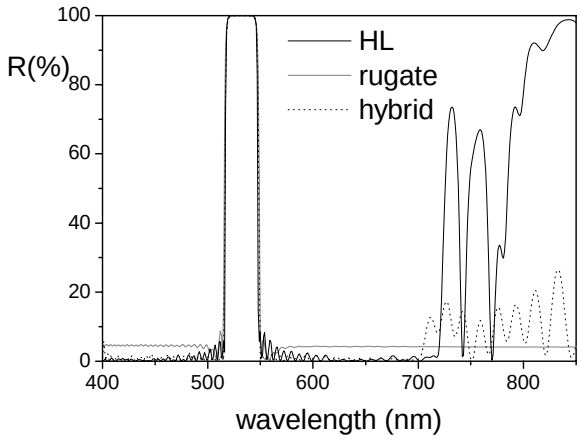

Figure 60. The pass band of the rugate filter is significantly wider than the band of the hybrid and HL one.

5.3. Deposited AR samples

When comparing the results of the round robin experiment where hybrid AR coatings have been deposited by different techniques, one has to keep in mind that the thicker coating, deposited by RFS, is more challenging for production process than the thinner coatings, and therefore, the probability of errors is higher.

The IBS sample shows the lowest deviation from the theoretical spectrum (Table 9). This quasi-inhomogeneous coating is the only one that really corresponds to the proposed design, where ramps are replaced by 8 homogeneous refractive index layers. In this sense, EBE and RFS designs are only approximations for the corresponding coatings that have actually been deposited, where the changes in refractive index are realised as linear ramps and not as step functions as in the designs. One could argue that this is the reason for the superior performance of IBS samples in respect to EBE and RFS samples. However, it has been checked that a subdivision of the design ramps into 8 or 50 layers (later gives sublayers of around 2.5 nm of thickness and is a good approximation of linear ramps) gives a difference in theoretical performance that is too small to explain weaker matching in performance of EBE and RFS designs and samples. Therefore, the conclusion is that the quality of IBS samples really originates from the high stability of the process and reproducibility of the results in conjunction with the sophisticated *in-situ* broad band monitoring and not from its quasi-inhomogeneous nature.

The high deviation between optical performances of two RFS thicker samples deposited in different runs showing low reproducibility, may be attributed to spectral shifts (Figure 32) induced by a systematic error in thickness of the coatings.

5.4. Spectroscopic optical characterisation of the deposited samples

In the process of optical characterisation different EMTs for material mixtures have been tested. The lowest values of merit function were obtained when LL model was applied. Therefore, the presented models are using LL EMT.

5.4.1. Nb_2O_5 and SiO_2

The optical characterisation of pure material layers is a standard procedure used for calibration of thickness control and determination of optical constants. The studied samples show slightly negative inhomogeneity of refractive index (-1.022 for SiO_2 and -2.707 for Nb_2O_5), meaning that refractive index decreases with thickness. This can originate from unstable rates of deposition at the very beginning of the layer growth or warming of substrate during the process. However, inhomogeneity like this is quite usual in standard coatings.

The optical parameters found for the two materials are within expected values. They are used later for optical characterisation of the more complex hybrid AR coatings. The obtained thickness has been used for adjustment of tooling factor of the central quartz monitor that is controlling rate of deposition and thickness of pure material layers.

5.4.2. Sample with ten periods

The model obtained by optical characterisation of the sample with ten periods shows only a small (1.5%) error in the deposited thickness, small especially if taking into account the kind of thickness control available in the deposition plant. The errors in refractive indices, however, are bigger. The whole profile of the model is shifted upwards comparing with the design: n_M is higher about 6% and n_m about 3% in average. This suggests that there is excess of high index material to the low index material in the system, indicating the rate of deposition of Nb_2O_5 has been underestimated or/and the one of SiO_2 overestimated. The profile obtained from rates of deposition shows better correspondence in refractive indices with design and slightly bigger thickness error than the model (2.4%). This is expected because the rates and time of deposition have been adjusted after probes to the values that would give accordance with the desired result (design).

5.4.3. Hybrid antireflective samples

Generally speaking, the characterisation procedure led to a remarkable agreement between the simulated and experimental data and a model close (i.e. within the expected errors) to the initial design. Differences between the obtained model and the initial design can be explained in terms of deviations in the deposition process.

The optimisation of the refractive indices of SiO_2 of EBE and RFS samples, modelled with the Cauchy dispersion formula, enabled significant improvement of function of merit. On the contrary, no improvement was achieved by optimising the high index materials (except the need to include absorption in Ta_2O_5 of RFS as described above) or SiO_2 of IBS, regardless the used dispersion model. The differences to the data file refractive indices of EBE and RFS samples determined from samples with single layer of pure silica are between 1% and 2%, the higher corresponding to the RFS sample. Such difference could be explained by different conditions during the process of deposition (pressure or temperature of the substrate) or difference in growth of the material when it is deposited directly to the bare substrate or to the pre-evaporated coating. Besides, for the RFS sample a more probable explanation could be contamination with the high index material. In fact, the found difference in SiO_2 refractive index corresponds to 5% volume fraction of Ta_2O_5 inclusions. The origin of these inclusions could be that SiO_2 target becomes contaminated by Ta_2O_5 while the later is sputtered. Another possible reason could be as follows: all of the time during the deposition both sources must be kept running. So, at pure material deposition the other source is still running, although at extremely low power. This low power mode can be instable, depending of the process history. It should be possible to avoid this effect by running only one source for pure materials switching off the other completely and protecting it from contamination with a closed shutter. Possible undesired co-sputtering can also be reduced by using higher low-power limits.

The refractive index of the layer that was supposed to be pure silica in the model for IBS sample is higher than could be expected for this material (Table 16.). The reason for this, similar as for the case of SiO_2 of RFS, could be inclusions of TiO_2. The obtained refractive index of this layer corresponds to silica with 4% of volume fraction of titania. For co-deposition with the IBS technique specially prepared zone target has been used[90]. The mismatch in dependency of the refractive indices against the target position, leading to co-sputtering of both materials instead of only one of them, can originate from a slightly broadened ion beam[91]. An additional effect may arise from the contamination of the non-sputtered side of the target with the actual coating material. Optical characterisation points out that

higher than expected refractive indices of SiO_2 layers are crucial issues. Above suggested possible origins of these discrepancies must be checked in order to improve the process.

Regarding thicknesses, they remain within the expected errors of 6% for EBE and 3% for RFS and IBS. Only the third ramp of EBE model and the second one together with Ta_2O_5 layer of RFS model are out of these error ranges, improving the fits significantly. The model of EBE sample gives ramps starting and ending with higher refractive index compared to the design (Figure 38 a). This indicates that the content of Nb_2O_5 in the coatings was higher than expected, i.e. it was not well calibrated, that is in correspondence to the results of optical characterisation of the sample with ten periods, where n_M and n_m are also shifted upwards comparing to the expected values. On the contrary, the thickness of the pure Nb_2O_5 layer has smaller error because it was controlled by quartz crystal monitor and not by time of deposition as in the case of ramps. In the case of RFS it is possible that, due to the specific conditions during co-sputtering process mentioned before, the rate of deposition of Ta_2O_5 that was determined from samples coated with pure material and not in the process of co-deposition, is not repeatable in the process of co-deposition, or it suffers from larger deviations which resulted in the error in the thickness of the Ta_2O_5 layer. The true origin of so high thickness error still should be studied.

It must be highlighted that the characterisation started from the simplest model and minimal number of parameters. New parameters (coefficients of dispersion formulas and extinction) were gradually introduced only when trials would confirm it was the only way for significant reduction of merit function that otherwise would remain high. The same applies for increasing limits to some parameters, such as thickness of constant refractive index mixture layer in EBE model or Ta_2O_5 layer in RFS model. Also, the starting designs were modified within the expected limits and subjected to optimisation. The optimisation would stop either in merit function significantly higher or very close to the one of the reported optimised model, the later always giving refractive index profile within the given parameter uncertainties and only slightly different from the reported one.

Regarding the related SIMS measurements, instead of steep transition between pure Nb_2O_5 and SiO_2 layers, around 110 nm in depth, it is possible to see rather smooth change in concentration of the materials through some 15 nm (Figure 42). Besides, in Nb_2O_5 layer some SiO_2 has been detected. This is probably a consequence of simultaneous detection of ions sputtered from different layers, for example due to conical shape of the hole drilled throughout the sample. It results in systematic errors in concentration and lowers the contrast of refractive indices in the profile obtained by SIMS (Figure 43).

The original targeted design presents a closer initial guess to the final model obtained previously, compared to the SIMS based. However, despite of all this and the fact that the initial SIMS based design was breaking the thickness limits of 6% that were imposed in the previous optical characterisation, the newly obtained model is practically the same as the previous one (Figure 44, Table 17 and Table 14). This confirms that SIMS is able to give refractive index profile good enough to be used as an initial design in optical characterisation. It should be only taken into account that the limits set to thickness during optimisation should be less restrictive than those expected by errors in deposition by EBE.

The refractive index profile obtained by optical characterisation involving only spectrophotometric measurements is nearly the same as the model obtained including ellipsometry as well (Table 17). Value of merit function calculated for only reflectance and transmittance (discrepancies from R and T measurements only) of the new model is 3 times lower than of the corresponding value of the previous model, both being well below 1. It must be highlighted that the results of optical characterisation having merit function values lower that 1 indicate that the simulation is within the experimental error margin and therefore, taking into account error of measurements, all the models with the merit functions values below 1 are equally acceptable.

From confidence limits analysis (Table 19) it is possible to see that the percents of uncertainties are 1.5 to 4 times higher if only reflectance and transmittance measurements have been used. Also, comparison of calculated curvature matrices shows that in this case the matrix elements are significantly higher than in the case when ellipsometry measurements were included. This implies that minimum of merit function is narrower (i.e. better defined) in comparison when only spectrophotometric measurements are used, that evidences higher stability of solution. Thus, the complementary use of ellipsometric data results in a more realistic model.

Finally, the importance of setting realistic limits to the parameters in optical characterisation has to be highlighted as a critical issue in characterisation of complex systems such as AR hybrid coatings. Although the optical system defined with both, spectrophotometric and ellipsometry measurements, can be, as shown, considered as well defined, the optimisation procedures having parameters without set limits were ending in solutions with highly unrealistic values of parameters, very often even with high values of merit function. Setting realistic limits and, if necessary, increasing them gradually, is the optimisation strategy that was leading to the realistic solutions with acceptable merit function values,

also for the examples when ellipsometry measurements were not included into optical characterisation or when initial solution was SIMS based - further from the final model than the design.

5.5. Mixture samples

Since the band gap for SiO_2 is around 8 eV (160 nm) and for Nb_2O_5 around 3.3 eV (375 nm), for the spectral range of performed optical characterisation Cauchy model is appropriate for SiO_2 and low content Nb_2O_5 samples, while for Nb_2O_5 and samples with high content of this material Tauc-Lorentz model is more appropriate. Due to significant scattering of Nb_2O_5 sample annealed at 750°C (Figure 47 a)), optical characterisation could not have been performed. Also due to scattering, but lower in this case, for n_M sample instead of Tauc-Lorentz model that is appropriate for the samples with high content of Nb_2O_5, Cauchy model has been applied. In combination with exponential absorption law it simulates the effect of scattering more successfully than Tauc-Lorentz that is not able to account for optical losses below band-gap. Also, reflectance and transmittance measurements in the range 400-900 nm (where scattering is lower than 1%) have been used for characterisation of this sample. The other samples don't show significant scattering (Figure 47 b)).

The thicknesses obtained from optical characterisation are higher than those calculated from deposition rates (Table 20), possibly because of higher porosity or changes in deposition conditions from one process to another. The thickness reduces with annealing temperature: around 7% upon annealing at 500°C and around 10% upon annealing at 750°C. Refractive indices increase with temperature: around 0.9% for n_M and n_{M-x} samples annealed at 500°C and 5% after treatment at 750°C. For the rest of the mixture layers this increase is around a half of the samples with high content of Nb_2O_5. This behaviour of indices and thicknesses indicates that density of the layers increases with annealing. Optical thickness (*nd*) reduces with annealing temperature.

Dispersion curves of AD mixtures follow the theoretical LL dispersion curves very well (Figure 48). The highest discrepancy from the curves is for n_{M-x} and n_{m+x} samples. The refractive indices at 570 nm depending on $f_v(SiO_2)$ are shown in Figure 61, together with the theoretical values calculated from LL and LIN models. For the calculated mixtures BG and MG models show nearly the same values as LIN. Due to the lack of experimental data for 750°C annealed Nb_2O_5, the approximate value 2.41, found in literature[92], has been taken for the simulations. It is clear that refractive indices of the samples follow LL and not LIN model, confirming appropriateness of application of LL model in optical characterisation. This is valid for both, AD and annealed samples, that is in contradiction to the

expectations that after thermal treatment mixtures should separate into phases and should be best described by BG EMT (similar to LIN).

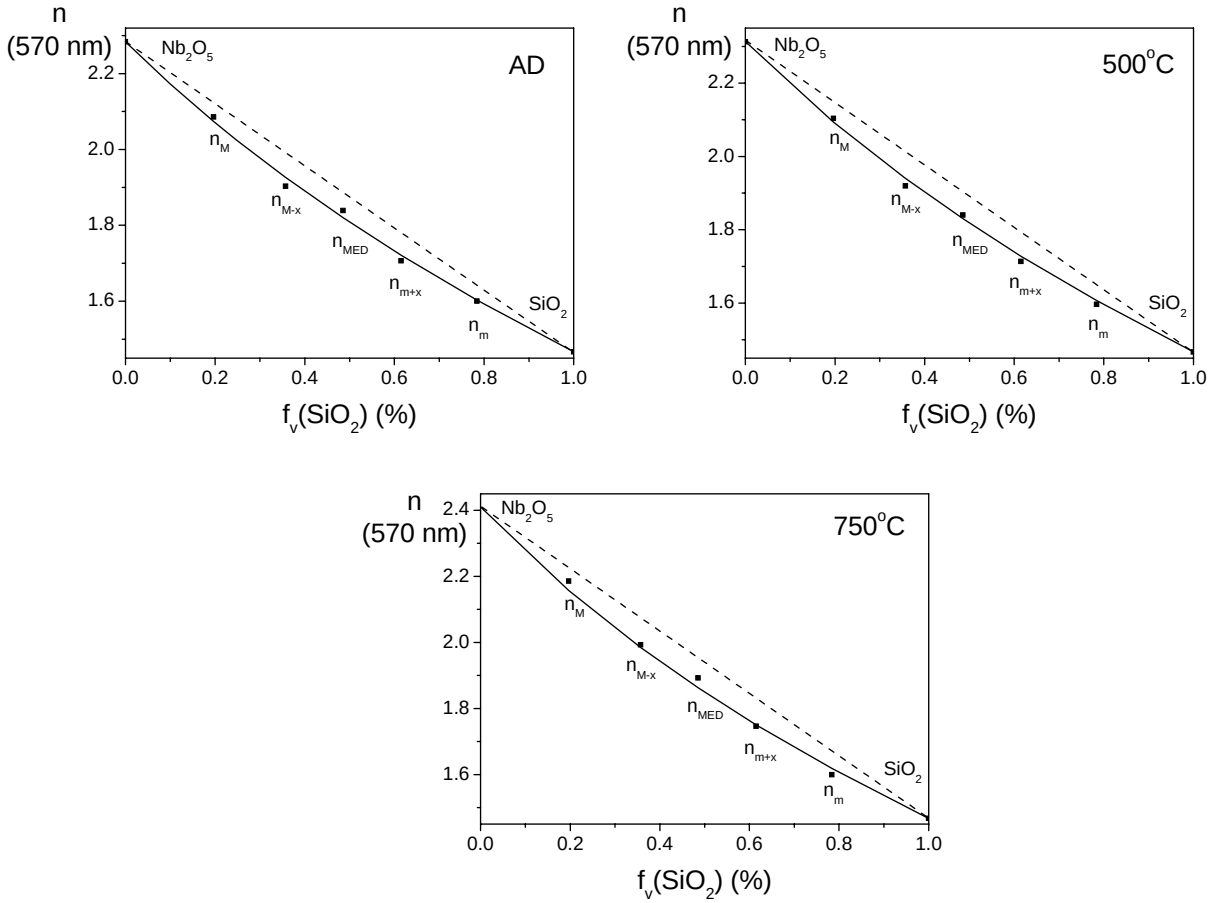

Figure 61. Refractive indices at wavelength 570 nm of the mixture samples (rectangles), together with theoretical curves for LL (solid line) and LIN model (dashes).

FTIR spectra of AD samples (Figure 49) show increase in intensity of bands at 1080 cm^{-1} and 804 cm^{-1} with increased content of SiO_2. The band assigned to Si-O-Nb bonds (around 920-930 cm^{-1}) is especially pronounced for n_m and n_{m+x} samples. Existence of this band suggests that SiO_2 and Nb_2O_5 are mixed at atomic level having no significant separation of phases. The change of intensity of these peaks with annealing temperature indicates breaking of Si-O-Nb bonds followed by creation of Si-O-Si bonds (increase of band at 1080 cm^{-1}). Thus, separation of phases occurs during temperature treatment. However, these bands remain visible even after annealing at 750°C (Figure 50, sample n_m) suggesting that the process is not completed. Notice increase of Si-O-Si band in Nb_2O_5 sample. It is attributed to the growth of native SiO_2 layer at interface with Si substrate due to annealing.

Water absorption bands show that all the AD samples have pores filled with water molecules or that water is adsorbed at the surface of the coating (Figure 51). In FTIR spectra measured three days upon annealing at 500°C (no change in spectra has been noticed after three days) these bands are significantly reduced or even absent (Table 21) and upon annealing at 750°C none of the samples shows water absorption. Reduction of thickness can be related to reduction of concentration of pores in the layer. Indeed, Figure 62 (the data from the Table 21) shows that area under water absorption peak is correlated with shrinking of the thickness. However, the samples after thermal treatment at 500°C already don't have water absorption bands, but their thickness reduces in even higher percent when annealed at 750°C. This effect cannot be attributed only to restructuring due to crystallisation because it is evidenced also for samples that did not crystallise. So, although there is no water absorption in the layer (i.e. open voids that can be filled with water molecules), there are still remained closed pores, so it can be further reduced in thickness with annealing.

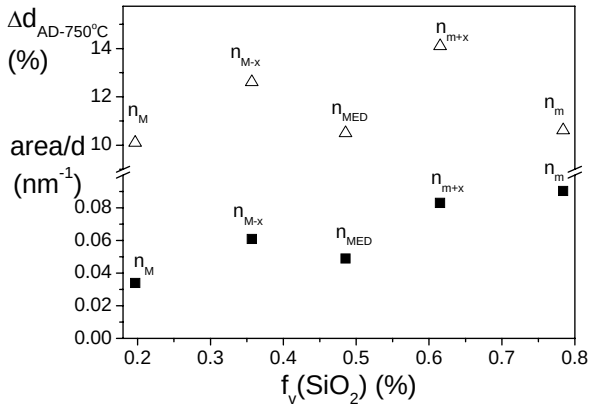

Figure 62. Graphical presentation of the data given in Table 21.

XRD shows (Figure 52) that the first crystallisation in the samples appears between 500°C and 750°C and only for samples with highest content of Nb_2O_5 (n_{M-x}, n_M and Nb_2O_5). The peaks found for n_{M-x} and n_M correspond to hexagonal crystal structure, while in the case of Nb_2O_5 sample it is clear splitting of peaks close to 28.5° and 36.7° that is characteristic for orthorhombic structure. The diffractograms of all the other samples present only halo from the Suprasil substrate and no diffraction pattern is distinguishable. The lack of defined XRD peaks indicates that Nb_2O_5 species are well dispersed in silica (and oppositely) as crystallites are smaller than 2-3 nm (detection limit), or they are present as an amorphous phase.

RMS roughness obtained from XRD analysis (Table 22) doesn't show increase of roughness upon annealing for the samples that have crystallised (n_M, n_{M-x}). It indicates that no big grains are formed on the surface. On the contrary, RMS roughness shows smoothening of the surface for these samples. It must be noticed that it is not expected that the method is appropriate for this level of roughness, but however, the tendency should be correct. For the same samples also density increases after annealing, that is in accordance with decreasing of thickness and lower water absorption found from optical characterisation and FTIR measurements. However, for the Nb_2O_5 sample RMS has significantly increased. This is related to the formation of big crystalline grains that highly contribute to the scattering of this sample.

Indeed, RMS values obtained from AFM measurements (Table 22) confirm the smoothening of surface of mixture samples with high content of Nb_2O_5 after annealing at 750°C and big grains at the surface of Nb_2O_5 sample (Figure 53 and Figure 54). The difference in RMS values of the two techniques for this sample can originate from the scale on which measurements have been performed (compare the two pictures of annealed Nb_2O_5 samples of Figure 53). RMS values obtained from XRD and AFM measurements are in accordance with the level of scattering found in the annealed mixture samples (Figure 63).

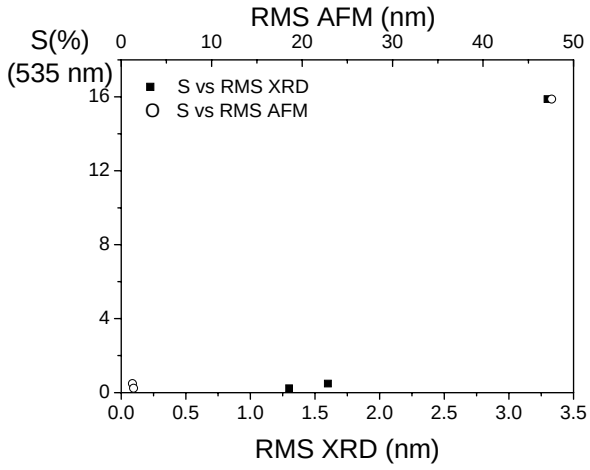

Figure 63. Scattering of annealed Nb_2O_5, n_M and n_{M-x} samples versus RMS values obtained from both, XRD and AFM presented.

TEM diffractogram pattern of AD Nb_2O_5 and n_M samples (Figure 56 and Figure 57) confirm amorphous structure of these samples found by XRD. The spots originate from reflections on Si crystalline structure of the substrate, while rings indicate amorphous structure of the layer. In HRTEM

images it is possible to see 4-7 nm of SiO_2 layer at the interface between the substrate and the coating that is previously mentioned native film that grows on Si exposed to the atmosphere. It is possible to see that the structure of the layers is porous, that is again in accordance with FTIR results. Pores are elongated going from the bottom to the top of the coating. In the first 7 nm of growth there are no pores. Thus, the HRTEM image of n_M sample demonstrates uniform (besides pores) distribution of elements across the layer. The thickness of the coatings for Nb_2O_5 and n_M AD samples found by TEM are 450±20 nm that corresponds to the result from optical characterisation.

Diffractogram of the n_M sample annealed at 750^{o}C (Figure 58) shows that the layer is well crystallised, as expected from XRD results. There is no preferable orientation of the structure in relation to the Si substrate (no overlap with Si substrate reflections). TEM image demonstrates that the sample is multilayered film of total thickness 400±20 nm, again in agreement with thickness from optical characterisation. The native SiO_2 layer has approximately doubled with annealing. This is related to the development of FTIR Si-O-Si band in Nb_2O_5 sample. Z-contrast image indicates that 10-30 nm thick layers consist of element with high atomic number (Nb). They are separated by layers of 1-3 nm of light element (Si). Although the layered structure demonstrates separation of the mixture into phases, HRTEM images show that they are not well defined. This can be related to the results of FTIR that Si-O-Nb bands of some samples remain detectable even after annealing at 750^{o}C, indicating that the process of separation in phases is not completed. This can be correlated with optical characterisation results showing that refractive indices of the mixtures are best described by LL EMT even upon annealing. Indeed, the limits of phase size for BG and MG theory to become effective is 3-30 nm[57] (visible to mid-infrared wavelengths). The uncompleted separation of phases into layers of 1-3 nm is obviously under this limit. Therefore, LL model should be implemented into the rugate design software to simplify linking design and volume fraction values that should be controlled in the deposition process to obtain desired refractive index profile.

The restructuring of the annealed n_M coating into layers is unexpected. However, it can be related to the previous study[33] that has shown periodical regions of higher and lower content of SiO_2 in the mixture coating that was deposited as a layer of constant refractive index. This periodicity has been related to the rotation of the sample placed at calotte and lateral positions of evaporation material crucibles (Figure 26) indicating that the mixture of materials in the vapour is not uniform in the chamber. Above the crucible the concentration of the corresponding material in the vapour is higher. It

is possible that during annealing, due to crystallisation, the regions poor in one material become even more depleted resulting in layered structure more pronounced than in AD coating.

6. Conclusions

Hybrid optical coatings presented in this work are a synthesis of dielectric homogeneous and gradient index layers. It is demonstrated that hybrid AR designs show excellent optical performance in broad angular range. When compared to the equivalent classical HL design the hybrid designs demonstrates similar or even better optical performance. These designs may be practically produced by co-evaporation of a high and a low index coating materials. Besides good optical performance, small physical thickness, low number of corner points, segments starting and finishing only in maximal and minimal allowed refractive indices of the mixtures and absence of refractive index values close to that of ambient (air) make these **designs feasible and affordable as broad angular range antireflective coatings.**

Comparison of classical HL, rugate and hybrid notch design, optimised to satisfy the same requirements, showed that **the graded index designs need more thickness for the same optical density than the HL stack. However, the advantage of the gradient index approach is better sidelobes and ripple suppression, especially in the case of the rugate design. The hybrid design has simpler refractive index profile compared to the rugate and is easier to adapt to different deposition systems. It is shown that for the set specifications the HL design is more favourable than the rugate approaches.** In fact, as a conclusion from the maximum principle, in the case of normal incidence the optimum design will be the one using only two materials, having maximal possible refractive index contrast. Therefore, it is not astonishing that the HL-stack shows the best optical performance. **In the case of oblique incidence, this conclusion holds no more and then gradient index designs may show similar or even better optical properties than their HL-counterparts, as it has been demonstrated for the case of omnidirectional broadband AR coatings.** Together with the expected better mechanical properties, replacement of classical coatings with hybrids is feasible and justified.

Successful coating processes for the fabrication of hybrid antireflection coatings are demonstrated. It is shown that the samples with the best performances and reproducibility are obtained by IBS, demonstrating the high stability and reproducibility of this concept. Very good results are obtained by RFS as well. The sputtering technique, having low rates of deposition, enables stable and precise deposition of mixture films. Omnidirectional AR-coatings obtained by EBE, which allows significantly higher deposition rates than the considered sputter processes, show also good optical performance. There is still space for further improvement of the experimental set-up for the EBE, such

as more precise calibration and control of rates of deposition. Although EBE samples were, as expected, less successful due to more difficulties in control of the process due to high rates of deposition, it is of worth to invest time and effort into improvements because this technique, having the highest rate of deposition, requires least time for coating deposition and is the most commonly used technique.

Optical characterisation has been successfully performed for analysis of hybrid antireflective coatings. Remarkable agreement between simulated and experimental data has been achieved with realistic and reliable final models while number of optimisation parameters was kept as low as possible and their values were maximally controlled in the process of optimisation. It must be mentioned that different effective medium theories were tested to describe the optical constants of the samples. Thus, using Bruggeman formula, for example, merit functions were about 50% higher than those obtained by Lorentz-Lorenz.

Setting realistic limits to the optical characterisation parameters is the critical issue for the optimisation strategy of characterisation of complex systems such as AR hybrid coatings, for obtaining realistic solutions with acceptable values of merit function.

The resulting models were shown to be helpful for determination of errors of deposition process for all three applied techniques. Thus, it has been found that the coating thicknesses were controlled mainly within the expected accuracy. The main problem in the deposition of the studied samples is control of the desired refractive index by means of determination of deposition rates ratios of the materials or by avoiding the undesired co-deposition when only low index material is supposed to be deposited.

It has been shown that SIMS, as one non-optical method, is not sufficient to define the refractive index profile of the given sample. Namely, the profile obtained by SIMS differs from the model significantly more than the targeted design. However, **SIMS based refractive index profile was good enough as initial design for optical characterisation** since starting from it a result very close to the previously obtained model has been achieved.

From comparison of the models obtained from optical characterisation using only spectrophotometric or including also ellipsometry measurements it is not possible to conclude which results are more reliable because of similar profiles and optical performances. However, after taking a look at confidence limits of the optimisation parameters, it becomes clear that uncertainties of the

parameters are much lower when all the measurements are involved. This confirms that **ellipsometry measurements are significantly contributing to the reliability of optical characterisation results.**

Results of optical characterisation of mixture samples show that refractive indices of both, as deposited and annealed samples, follow LL EMT and not LIN as it has been assumed for relating designs with deposition parameters. Structural analysis of as deposited samples (FTIR, XRD diffractograms, TEM) shows that the materials are well mixed, at atomic level (Si-O-Nb bonds). There is no separation into phases for these samples, which is condition for validity of LL EMT. After annealing the materials in the mixture layers show phase separation and crystallisation (FTIR, XRD, TEM, AFM, scattering). The process of separation remains uncompleted and size of phase grains insufficient (FTIR, HRTEM) after annealing at 750^{o}C for BG or LIN EMT to become effective for Nb_2O_5 - SiO_2 mixtures. **Thus, LL EMT has been shown as the most appropriate model for Nb_2O_5 - SiO_2 mixtures** both, by optical characterisation and by relating optical parameters of the mixtures by the structure of the mixtures. Therefore, it is recommended to implement LL model into the rugate design software for the purpose of simplifying the transition of design to the corresponding deposition process.

References

[1] W. H. Southwell "Spectral response calculations of rugate filters using coupled-wave theory", J. Opt. Soc. Am. A **5**, 1558-1564 (1988).

[2] T. D. Rahmlow, Jr., J. E. Lazo-Wasem " Rugate and discrete hybrid filter designs", Proc. SPIE **3133**, 25-35 (1997).

[3] P. G. Verly, J. A. Dobrowolski "Iterative correction process for optical thin film synthesis with Fourier transform method", Appl. Opt. **29**, 3672-3684 (1990).

[4] D. Rats, D. Poitras, J. M. Soro, L. Martinu, J. von Stebut "Mechanical properties of plasma-deposited silicon-based inhomogeneous optical coatings", Surf. Coat. Technol. **111**, 220-228 (1999).

[5] M.-A. Raymond, S. Larouche, O. Zabeida, L. Martinu, J. E. Klemberg-Sapieha "Tribological properties of PECVD optical coatings", *Proceedings of the 44th Annual Technical Conference of Society of Vacuum Coaters*, 301-305, Society of Vacuum Coaters, Albuquerque, N. Mexico, 2001.

[6] R. Vernhes, O. Zabeida, J. E. Klemberg-Sapieha, L. Martinu "Single materal inhomogeneous optical filters based on microstructural gradients in plasma-deposited silicon-nitride", Appl. Opt. **43**, 97-103 (2004).

[7] D. Ristau, H. Schink, F. Mittendorf, J. Ebert, H. Welling "Laser induced damage of dielectric systems with gradual interfaces at 1.064 μm", NIST Spec. Publ. No. 775, pp. 414-426, 1988.

[8] A. Macleod "Optical coatings from design through manufacture", Thin Film Center Inc., Tucson, 2004.

[9] R. R. Willey "Practical design and production of thin films", Marcel Dekker, New York, Basel, 2002.

[10] H. Zorc, V. Janicki, A. Peršin "Narrow band reflector coatings: design procedures", Appl. Opt. **37**, 4249-4253 (1998).

[11] A. V. Tikhonravov, M. K. Trubetskov, G. DeBell "Application of the needle optimization technique to the design of optical coatings", Appl. Opt. **35**, 5493-5508 (1996).

[12] A. V. Tikhonravov "Some theoretical aspects of thin-film optics and their applications", Appl. Opt. **32**, 5417–5426 (1993).

[13] J. P. Borgogno, B. Lazarides, E. Pelletier "Automatic determination of the optical constants of inhomogenous thin films", Appl. Opt. **21**, 4020-4029, (1982).

[14] B. G. Bovard "Rugate filter theory: an overview", Appl. Opt. **32**, 5427-5442 (1993).

[15] D. Poitras, S. Larouche, L. Martinu "Design and plasma deposition of dispersion-corrected multiband rugate filters", Appl. Opt. **41**, 5249-5255 (2002).

[16] D. A. Bruggeman "Berechnung verschiedener physikalischer Konstanten von heterogenen Substanzen", Ann. Phys. 24, 636-679, (1935).

[17] L. Lorenz "Über die Refractionsconstante", Ann. Phys. 11, 70-103 (1880).

[18] J. C. Maxwell Garnett "Colours in metal glasses and metallic films", Philos. Trans. R. Soc. A **203**, 385-420 (1904).

[19] A. V. Tikhonravov, M. K. Trubetskov, T. V. Amotchkina, M. A. Kokarev, N. Kaiser, O. Stenzel, S. Wilbrandt, D. Gäbler "New optimisation algorithm for the synthesis of rugate optical coatings", Appl. Opt. **45**, 1515-1532 (2006).

[20] X. Wang, H. Masumoto, Y. Someno, T. Hirai "Microstructure and optical properties of amorphous TiO_2-SiO_2 composite films synthesized by helicon plasma sputtering", Thin Solid Films, **338**, 105-109 (1999).

[21] S. Larouche, H. Szymanowski, J. E. Klemberg-Sapieha, L. Martinu "Microstructure of plasma-deposited SiO_2/TiO_2 films", J. Vac. Sci. Technol. A **22(4)**, 1200-1207 (2004).

[22] J.-S. Chen, S. Chao, J.-S. Kao, H. Niu, C.-H. Chen "Mixed films of TiO_2-SiO_2 deposited by double electron-beam evaporation", Appl. Opt. **35**, 90-96 (1996).

[23] I. M. Thomas "Method for the preparation of porous silica antireflection coatings varying in refractive index from 1.22 to 1.44", Appl. Opt. **31**, 6145-6149 (1992).

[24] P. Prene, J. J. Priotton, L. Beavrain, P. Belleville "Preparation of a sol-gel broadband antireflective and scratch resistant coating for blast shields of the French laser LIL", J. Sol-Gel Sci. Techn. **19**, 533-537 (2000).

[25] H. Bartzsch, S. Lange, P. Frach, K. Goedicke "Graded refractive index layer system for antireflective coatings and rugate filters deposited by reactive pulse magnetron sputtering", Surf. Coat. Technol. **180-181**, 616-620 (2004).

[26] M. F. Ouellette, R. V. Lang, K. L. Yan, R. W. Bertram, R. S. Owles, D. Vincent "Experimental studies of inhomogeneous coatings for optical applications", J. Vac. Sci. Technol. A, **9**, 1188-1192 (1991).

[27] A. Piegari, G. Emilliani "Analysis of inhomogeneous thin films by spectrophotometric measurements", Thin Solid Films **171**, 243-250 (1989).

[28] G. Parjadis de Lariviere, J. M. Frigerio, J. Rivory, F. Abeles "Estimate of the degree of inhomogeneity of the refractive index of dielectric films from spectroscopic ellipsometry", Appl. Opt. **31**, 6056-6061 (1992).

[29] P. Chindaudom, K. Vedam "Characterisation of inhomogeneous transparent substrates by spectroscopic ellipsometry: refractive indices *n(λ)* of some fluoride-coating materials", Appl. Opt. **33**, 2664-2671 (1994).

[30] V. Janicki, H. Zorc "Refractive index profiling of CeO_2 thin films using reverse engineering methods", Thin Solid Films **413**, 198-202 (2002).

[31] D. Franta, I. Ohlidal, D. Munzar, J. Hora, K. Navratil, C. Manfredotti, F. Fizzotti, E. Vittone "Complete optical characterisation of imperfect hydrogenated amorphous silicon layers by spectroscopic ellipsometry and spectroscopic reflectometry", Thin Solid Films **343-344**, 295-298 (1999).

[32] D. Franta, I. Ohlidal "Optical characterisation of inhomogeneous thin films of ZrO_2 by spectroscopic ellipsometry and spectroscopic reflectometry", Surf. Interface Anal. **30**, 574-579 (2000).

[33] R. Leitel, O. Stenzel, S. Wilbrandt, D. Gäbler, V. Janicki, N. Kaiser "Optical and non-optical characterisation of Nb_2O_5-SiO_2 compositional graded-index layers and rugate structures", Thin Solid Films **497**, 135-141 (2006).

[34] V. Janicki, S. Wilbrandt, O. Stenzel, D. Gäbler, N. Kaiser, A. Tikhonravov, M. Trubetskov, T. Amotchkina "Hybrid optical coating design for omnidirectional antireflection purposes", J. Opt. A: Pure Appl. Opt. **7**, L9-L12 (2005).

[35] V. Janicki, M. Lappschies, B. Görtz, D. Ristau, U. Schallenberg, O. Stenzel, N. Kaiser "Comparison of gradient index and classical designs of narrow band notch filter", in *Advances in Optical Thin Films II*, C. Amra, N. Kaiser, H. A. Macleod, eds., Proc. SPIE **5963,** 5963-60 (2005).

[36] A. V. Tikhonravov, M. K. Trubetskov, T. V. Amotchkina, M. A. Kokarev, N. Kaiser, O. Stenzel, S. Wilbrandt "General approach to the synthesis of rugate coatings", *Proceedings of VI international conference "Prikladnaja Optika"* **3**, 12-16, 2004.

[37] V. Janicki, R, Leitel, S, Wilbrandt, O, Stenzel, D, Gäbler, N. Kaiser "Design of hybrid coatings composed of homogeneous layers and refractive index gradients", in *Advances in Optical Thin Films II*, C. Amra, N. Kaiser, H. A. Macleod, eds., Proc. SPIE **5963,** 397-404 (2005).

[38] V. Janicki, D. Gäbler, S. Wilbrandt, R. Leitel, O. Stenzel, N. Kaiser, M. Lappshies, B. Görtz, D. Ristau, C. Rickers, M. Vergöhl "Deposition and spectral performance of an inhomogeneous wide-angular antireflective coating", Appl. Opt. **45**, 7851-7857 (2006).

[39] V. Janicki, J. Sancho-Parramon, O. Stenzel, M. Lappshies, B. Görtz, C. Rickers, C. Polenzky, U. Richter "Optical characterization of hybrid antireflective coatings using spectrophotometric and ellipsometric measurements", Appl. Opt. **46**, 6084-6091 (2007).

[40] S. W. Wang, X. X. Huang, J. K. Guo, B. S. Li "Synthesis and characterization of yttria-stabilized tetragonal zirconia polycrystalline powder coated with silica layers", Mater. Lett. **28**, 43-46 (1996).

[41] N. Özer, M.D. Rubin, C. M. Lampert "Optical and electrochemical characteristics of niobium oxide films prepared by sol-gel process and magnetron sputtering", Sol. Energ. Mat. Sol. C. **40**, 285-296 (1996).

[42] A. Pawlicka, M. Atik, M. A. Aegerter " Synthesis of multicolour Nb_2O_5 coatings for electrochemic devices", Thin Solid Films **301**, 236-241 (1997).

[43] M. Paulis, M. Martín, D. B. Soria, A. Díaz, J. A. Odriozola, M. Montes "Preparation and characterization of niobium oxide for the catalytic aldol condensation acetone", Appl. Catal. A **180**, 411-420 (1999).

[44] International Centre for Diffraction Data, Joint Committee on Powder Diffraction Standards, Powder Diffraction File, 1601 Park Lane, Swarthmore, PA 19081, USA.

[45] M. S. P. Francisco, Y. Gushikem " Synthesis and characterization of SiO_2-Nb_2O_5 systems prepared by sol-gel method: structural stability studies", J. Mater. Chem. **12**, 2552-2558 (2002).

[46] M. Fox "Optical properties of solids", Chapter 2.2, Oxford University Press, New York, 2001.

[47] E. Palik, editor "Handbook of Optical Properties", Academic Press, San Diego, 1991.

[48] G. E. Jellison Jr., F. A. Modine " Parametrization of the optical functions of amorphous materials in the interband region", Appl. Phys. Lett. **69,** 371-373 (1996).

[49] G. E. Jellison Jr., F. A. Modine "Erratum: Parametrization of the optical functions of amorphous materials in the interband region" [Appl. Phys. Lett. **69,** 371-373 (1996)], Appl. Phys. Lett. **69,** 2137-2139 (1996).

[50] J. Tauc, R. Grigorovici, A. Vancu "Optical properties and electronic structure of amorphous germanium", Phys. Stat. Sol. **15,** 627-637 (1966).

[51] A. Macleod "Thin films optical filters", 3rd Ed., pp. 191, Institute of Physics Publishing, Bristol and Philadelphia, 2001.

[52] S. A. Furman, A. V. Tikhonravov "Basics of optics of multilayer systems", Frontiers, Giff-sur-Yvette, 1992.

[53] P. Chindaudom, K. Vedam "Studies on inhomogeneous transparent optical coatings on transparent substrates by spectroscopic ellipsometry", Thin Solid Films **234**, 439-442 (1993).

[54] D. Franta, I. Ohlidal "Calculation of the optical quantities characterizing inhomogeneous thin film using a new mathematical procedure based on the matrix formalism and Drude approximation", in *Proceedings of the 12th Czech-Slovak-Polish optical conference*, J. Perina, M. Hrabovsky, J. Krepelka eds., Proc. SPIE **4356**, 207-212 (2001).

[55] C. K. Carniglia "Ellipsometric calculations for nonabsorbing thin films with linear refractive index gradients", J. Opt. Soc. Am. A **7,** 848-856 (1990).

[56] A. V. Tikhonravov, M. K. Trubetskov, B. T. Sullivan, J. Dobrowolski "Influence of small inhomogeneities on the spectral characteristics of single thin films", Appl. Opt. **36**, 7188-7198 (1997).

[57] G. A. Niklasson, C. G. Granqvist, O. Hunderi "Effective medium models for the optical properties of inhomogeneous materials", Appl. Opt. **20**, 26-30 (1981).

[58] D. E. Aspnes "Optical properties of thin films", Thin Solid Films **89**, 249-262 (1982).

[59] D. E. Aspnes "Microstructural information from optical properties in semiconductors", in *Optical characterization techniques for semiconductor technology*, D. E. Aspnes, R. F. Potter, S. S. So, eds., Proc. SPIE **276**, 188-195 (1981).

[60] J. A. Woollam, P. G. Snyder "Fundamentals and applications of variable angle spectroscopic ellipsometry", Mat. Sci. Eng. B **5**, 279-283 (1990).

[61] R. M. Azzam, N. B. Bashara "Ellipsometry and polarized light", pp. 364-366, North-Holland, Amsterdam, 1977.

[62] R. W. Collins "Automatic rotating element ellipsometers: Calibration, operation and real-time applications", Rev. Sci. Instrum. **61**, 2029-2062 (1990).

[63] S. N. Jasperson, S. E. Schnatterly "An improved method for high reflectivity ellipsometry based on a new polarization modulation technique", Rew. Sci. Instrum. **40**, 761-767 (1969).

[64] H. G. Tompkins, W. A. McGahan "Spectroscopic ellipsometry and reflectometry. A User's guide", John Willey and Sons, New York, 1999.

[65] A. V. Tikhonravov, M. K. Trubetskov, A. V. Krasilnikova "Spectroscopic ellipsometry of slightly inhomogeneous nonabsorbing thin films with arbitrary refractive-index profiles: theoretical study", Appl. Opt. **37**, 5902-5911 (1998).

[66] A. V. Tikhonravov, M. K. Trubetskov, A. V. Krasilnikova, E. Masetti, A. Duparre, E. Quesnel, D. Ristau, "Investigation of the surface micro-roughness of fluoride films by spectroscopic ellipsometry", Thin Solid Films **397**, 229-237 (2001).

[67] O. Stenzel, S. Wilbrandt, D. Gäbler, N. Kaiser, A. V. Tikhonravov, M. K. Trubetskov, T. V. Amotchkina, M. A. Kokarev "Refractive indices of SiO_2 and Nb_2O_5 mixture films", *Proceedings of VI international conference "Prikladnaja Optika"* **3**, 34-38 (2004).

[68] W. H. Press, S. A. Teukolsky, W.T. Vetterling, B. P. Flannery "Numerical Recepies in C" (Cambridge University Press, New York, 1992).

[69] S. Bosch, J. Ferré-Borrull, J. Sancho-Parramon, "A general-purpose software for the optical characterisation of thin films: specific features for microelectronic applications", Solid State Electron. **45**, 703-709, (2001).

[70] P. H. Berning, "Physics of thin films", Vol. 1, 69-121, New York, Academic Press, 1963.

[71] W. H. Press, S. A. Teukolsky, W. T. Vetterling, B. P. Flannery "Numerical Recipes in C", Cambridge University Press, New York, 1992.

[72] Z. Knittl "Optics of thin films" (John Willey & Sons, 1976.) pp. 41-68.

[73] A. Macleod "Optical coatings from design through manufacture", pp. 55, 145, Thin Film Center Inc., Tucson, 2004.

[74] R. R. Willey "Practical design and production of thin films", pp. 65-83, Marcel Dekker, New York, Basel, 2002.

[75] J. A. Dobrowolski, D. Poitras, P. Ma, H. Vakil, M. Acree "Toward perfect antireflection coatings: numerical investigation", Appl. Opt. **41**, 3075-3083 (2002).

[76] D. Poitras, J. A. Dobrowolski "Toward perfect antireflection coatings. 2. Theory", Appl. Opt. **43**, 1286-1295 (2004).

[77] A. Kaless, U. Schulz, P. Munzert, N. Kaiser "NANO-motheye antireflection pattern by plasma treatment of polymers", Surf. Coat. Technol. **200**, 58-61 (2005).

[78] E. Lorenzo, C. J. Oton, N. E. Capuj, M. Ghulinyan, D. Navarro-Urrios, Z. Gaburro and L. Pavesi "Porous silicon-based rugate filters", Appl. Opt. **44**, 5415-5421 (2005).

[79] W. H. Southwell "Extended-bandwidth reflector designs by using wavelets", Appl. Opt. **36**, 314-318 (1997).

[80] W. H. Southwell "Rugate filter sidelobe suppression using quintic and rugated matching layers", Appl. Opt. **28**, 2949-2951 (1989).

[81] W. H. Southwell "Using apodization function to reduce sidelobes in rugate filters", Appl. Opt. **28**, 5091-5094 (1989).

[82] R. R. Willey "Practical design and production of thin films", pp. 102, Marcel Dekker, New York, Basel, 2002.

[83] H. Ehlers, K. Becker, R. Beckmann, N. Beermann, U. Brauneck, P. Fuhrberg, D. Gäbler, S. Jakobs, N. Kaiser, M. Kennedy, F. König, S. Laux, J. C. Müller, B. Rau, W. Riggers, D. Ristau, D, Schäfer, O. Stenzel "Ion assisted deposition processes: industrial network IntIon", in *Advances in Optical Thin Films*, C. Amra, N. Kaiser, H. A. Macleod, eds., Proc. SPIE **5250,** 646-655 (2004).

[84] M. Lappschies, B. Görtz, D. Ristau "Application of optical broad band monitoring to quasi-rugate filters by ion beam sputtering", to be published in Appl. Opt.

[85] M. Lappschies, B. Görtz, D. Ristau "Optical monitoring of rugate filters", in *Advances in Optical Thin Films II*, C. Amra, N. Kaiser, H. A. Macleod, eds., Proc. SPIE **5963,** 547-555 (2005).

[86] K. Starke, T. Gross, M. Lappschies, D. Ristau "Rapid prototyping of optical thin film filters", in *Optical and Infrared Thin Films*, M. L. Fulton, ed., Proc. SPIE **4094,** 83-92 (2000).

[87] V. Janicki, J. Sancho-Parramon, H. Zorc "Refractive index profile modelling of dielectric inhomogeneous coatings using effective medium theories", to be published in Thin Solid Films.

[88] E. B. Pereira, M. M. Pereira, Y. L. Lam, C. A. C. Perez, M. Schmal "Synthesis and characterization of niobium oxide layers on silica and interaction with nickel", Appl. Catal. A **197**, 99-106 (2000).

[89] S. Laux, W. Richter "Packing-density calculation of thin fluoride films from infrared transmission spectra", Appl. Opt. **35**, 97-101 (1996).

[90] M. Lappschies, B. Görtz, D. Ristau "Application of optical broadband monitoring to quasi-rugate filters by ion beam sputtering", Appl. Opt. **45**, 1502-1506 (2006).

[91] M. Lappschies, B. Görtz, D. Ristau "Optical monitoring of rugate filters", Proc. SPIE 5963, pp.1Z-1 (2005).

[92] J.-P. Masse, H. Szymanowski, O. Zabeida, A. Amassian, J. E. Klemberg-Sapieha, L. Martinu "Stability and effect of annealing on the optical properties of plasma-deposited Ta_2O_5 and Nb_2O_5 films", Thin Solid Films **515**, 1674-1682 (2006).